AD/A-003 036

CRITICAL HEAT FLUXES FOR CURVED AND STRAIGHT SURFACES DURING SUBCOOLED FLOW BOILING

Thomas G. Hughes

Pennsylvania State University

Prepared for:

Naval Sea Systems Command

7 June 1974

PII Redacted

REPORT DOCUMENTATION PAGE	READ INSTRUCTIONS BEFORE COMPLETING FORM

1. REPORT NUMBER	2. GOVT ACCESSION NO.	3. RECIPIENT'S CATALOG NUMBER
TM 74-194		AD/A - 003036

4. TITLE (and Subtitle)	5. TYPE OF REPORT & PERIOD COVERED
CRITICAL HEAT FLUXES FOR CURVED AND STRAIGHT SURFACES DURING SUBCOOLED FLOW BOILING	Ph.D. Thesis
	6. PERFORMING ORG. REPORT NUMBER
	TM 74-194

7. AUTHOR(s)	8. CONTRACT OR GRANT NUMBER(s)
Thomas George Hughes	N00017-73-C-1418

9. PERFORMING ORGANIZATION NAME AND ADDRESS	10. PROGRAM ELEMENT, PROJECT, TASK AREA & WORK UNIT NUMBERS
The Pennsylvania State University Applied Research Laboratory P. O. Box 30, State College, PA 16801	

11. CONTROLLING OFFICE NAME AND ADDRESS	12. REPORT DATE
Naval Sea Systems Command Department of the Navy Washington, DC 20360	November 1974
	13. NUMBER OF PAGES
	161

14. MONITORING AGENCY NAME & ADDRESS(If different from Controlling Office)	15. SECURITY CLASS. (of this report)
	Unclassified, Unlimited
	15a. DECLASSIFICATION/DOWNGRADING SCHEDULE

16. DISTRIBUTION STATEMENT (of this Report)

Approved for public release, distribution unlimited, per Naval Sea Systems Command, July 24, 1974.

17. DISTRIBUTION STATEMENT (of the abstract entered in Block 20, If different from Report)

Approved for Public Release, Distribution Unlimited per NAVSEA 7/24/74

18. SUPPLEMENTARY NOTES

19. KEY WORDS (Continue on reverse side if necessary and identify by block number)

Correlation Functions
Critical Heat Flux
Freon 113
Nucleate Boiling

Subcooled Flow
Vapor Bubble Cycle

20. ABSTRACT (Continue on reverse side if necessary and identify by block number)

Experimental and analytical studies of the critical heat flux for subcooled flows of Freon 113 over concave, convex and straight surfaces have been conducted. Correlation functions for the critical heat flux on each surface have been developed from an idealized model of the vapor bubble cycle in nucleate boiling. These functions have been evaluated and compared with data collected in an experimental apparatus, constructed as part of this investigation.

Details of the apparatus design and operating procedures are given. (Cont)

1a

20. The results of 274 critical heat flux experiments are reported and summarized in tabular and graphical form.

The analytical and experimental phases of the investigation both indicate that the critical heat flux is increased for all surfaces by increases in velocity and subcooling. In addition, the concave surface was found to sustain critical heat fluxes of between 1.5 and 2.0 times those for the convex surface, depending upon the velocity and subcooling of the bulk fluid. The straight surface was found to sustain between 1.0 and 1.2 times the critical heat flux magnitudes accommodated by the convex surface.

The primary conclusion of the investigation was that concave surfaces permit substantially higher critical heat fluxes than straight surfaces which, in turn, permit somewhat higher critical heat fluxes than convex surfaces.

ABSTRACT

An analytical and experimental investigation of the critical
heat flux on concave, convex and straight heated surfaces has been
carried out for subcooled, flow boiling in Freon 113. A total of
274 experiments have been conducted at five mean velocities and four
subcoolings. The analytical study and the experimental data indicate
that for equal velocity and subcooling, concave surfaces sustain
larger critical heat fluxes than straight surfaces which, in turn,
sustain larger critical heat fluxes than convex surfaces. The
analytical results are compared with the experimental results of
this and other work.

An idealized vapor bubble cycle has been defined and is used
as the basis for a critical heat flux model. In the model, vapor
bubbles are assumed to depart from the heated surface when they
have grown to the edge of the hydrodynamic sublayer. The frequency
of the idealized vapor bubble cycle has been derived and combined
with expressions for the energy associated with each vapor bubble
cycle and the number of active sites present to produce a critical
heat flux expression. The resulting expression contains only one
empirical constant.

Expressions for the ratio of the critical heat flux between
concave and convex surfaces, and between straight and convex
surfaces have been derived. These expressions contain no empirical
constants and predict that for the conditions of this
study, the concave surface will sustain critical heat fluxes of
between 1.5 and 2.0 times those for the convex surface, depending upon

the radial acceleration and subcooling of the bulk fluid. The straight surface was predicted to sustain between 1.0 and 1.2 times the critical heat flux magnitudes accommodated by the convex surface.

An experimental, closed loop boiling apparatus with interchangeable curved and straight test sections was constructed for this study. Details of the apparatus design and operating procedures for the experimental program are given.

Tabular summaries of the experimental data are presented for all surfaces, along with graphical comparison of the experimental and analytical results.

ACKNOWLEDGMENTS

The author would like to express his appreciation for the timely and helpful guidance provided by Professor D. R. Olson, who supervised this investigation. His questions, suggestions, and advice, freely offered throughout the course of the investigation, stimulated an interest and insight into the problem that would not otherwise have been present.

The author also wishes to acknowledge the support of the Applied Research Laboratory under contract with the Naval Ordnance Systems Command, and Professor M. T. Pigott in particular for his role in monitoring this study as part of the E/F program.

TABLE OF CONTENTS

TABLE OF CONTENTS (CONTINUED)

LIST OF TABLES

LIST OF FIGURES

LIST OF FIGURES (CONTINUED)

LIST OF FIGURES (CONTINUED)

LIST OF FIGURES (CONTINUED)

NOMENCLATURE

Symbol	Description
A	Geometry factor defined by Equation (A.13) (1/in)
A_c	Conduction area during the waiting period (in^2)
A_I	Area of bubble influence (in^2)
A_n	Area of infinitesimal segment of sphere perpendicular to y direction (in^2)
A_s	Area of segment of spherical surface (in^2)
A_T	Total area of heated surface (in^2)
a	Drag coefficient for sphere
B	Dimensional group defined by Equation (2.40) (1/sec)
C	Constant
C_p	Specific heat of liquid at constant pressure (BTU/lb_m-°F)
C_1	First integration constant
C_2	Second integration constant
D_h	Hydraulic diameter (in)
d	Bubble departure diameter (in)
e	Natural base logarithm
F_y	Force on vapor bubble (lb_f)
f	Bubble cycle frequency (1/sec)
f_c	Friction factor for curved channel
g	Standard acceleration of gravity (in/sec^2)
g_c	Dimensional constant ($lb_m \cdot in/lb_f$-sec^2)
H	Dimensional group defined by Equation (2.29) (°F)
h	Film coefficient (BTU/sec-in^2-°F)
h_{fg}	Latent heat of vaporization (BTU/lb_m)

NOMENCLATURE (CONTINUED)

Symbol	Description
i	Convex surface subscript
J	Perimeter of fin (in)
K	Area of influence proportionality factor
k	Thermal Conductivity (BTU/sec-in-°F)
k_1	Thermal conductivity of liquid (BTU/sec-in-°F)
L,l	Length (in)
M	Dimensional group defined by Equation (B.2)
N_T	Number of active sites
n	Exponent
o	Concave surface subscript
P	Dimensional group defined by Equation (2.43) (in/sec^2)
P_{ℓ}	Pressure at centerline of channel (lb_f/in^2)
p	Pressure (lb_f/in^2)
q	Heat energy (BTU)
$\dot{q}''$	Heat energy flux (BTU/sec-in^2)
R	Channel radius (in)
R_{ℓ}	Channel centerline radius (in)
Re	Reynolds number
R_i	Channel inside radius (in)
R_m	Channel radius of zero shear stress (in)
R_o	Channel outside radius (in)
r	Radius of growing bubble (in)
r_h	Hydraulic radius (in)
S	Cross sectional area of fin (in)

NOMENCLATURE (CONTINUED)

Symbol	Description
s	Straight surface subscript
T	Temperature (°F)
T_b	Bulk fluid temperature (°F)
T_c	Complete temperature difference, $T_W - T_b$ (°F)
T_e	Wall superheat, $T_W - T_{SAT}$ (°F)
T_m	Mean quiescent layer temperature at t_1 (°F)
T_s	Subcooling, $T_{SAT} - T_b$ (°F)
T_{SAT}	Saturation temperature (°F)
T_W	Wall temperature (°F)
t	Time (sec)
t_1	Waiting period defined by Equation (2.28) (sec)
t_2	Wall growth period defined by Equation (2.35) (sec)
t_3	Migration period defined by Equations (2.41), (2.50), (2.54) (sec)
U	Velocity of bubble center of mass (in/sec)
U_o	Initial velocity in migration period defined by Equation (2.37) (in/sec)
V	Velocity of fluid in channel (in/sec)
V_m	Mean channel velocity (in/sec)
v_*	Shear velocity defined by Equation (2.9) (in/sec)
W	Dimensionless hydrodynamic sublayer thickness
X	Dependent variable in standard deviation expression
y	Perpendicular distance from heated surface (in)
y^*	Conduction layer thickness defined by Equation (2.27) (in)

NOMENCLATURE (CONTINUED)

Symbol	Description
α	Thermal diffusivity (in^2/sec)
β_{fs}	Fluid-surface constant ($^\circ$F $\sqrt{sec}$ $\sqrt{in}$)
θ	Angular position along curved channel
μ	Dynamic viscosity (lb_m/sec-in)
ν	Kinematic viscosity (in^2/sec)
π	Dimensionless constant
ρ	Density (lb_m/in^3)
ρ_1	Density of liquid (lb_m/in^3)
ρ_v	Density of vapor (lb_m/in^3)
σ	Standard deviation defined by Equation (C.1)
τ	Shear stress (lb_f/in^2)
τ_w	Wall shear stress (lb_f/in^2)
ϕ	Angle between bubble radius and y direction axis

CHAPTER I

INTRODUCTION

1.1   General Statement of the Problem

Nucleate boiling is a process in which energy is transferred
from a heated solid surface to an adjacent liquid by the periodic
production of discrete vapor bubbles at the solid-liquid interface.
This process is unusually conducive to heat transfer at the interface,
and allows large heat fluxes to be transmitted from the solid to
the liquid, while small temperature differences are maintained
between them. When the adjacent liquid is quiescent, the process is
called pool boiling. If the liquid is agitated or forced to flow in
confining tubes, it is called flow or forced convection boiling.
Saturated boiling occurs when the liquid is at saturation conditions
and subcooled boiling occurs when the bulk liquid temperature is
below saturation conditions. The intense agitation caused by the
periodic production of vapor bubbles at the solid surface is used as
the basis for various hypotheses which seek to explain the unusually
large heat fluxes which may be obtained in boiling systems.

Some practical devices make use of a number of these
processes together. Once through vapor generators normally span
the range of forced convection boiling regimes as shown in Figure 1.
The present study is concerned exclusively with the subcooled
flow boiling regime.

The combination of large heat fluxes and small temperature
differences has stimulated the application of the boiling process
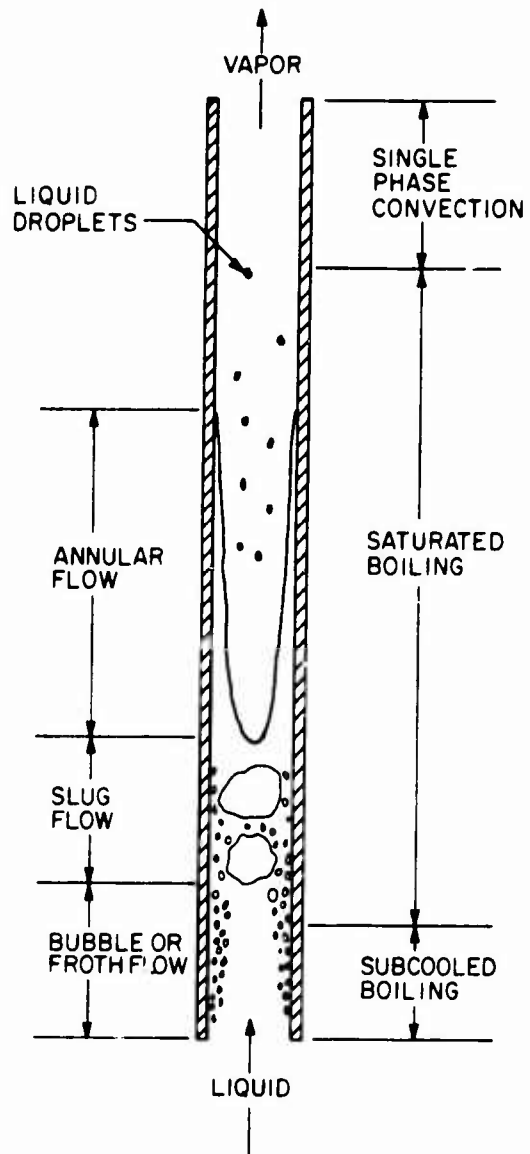
Figure 1   Flow Boiling Regimes

to many contemporary problems; included are once through vapor
generators, nuclear reactor core cooling, electronics package
cooling, and rocket engine fuel vaporization. In each of these
applications a region exists where subcooled liquid flows along a
heated surface. Figure 2 represents the heat transfer performance
of such a surface as its temperature is increased. In region A-B,
the heat transfer process is by forced convection alone and involves
no formation of vapor bubbles at the heated surface. Point B,
the point of incipience, marks the first appearance of vapor bubbles,
and is followed by a transition region B-C. In this region,
bubble formation is irregular and sporadic, and may be affected
by such variables as surface finish, dissolved gases, and thermal
history. At point C, the fully developed boiling region is
entered and is characterized by the periodic formation of discrete
vapor bubbles. The frequency and number of bubbles thus produced
increase with increasing wall temperature until the critical heat
flux, point D, is reached. Continued increases in the surface
temperature will be accompanied by decreasing heat fluxes in region
D-E. In this transition region, alternate patches of vapor and
liquid will blanket the surface until at E, the film boiling
region E-G is entered. In film boiling, the subcooled liquid and
heated surface are separated by a thin layer of vapor. This vapor
layer produces a substantial resistance to heat transfer; the
dominant mechanism becomes radiation and the associated surface
temperatures are frequently beyond the melting point of the heater
material. When the energy supplied to the heater is constant, as
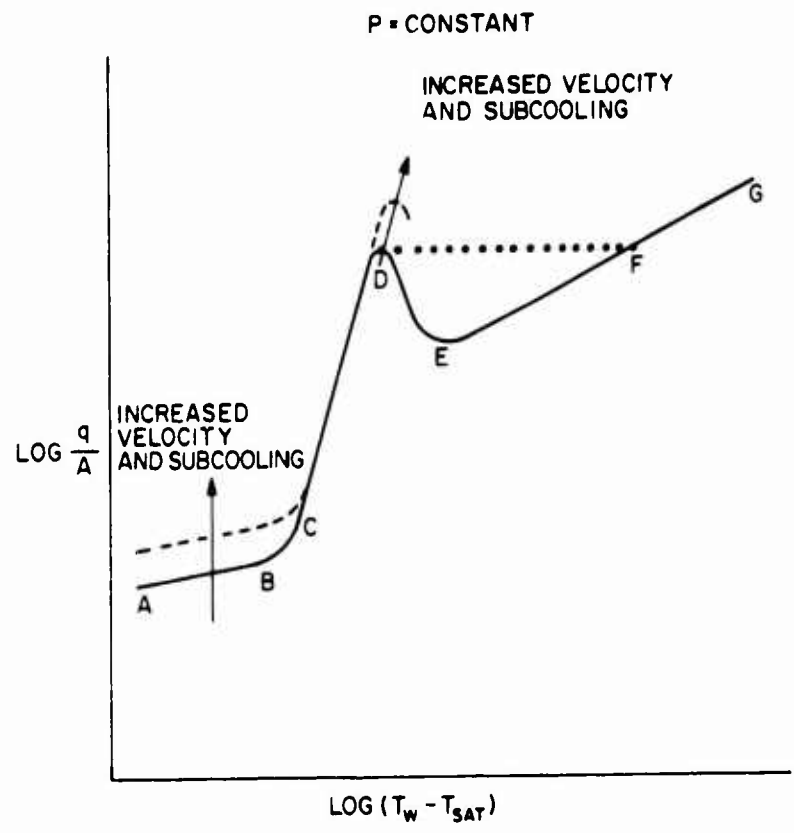
Figure 2   Typical Subcooled Flow Boiling Heat Flux Curve

opposed to the surface temperature, the critical heat flux D is followed by a rapid transition along D-F to film boiling. In such cases the heater invariably melts because of the extremely high surface temperature necessary to produce the critical heat flux in film boiling. Increasing the velocity of the liquid or decreasing its temperature (increased subcooling) will primarily alter region A-B of the curve and the critical heat flux D; both will be displaced upward while the remainder of the curve will be essentially unchanged (dashed line, Figure 2).

Many practical applications of subcooled forced convection boiling involve the constant heat flux mode of operation, and in these applications the region beyond the critical heat flux must be avoided to prevent material failures. The ability to predict the critical heat flux for various systems is therefore desirable. Because of the extreme complexity of the subcooled flow boiling process, no general mathematical prediction of the critical heat flux magnitude has yet been obtained. Efforts to date have centered around obtaining empirical correlations of experimental data for specific heater geometries and fluid-surface combinations. A more general correlation technique with a stronger physical basis is needed. The inclusion of varied surface geometries in such studies is desirable

1.2   The Critical Heat Flux

The varied character of the nucleate boiling process at low, intermediate, and high heat fluxes has resulted in three primary areas of study; incipient boiling, fully developed boiling,

and the critical heat flux. In high energy density applications,
the critical heat flux is of primary importance since it represents
the upper boundary at which a system can be safely operated. In
constant heat flux devices such as nuclear reactor cores, electrical
resistance heaters, and liquid metal combustors, an excursion beyond
the critical heat flux will result in a rapid transition to the
film boiling regime. This transition will be accompanied by a
precipitous increase in the heater temperature and its probable
failure.

A substantial number of specific experiments have been
conducted in the investigation of this phenomenon. The majority
have dealt with   ical upflow in a tube and annular flow over a
heated internal tube. The former is analogous to nuclear reactor
core cooling, while the latter allows experimental observations of
the boiling surface. A large number of terms have evolved to
describe the observations in these experiments. Terms such as
departure from nucleate boiling, burnout, peak heat flux, and the
critical heat flux have been used to describe approximately
equivalent phenomena. Although slight variations in the definition
of each term might be given by separate investigators, the
underlying concept is the same and is illustrated in Figure 3.
Figure 3 represents the changing distribution of vapor near the
heated surface as the critical heat flux is approached. At the
lowest heat flux shown $(\dot{q}_1")$, discrete bubbles are periodically
formed at fixed locations along the solid-liquid interface. As the
heat flux is increased, the frequency and number of bubbles increases

$$q_1 < q_2 < q_3$$

FLOW →

$\dot{q}_1''$

FLOW →

$\dot{q}_2''$

FLOW →

$\dot{q}_3''$
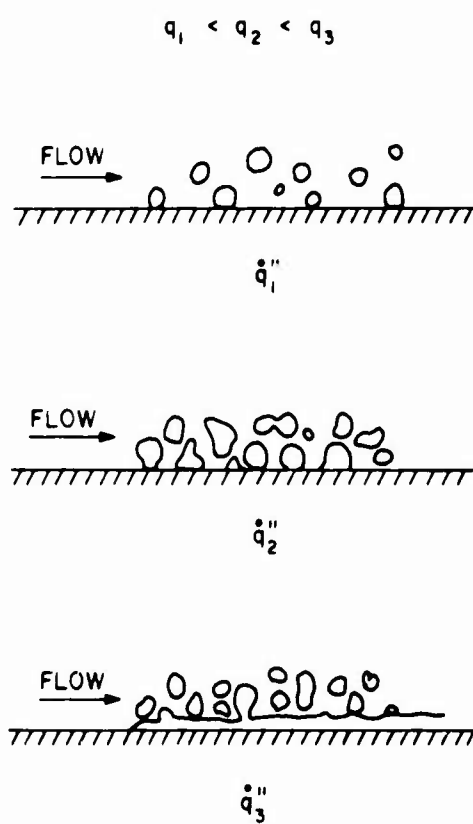
Figure 3   Vapor Behavior Near a Heated Surface Approaching the
Critical Heat Flux

until individual bubbles begin to agglomerate into irregular patches
of vapor ($\dot{q}_2"$). Finally the rate of formation of vapor becomes so
great ($\dot{q}_3"$) that the liquid is effectively prevented from reaching
the surface, or conversely the vapor can no longer be removed from
the surface and a transition to film boiling will occur. In this
study the critical heat flux will be defined as the maximum heat
flux which can be continuously sustained by a boiling surface without
the occurrence of a transition to film boiling.

The occurrence of the critical heat flux becomes, in its
simplest approximation, a contest between the liquid and vapor
phases for the region adjacent to the heated surface. Subcooled
liquid must continually be able to reach the heated surface, while
the vapor produced must be condensed or removed. Since the forces
on a particle of flowing fluid are affected by the shape of channel
in which the flow occurs, channel geometry is expected to have an
effect on the distribution of liquid and vapor, and hence, on the
critical heat flux magnitude. Such effects have been found for
vertical and horizontal tubes, rod bundles, and annular channels.
Indeed, heater geometry is a prominent variable in most critical heat
flux experiments.

Although many common boiling devices such as steam generators
employ coiled tubes, few investigations of the critical heat flux
have been performed for this configuration. Coiled tube experiments
have neglected subcooled boiling, which produces the highest possible
boiling heat fluxes, and failed to account for the very different
body forces encountered by fluid particles at different locations

around the circumference of a cross section of a coiled tube.
The limiting boiling conditions in a coiled tube can be approximated
by flow between convex and concave surfaces, Figure 4. Flow in such
a channel produces two important effects: (1) a radially increasing
pressure gradient, and (2) a centripetal force tending to move all
particles toward the concave surface. It is seen that the radial
pressure gradient will tend to remove vapor from the concave surface
and hold vapor to the convex surface. The centripetal force will
tend to move the more dense liquid away from the convex surface
and toward the concave surface. Clearly, the combined effect of
the pressure gradient and centripetal force is to move liquid
toward the concave surface and restrict vapor movement away from the
convex surface. It is hypothesized that the result of this preferential
wetting of the concave surface will allow higher values of the
critical heat flux to be sustained on the concave surface than the
convex. Intuitively, the critical heat flux for a straight surface
should fall between that of a convex and concave surface for similar
flow conditions.

1.3 Previous Related Studies

Tong (1) has characterized the critical heat flux as a
hydrodynamic phenomenon. The basic assumption is that a critical
volume of vapor injection at the heated surface causes a boundary
layer separation, followed by the vaporization of the stagnant
fluid adjacent to the wall. The critical mass flux required for
separation is obtained from classical hydrodynamics. The momentum
of an equivalent mass flux of vapor, generated at the critical heat
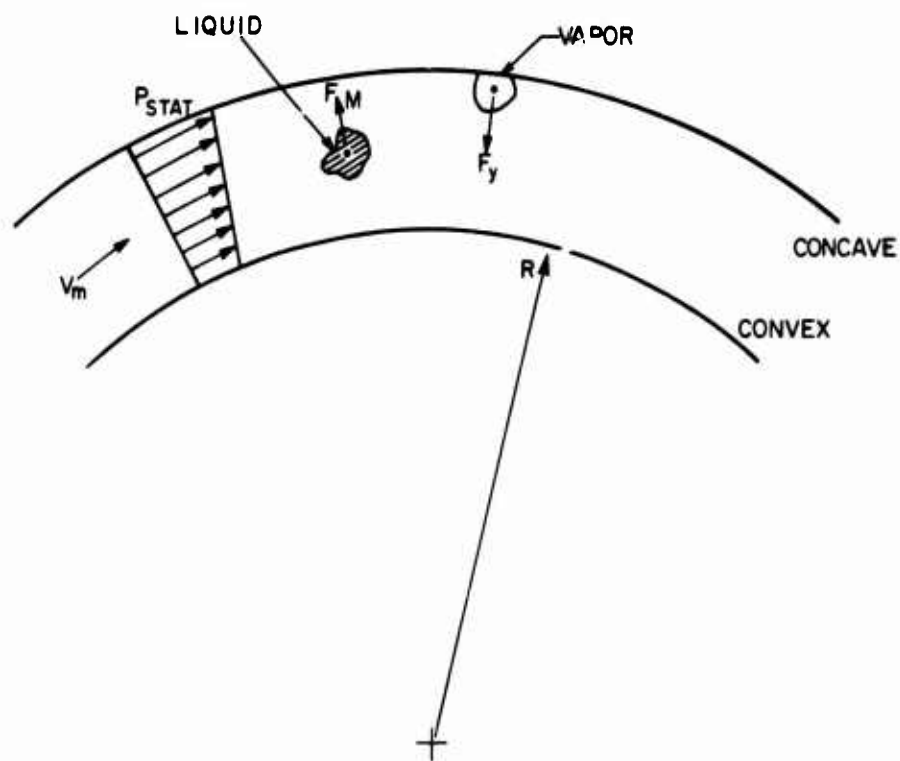
Figure 4 Behavior of Liquid and Vapor Fluid Particles in Curved
         Flow

flux, is then related to mean flow properties and the friction factor for the channel in use. This procedure provides an expression of the critical heat flux in terms of fluid properties, the mean liquid velocity, and the friction factor. The friction factor is assumed to be a function of subcooling and Reynolds number, where the power of the Reynolds number is arbitrarily taken to be half way between that for laminar flow and that for turbulent flow over a rough surface. The effect of subcooling is accounted for by including an experimentally determined "constant" that is a function of the degree of subcooling. Data selected from the experiments of other investigators has been correlated to within 25 percent by this method.

Purcupile and Gouse (2) have taken a similar point of view in which the energy transferred is assumed to be the sum of the energy required to produce the vapor and the energy contained in the liquid displaced by the vapor. It is assumed that this ratio is a function of fluid properties and a pressure dependent "constant." Using this assumption, the critical heat flux can again be found in terms of a critical mass flux of injected vapor. The final expression obtained contains three empirical constants which must be evaluated from experimental data for a specified fluid and heater geometry.

Chang (3) has analyzed the critical heat flux in terms of a thin superheated layer of liquid adjacent to the heated surface. The critical heat flux is considered to occur as the result of the attainment of a limiting critical velocity of the vapor bubbles. No allowance for bubble agglomeration is made and the critical

velocity is deduced by an analysis of the dynamic forces to which an average bubble is subjected. Heat energy transferred both to the liquid and vapor is related to the critical velocity to obtain a critical heat flux expression for subcooled flow boiling. The resulting expression is quite complex and contains five empirical constants, four of which may change with surface geometry and boiling fluid.

Using experimental data collected in similar experiments at the University of California at Los Angeles, Massachusetts Institute of Technology, and Purdue University, Jens and Lottes (4) were able to obtain a purely empirical relationship describing the critical heat flux for water flowing in electrically heated, vertical tubes of small diameter. The relationship obtained was:

$$\left(\frac{\dot{q}''}{10^6}\right)_{B.O.} = C\left(\frac{\rho V_m}{10^6}\right)^n (T_{SAT} - T_b)^{0.22} \quad , \tag{1.1}$$

where the coefficient C and the exponent n were determined to be functions of pressure. The absence of fluid properties in the correlation restricts its use to the fluid for which it was developed (water). The UCLA data was correlated to within 23 percent by this expression, while the Purdue data was correlated to within 60 percent.

Without proposing a model for the flow boiling critical heat flux, Gambill (5) suggested that the critical heat flux could be described as the sum of a non-boiling convective contribution, and a boiling contribution. An expression for the boiling contribution was taken from earlier work on saturated and subcooled pool boiling,

while the non-boiling contribution was described with traditional

forced convection expressions (such as the Colburn equation). The

resulting expression contained two empirical constants and correlated

water data for a variety of tube configurations to within 96 percent.

Correlations restricted to one data set alone were improved to

variations of as little as 12 percent.

Bernath (6) has correlated other experimenters' critical heat

flux data using a turbulent mixing theory. It was assumed that the

intense agitation of the boiling process created a homogeneous

"froth" of liquid and vapor near the heated surface. This layer

was supposed to have a conductivity and thickness which could be

taken together as a traditional film coefficient. By direct

analogy to single phase heat transfer, the critical heat flux

expression became:

$$\left(\frac{\dot{q}}{A_T}\right)_{CHF} = h_{CHF}(T_w - T_b)_{CHF} \quad , \tag{1.2}$$

where the film coefficient, h_{CHF}, was a function of pressure and

velocity (at the very least). Existing data was then used to find

empirical relationships for the critical heat flux film coefficient.

This type of correlation is beset by many difficulties; among them

are a lack of a strong physical basis, the lack of generality of

the film coefficient for various fluids and heater geometries, and

most seriously, the inclusion of the wall temperature in the

relationship. Wall temperatures are not known without experimentation,

which would also reveal the heat flux sought.

DeBartoli, et al., (7) have presented an extensive summary of forced convection burnout studies in rectangular channels and round tubes. Included are discussions of experimental techniques, the effects of numerous variables on the critical heat flux, a review of existing burnout correlations and the application of burnout data to nuclear reactor design.

A purely experimental study of the critical heat flux for Freon 12 flowing in vertical, electrically heated tubes was reported by Stevens, Elliot, and Wood (8). The effects of mass velocity, tube length to diameter ratio, and exit quality of the Freon were presented graphically along with a discussion of the basic boiling curve. Voluminous experimental data was reported, but no analytical modeling was included.

The results of 4,389 critical heat flux experiments for water flowing in vertical heated tubes have been compiled by Thompson and MacBeth (9). The results of attempts to fit this data to polynomials, with coefficients determined by computer analysis, were reported. As many as twelve coefficients have been used to describe the polynomials at a given pressure.

A summary of critical heat flux correlations, as applied to water-cooled nuclear reactors, has been presented by Milioti (10). Fifty-nine references, including some already discussed, were assembled and briefly described. In general, they involve empirical relationships of the type already discussed.

A photographic study of the bubbly boundary layer at the critical heat flux has been reported by Mattson (11). Freon 113 was forced to flow over a heated ribbon on one side of a rectangular

channel while photographic records of bubble behavior at the critical heat flux were made. Average bubble sizes at departure were measured as well as bubble population densities for various conditions. The occurrences of the critical heat flux was shown to entail no abrupt change in flow regime; only a continual increase in bubble size and frequency until the surface was vapor blanketed. Thirty-nine critical heat flux data points were obtained and reported.

Boiling experiments in curved tubes are exceedingly rare, and do not separate the effects of boiling on a concave surface and a convex surface. In an investigation by Carver, Kakarala, and Slotnik (12), two bend radii were employed and temperature measurements were made at 30° intervals around the tube cross section. Inlet fluid quality was increased until a transition to film boiling was indicated at each location by a sharp increase in wall temperature. Average film coefficients for the curved configuration were shown to be higher than for equivalent straight sections and the data revealed that nucleate boiling was more effectively maintained on the concave surface than on the convex surface (although this observation was not made by the investigators). No theoretical analysis was included.

A similar scheme was used by Owhadi (13) to study boiling in a heated coil for water flowing at atmospheric pressure. Heat transfer coefficients were reported at 90° intervals on the tube cross section circumference. In general, the highest coefficients occurred on the concave surface (tube wall farthest from the coil axis). Since many boiling experiments have discovered the

existence of high and low pressure boiling regimes, the application

of this work to high pressure cases does not appear to be warranted.

The experiments of both Owhadi (13) and Carver (12) involved

a constant power supplied to a test section having (by direct

observation) film coefficients that varied around the tube

circumference. This gave rise to a circumferential variation in

heat flux that could not be measured in these experiments. Since

the boiling processes on the concave and convex portions of the tube

surface can readily be seen as limiting cases, further investigations

of each, as well as their relationship to each other, are indicated.

Duchatelle, DeNucheze, and Robin (14) performed similar

experiments for pressurized water flows with three separate diameter

tube coils. The experimental procedures and observations were

similar to those of Carver, et al. In addition, an attempt was

made to correlate the critical inlet quality with heat flux, mass

velocity and pressure. Four numerical constants in the resulting

expression were evaluated by the method of least squares. The

resulting empirical expression, restricted to water in coiled tubes,

correlated the 75 data points obtained to within 10 percent. In

this study, the tube coils were heated with a counterflow of hot NaK.

1.4   Specific Objectives of the Study

Subcooled forced convection nucleate boiling is important

primarily because of the extremely high rates of heat transfer

possible with only modest heater surface temperatures. The limiting

heat fluxes at which subcooled forced convection nucleate boiling

may be sustained are influenced by many variables, including the

geometric path to which the flow is constrained. There is
evidence that flow in coiled tubes is superior to flow in straight
tubes for maintaining nucleate boiling to the highest possible
heat fluxes. However, it can be shown that the complex flow
patterns in coiled tubes give rise to fundamentally different
boiling situations at different locations around the circumference
of the tube cross section. A good basic view of the limiting
boiling situations inside a coiled tube may be obtained by
investigating the boiling processes over convex and concave heated
surfaces.

In light of this, the specific objectives of this investigation
were:

1. The study of the critical heat flux, by experiment and
    analysis, for the flow of a subcooled liquid over
    concave, convex, and straight heated surfaces.

2. The development of an analytical model for the critical
    heat flux on such surfaces, based on an idealized
    vapor bubble cycle, and requiring only fluid properties
    and a single empirical constant for evaluation.

3. The determination of purely analytical expressions
    predicting the ratios of the critical heat flux between
    concave, convex and straight surfaces.

CHAPTER II

THEORETICAL CONSIDERATIONS

2.1 Description of the Physical Phenomena

The physical phenomena associated with flow boiling near the
critical heat flux are extremely complicated. The periodic generation
and collapse or departure of vapor bubbles from the surface has not
yet been exactly modeled by any investigator. Directly accounting
for every system variable has usually been avoided in favor of
seeking simplified correlations of experimental data. Such
correlations, often lacking any physical basis, may include
numerous experimental constants to obtain a good fit of the data.

The subcooled flow boiling process has been studied by a
number of investigators. A "bubbly boundary layer" has been
described by Jiji and Clark (15). The bubbly boundary layer,
illustrated in Figure 5, is not to be confused with the traditional
hydrodynamic boundary layer. The bubbly boundary layer refers to
that region adjacent to the heated surface containing vapor bubbles
at various stages of growth and collapse. At low system pressures
it is about as thick as the diameter of the average bubble contained
within it (15) while at high pressures it may be an order of
magnitude thicker than the largest bubble present (11). The high
pressure regime is much more commonly encountered.

Increasing velocities and subcoolings are accompanied by
decreasing bubble boundary layer thicknesses, while increasing
heat fluxes result in thicker bubble boundary layers. At any fixed

$T_w > T_{SAT} > T_b$

BULK FLUID AT T_b

EDGE OF BUBBLY
BOUNDARY LAYER

EDGE OF HYDRODYNAMIC
SUBLAYER

FLOW →

BUBBLE GENERATION
AND GROWTH

WALL AT T_w
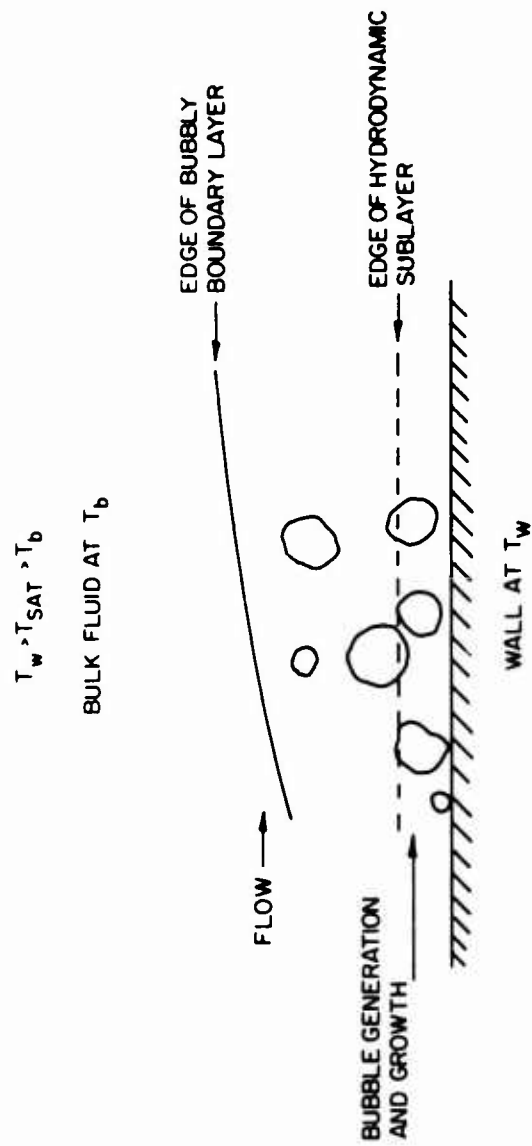
Figure 5   The Bubbly Boundary Layer

velocity and subcooling, increasing heat fluxes bring about
increased rates of bubble production at any given active site.
As the critical heat flux is approached, Mattson (11) has found that
"there are no abrupt changes in bubble size, bubble population
density, bubble flow trajectory, bubble boundary layer thickness, or
bubble boundary layer slope. That is, there is no abrupt change
in flow regime at (the critical heat flux)."

2.2   Mechanisms of Boiling Heat Transfer

It is generally agreed that the excellent heat transfer
rates associated with nucleate boiling are due to the intense
agitation stemming from the growth cycle of vapor bubbles at the
heated surface. Various investigators have attempted to describe
boiling heat transfer mechanisms capable of accounting for the large
heat fluxes typical of boiling surfaces. A summary of four basic
categories into which many of these mechanisms may be placed is
presented by Forster and Grief (16), and includes virtually all of
the concepts contained in other work (17, 18, 19).

Theories of microconvection in the sublayer hold that the
main energy flow is from the heated surface to the liquid separating
growing bubbles at the heated surface. Since, even in the case of
forced convection, unrealistically high velocities would be required
to achieve boiling film coefficients, it is hypothesized that the
growing bubbles create large local velocities in the sublayer.
These velocity fluctuations are assumed to be randomly directed and
large enough to produce the high boiling film coefficients. This
hypothesis is weakened by its inability to explain the relative

insensitivity of the fully developed boiling regime to changes in subcooling.

In another suggested mechanism (16), the growing bubbles are hypothesized to act like an apparent increase in surface roughness, which tends to increase the turbulent exchange of liquid between the heating surface and bulk fluid. With this mechanism heat transfer coefficients could be obtained from pressure drop information by using Reynolds' analogy. Since frictional effects for internal flows are a function of the mean roughness height to pipe diameter ratio, the same would be expected of the boiling process. Experiments have shown little effect of pipe diameter on heat flux for similar boiling conditions, however, and this seems to discredit the apparent surface roughness mechanism.

It is intuitively appealing to consider that the latent heat of vaporization, supplied to form each bubble, accounts for a substantial portion of the energy exchanged at a boiling surface. To investigate this hypothesis, Forster and Grief (16) used data supplied by other investigators and computed the quantity of heat transfer that might be attributed to this mechanism. The computation was made by using motion pictures to obtain the number, maximum size, and frequency of bubbles produced at a heated surface. The vapor volume produced was computed as the product of these values. The volume was then multiplied by the density of the vapor and the heat of vaporization to obtain the heat flux associated with vapor production. It was found to be only a few percent of the total observed experimentally.

A vapor-liquid exchange mechanism is favored by Forster and Grief and, indeed, seems to be the most popular mechanism yet suggested. In the vapor liquid exchange mechanism, a layer of heated liquid is first formed and then expelled into the cooler core liquid by the growing bubble. In effect, a growing vapor bubble displaces an equal volume of heated liquid from the sublayer adjacent to the heater surface to the cooler core region. The recently departed vapor bubble is replaced by cooler liquid and the cycle is repeated, displacing hot liquid from the surface to the core. The energy associated with this process has been estimated by Forster and Grief (16) to be as much as several hundred times the energy associated with latent heat mechanisms. Since latent heat mechanisms have been shown to account for several percent of observed boiling heat fluxes, this exercise demonstrates that the vapor-liquid exchange mechanism is at least potentially capable of explaining the high heat fluxes of nucleate boiling.

2.3 The Model

In this work a greatly simplified model of the boiling process has been developed for the critical heat flux. This model assumes that the critical heat flux occurs when a critical packing density of active sites is reached and that an average vapor bubble will depart the surface when its diameter grows to the thickness of the hydrodynamic sublayer. The actual value of this thickness is open to speculation, but a trial value will be chosen later to demonstrate this concept.

The model describes an idealized vapor bubble cycle that occurs at every active site and consists of three distinct time periods summarized in Figure 6. At every active site attention is focused on a cylindrical region of diameter and height d. This region is initially filled with liquid at the bulk fluid temperature. During the waiting period heat is conducted into the subcooled liquid until a temperature profile suitable for bubble growth is formed adjacent to the wall.

The beginning of bubble growth marks the end of the waiting period and the beginning of the attached growth period. The bubble is then assumed to grow to a diameter, d, while contacting the wall. Additional heat is transferred to support bubble growth during this period, which ends when the bubble leaves the surface.

The migration period begins when the bubble of diameter, d, leaves the surface with an initial velocity equal to its radial growth rate at the end of the attached growth period. Bubble condensation is neglected during this period and the migration period is considered over when the bubble has moved out of the hydrodynamic sublayer. Heat transfer during this period is neglected since the surface is partially insulated with vapor and superheated liquid. This theoretically accounts for the temperature fluctuations observed in the region of active sites by some experimentors. During migration, liquid at the bulk fluid temperature flows to the wall region and then the cycle is repeated.

By finding the duration of these three periods, a mean bubble cycle frequency can be computed. If an expression for the heat
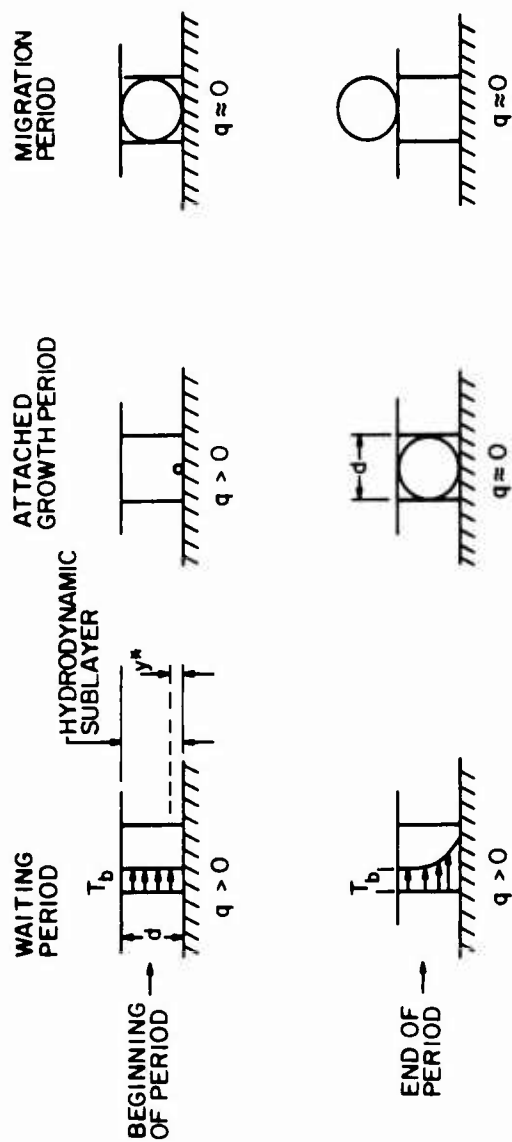
Figure 6 Periods of the Idealized Vapor Bubble Cycle

transfer during each cycle, q, and the critical number of active sites present can be developed, an overall heat flux expression can be written as follows:

$$\dot{q}'' = q \times f \times \left(\frac{N_T}{A_T}\right). \tag{2.1}$$

In this expression, q represents the sum of the heat transferred during the waiting period and the attached growth period. Each term of the right hand side of Equation (2.1) has been derived for the average idealized bubble cycle and the resulting expressions have been combined to express the critical heat flux, $\dot{q}''$.

2.4   Energy Transfer Associated with Ideal Bubble Cycle

The energy transfer associated with an idealized vapor bubble cycle at an average active site is the sum of the heat transferred during the waiting period and during the attached growth period:

$$\begin{bmatrix} \text{Heat Transfer} \\ \text{Per Cycle} \end{bmatrix} = \begin{bmatrix} \text{Heat Transfer During} \\ \text{Waiting Period} \end{bmatrix} + \begin{bmatrix} \text{Heat Transfer During} \\ \text{Attached Growth} \end{bmatrix} .$$

$$\tag{2.2}$$

Experiment and analysis indicate that an extremely thin layer of superheated liquid is required adjacent to the heated surface in order to achieve stable bubble growth at an active nucleation site (20). In this study, the thickness of such a layer will be defined as y^*, Figure 6, and it is assumed to contain a mass of liquid corresponding to the mass of vapor contained in a departing vapor bubble of diameter d. The expression for y^* will be developed later. The mass contained in a vapor bubble of diameter d is given by

$$\text{Mass of Vapor} = \rho_v \ \frac{\pi d^3}{6} \ . \tag{2.3}$$

It is assumed that the waiting period ends, and hence that vapor bubble growth begins, when the liquid at y* reaches saturation conditions. This assumption insures that a mass of liquid necessary for bubble growth has been heated to saturation conditions. The development of a temperature profile of the type shown in Figure 6 requires that energy in excess of that needed to raise the mass of liquid in the y* layer from bulk fluid conditions to saturation conditions must be supplied. If a quantity of heat equivalent to that required to produce a vapor bubble of diameter d from subcooled liquid at T_b is assumed added to the sublayer during the waiting period, this requirement is fulfilled. Such an assumption does not imply that a vapor bubble is actually formed during the waiting period, but rather insures that sufficient energy for vapor bubble growth would be present if it were concentrated in the y* layer instead of distributed throughout the hydrodynamic sublayer. According to this assumption, the quantity of heat transferred during the waiting period is then:

$$q_1 = \rho_v \ \frac{\pi d^3}{6} [C_p (T_{SAT} - T_b) + h_{fg}] = \rho_v \ \frac{\pi d^3}{6} (C_p T_s + h_{fg}) \ . \tag{2.4}$$

During the attached growth period, it is assumed that a bubble grows from the superheated liquid in the $y*$ layer and that all heat added is used to produce saturated vapor. Since the quantity of mass vaporized is described by Equation (2.3), the quantity of heat transferred during the attached growth period is

$$q_2 = \rho_v \frac{\pi d^3}{6} h_{fg} \quad . \tag{2.5}$$

Combining Equations (2.4) and (2.5) yields the total heat transfer associated with the bubble cycle at one active site,

$$q = \rho_v \frac{\pi d^3}{6}(C_p T_s + 2h_{fg}) \quad . \tag{2.6}$$

This expression requires only a relationship for bubble departure diameter for evaluation. The somewhat surprising presence of two heats of vaporization in Equation (2.6) stems from the energy transfer assumed necessary to initiate bubble growth. In essence, one heat of vaporization is used in heating the bulk liquid to a temperature profile suitable for bubble growth, while the second is consumed in actual vapor bubble generation.

Since the idealized vapor bubble cycle was assumed to occur in the region immediately adjacent to the heated surface, and because it is desirable to couple bubble departure diameter to bulk fluid velocity, the rather crude assumption has been made that vapor bubbles depart the heated surface at a diameter equal to some characteristic non-dimensional hydrodynamic sublayer thickness, W. General descriptions of the sublayer and its regions are offered by numerous authors including Martinelli [21] and Schlichting [22]. The non-dimensional thickness, W, is defined as:

$$W = \frac{y v_*}{\nu} \quad . \tag{2.7}$$

If the dimensional thickness, y, is replaced by the bubble diameter, d, the expression for bubble departure diameter becomes

$$d = y = \frac{W\nu}{v_*} \quad . \tag{2.8}$$

The definition for shear velocity is

$$v_* = \sqrt{\frac{\tau_w g_c}{\rho}} \quad , \tag{2.9}$$

and when Equation (2.9) is substituted into Equation (2.8) the following is obtained:

$$d = W\nu \sqrt{\frac{\rho}{\tau_w g_c}} \quad . \tag{2.10}$$

Visual observations of concave and convex boiling surfaces in this study indicated that the bubbles leaving the concave surface were smaller than those leaving the convex surface for equivalent fluid conditions. It is interesting to note that if the results of Eskinazi and Yeh (23) were used for the shear stress in Equation (2.10), a similar conclusion is reached.

In this investigation, the shear stress for concave and convex surfaces has been derived from a wall shear stress expression for two dimensional flow that has been reported by Wattendorf (24) and others:

$$\tau(R) = \frac{1}{2} \frac{\partial p}{\partial \theta} \left[1 - \left(\frac{R_m}{R} \right)^2 \right] \quad . \tag{2.11}$$

The pressure gradient in Equation (2.11) has been represented by the empirical correlation for the friction factor in coiled tubes obtained by Ito (25):

$$\frac{dp}{d\theta} = \frac{R_i + R_o}{2} \frac{f_c}{D_h} \frac{\rho V_m^2}{2g_c} \quad . \tag{2.12}$$

For large values of $Re \left(\dfrac{r_h}{R_{\ell}}\right)^2$ the following relation for the friction factor is suggested by Ito:

$$f_c = 0.316 \frac{\left(\dfrac{r_h}{r_{\ell}}\right)^{.1}}{(Re)^{.2}} \quad . \tag{2.13}$$

Equations (2.11), (2.12) and (2.13) may be combined, simplified and evaluated to give the shear stress at the inside (convex) and outside (concave) walls of the channel. The resulting expressions are:

$$\tau_i = 0.316 \frac{\rho V_m^2}{8g_c} \frac{\left(\dfrac{R_{\ell}}{r_h}\right)^{.9}}{(Re)^{.2}} \left[1 - \left(\frac{R_m}{R_1}\right)^2\right] , \tag{2.14}$$

$$\tau_o = 0.316 \frac{\rho V_m^2}{8g_c} \frac{\left(\dfrac{R_{\ell}}{r_h}\right)^{.9}}{(Re)^{.2}} \left[1 - \left(\frac{R_m}{R_o}\right)^2\right] . \tag{2.15}$$

Equation (2.10) can now be solved using Equations (2.14) and (2.15), for average bubble diameters at departure from the concave and convex surfaces. The resulting expressions are

$$d_o = \frac{5.04W}{\left[1 - \left(\dfrac{R_m}{R_o}\right)^2\right]^{1/2} \left(\dfrac{2R_{\ell}}{D_h}\right)^{.45}} \times \frac{D_h}{Re^{.9}} \quad . \tag{2.16}$$

$$d_i = \frac{5.04W}{\left[\left(\dfrac{R_m}{R_1}\right)^2 - 1\right]^{1/2} \left(\dfrac{2R_{\ell}}{D_h}\right)^{.45}} \times \frac{D_h}{Re^{.9}} \quad . \tag{2.17}$$

No experimental values for the size of bubbles departing curved
surfaces are available for comparison. However, the model can be
degenerated to the straight channel case where some experimental
data are available for comparison.

For a straight channel, the shear velocity has been derived
using the 1/7th power velocity distribution law (22),

$$v_\star = 0.15 V^{7/8} \left(\frac{\nu}{r_h}\right)^{1/8} .$$ (2.18)

Use of this power law restricts Equation (2.18) to Reynold's
numbers of less than 10^5. Substituting Equation (2.18) into
Equation (2.8) and simplifying gives the following result for
average departure diameters in a straight channel.

$$d_s = 6.12 \frac{W D_h}{Re^{7/8}} .$$ (2.19)

Assuming that bubbles depart when they first grow to the
edge of the turbulent core (W = 30) according to Martinelli (21),
values of d_s have been computed and superimposed on the work of
Mattson (11), Figure 7. The average departure diameter for these
assumptions was 0.0031 inches, a value that falls well within those
observed. Similar results have been obtained in other test cases.

2.5   Bubble Cycle Frequency

An analysis of the temperature profile buildup during the
waiting period has been performed by Han and Griffith (26). It is
their conclusion that "since the convection intensity near a solid
wall is damped down due to the no slip boundary condition for a solid
surface, the use of the pure conduction equation is justified in
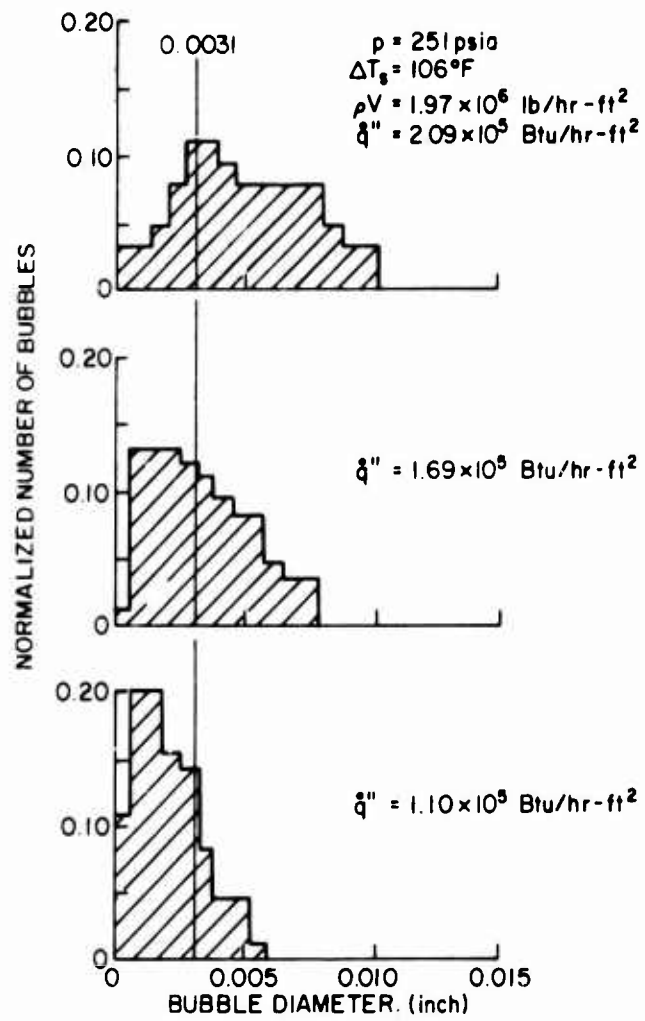
Figure 7   Calculated Departure Diameter Compared with the Data of Mattson

determining the temperature distribution in this thin layer of fluid near the heating surface." The one dimensional heat conduction equation

$$\frac{\partial^2 T}{\partial y^2} = \frac{1}{\alpha} \frac{\partial T}{\partial t} \quad . \tag{2.20}$$

has been solved for the following boundary and initial conditions.

Initial Condition: t = 0

$$T = T_b \text{ at all } y \tag{2.21}$$

Boundary Condition: t > 0

$$T = T_W \text{ at } y = 0$$
$$T = T_b \text{ at } y = \infty \tag{2.22}$$

The solution of Equation (2.20) is given by Carslaw and Jaeger (27) as

$$T - T_b = (T_W - T_b) \text{ erfc } \frac{y}{2\sqrt{\alpha t}} \quad . \tag{2.23}$$

In the region immediately adjacent to the wall, Equation (2.23) can be approximated (26) by a straight line with a slope equal to that of Equation (2.23) evaluated at y = 0,

$$\frac{\partial T}{\partial y}\bigg)_{y=0} = - \frac{T_W - T_b}{\sqrt{\pi \alpha t}} = - \frac{T_c}{\sqrt{\pi \alpha t}} \quad . \tag{2.24}$$

In accordance with the assumptions of Section 2.4, Figure 8 represents the idealized temperature profile adjacent to the heated surface just at the end of the waiting period. The length of the waiting period can be computed from the solution of Equation (2.24),
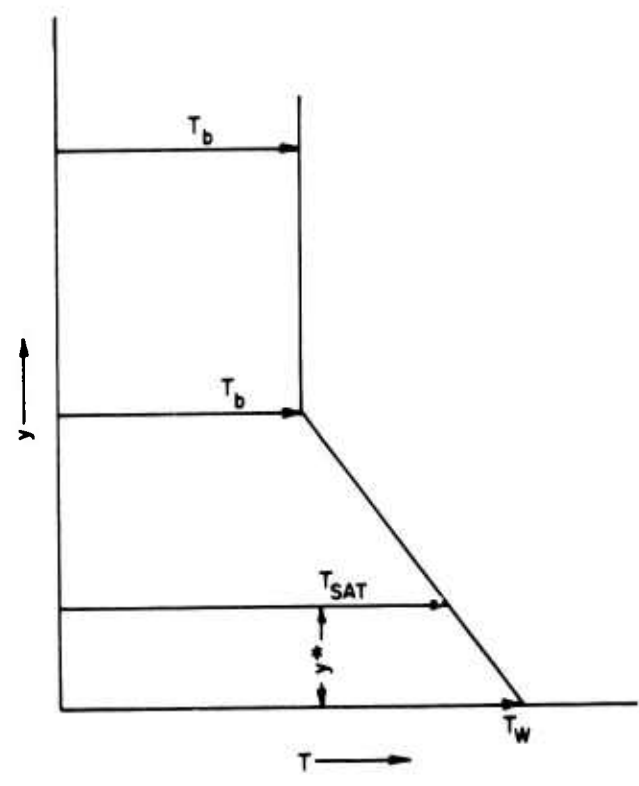
Figure 8   Assumed Temperature Profile in the Sublayer Prior to
Bubble Growth

using the temperature profile of Figure 8 to obtain

$$\frac{T_W - T_{SAT}}{y^*} = \frac{T_W - T_b}{\sqrt{\pi \alpha t_1}} \quad .$$
(2.25)

The value of y^* can be obtained by equating the mass of liquid in the y^* layer and the mass of vapor in a departing bubble:

$$y^* \frac{\pi d^2}{4} \rho_1 = \rho_v \frac{\pi d^3}{6} \quad ,$$
(2.26)

$$y^* = \frac{2}{3} \frac{\rho_v}{\rho_1} d \quad .$$
(2.27)

Combining Equations (2.25) and (2.27) produces an expression for the waiting period:

$$t_1 = \frac{4}{9\pi\alpha} \left(\frac{\rho_v}{\rho_1}\right)^2 \left(\frac{T_c}{T_e}\right)^2 d^2 \quad .$$
(2.28)

By equating the integral of the heat conducted to the liquid during the waiting period and the quantity of heat assumed added during the waiting period (Equation [2.4]), the wall temperature can be expressed in terms of other system variables,

$$\int_0^{t_1} q'' A_c dt = \int_0^{t_1} k_1 A_c \left.\frac{\partial T}{\partial y}\right|_{y=0} dt = \rho_v \frac{\pi d^3}{6}(h_{fg} + C_p T_s)$$
(2.29)

Using Equation (2.24) for the temperature gradient at the wall and Equation (2 28) for t_1, the following expressions result:

$$\frac{T_c^2}{T_e} = \frac{\pi\alpha\rho_1}{2k_1} (h_{fg} + C_p T_s) \equiv H \quad ,$$
(2.30)

and since,

$$T_e = T_c - T_s \quad , \tag{2.31}$$

then

$$T_c^2 - HT_c + HT_s = 0 \quad . \tag{2.32}$$

Equation (2.32) can be solved by the quadratic formula to obtain,

$$T_c = \frac{H}{2} + \frac{\sqrt{H^2 - 4HT_s}}{2} \quad . \tag{2.33}$$

The wall temperature has, therefore, been represented by generally known system properties.

The period of attached growth is the time required for a bubble to grow from incipience to departure diameter. This period has been evaluated making use of the asymptotic growth expression of Plesset and Zwick [28] for vapor bubbles in a superheated liquid. The use of this expression requires the rather gross assumption that during attached growth, the vapor bubble is always pushing a layer of superheated liquid ahead of it, and for that reason does not recognize the distant presence of subcooled liquid. The mean temperature of this layer of superheated liquid has been taken as the linear average of the initial mean temperature of the y^* layer and the saturation temperature. The Plesset and Zwick expression for radial bubble growth then gives:

$$\frac{dr}{dt} = \left(\frac{3}{\pi\alpha}\right)^{1/2} \frac{k_1 T_e}{4\rho_v h_{fg}} t^{-1/2} \quad , \tag{2.34}$$

which can be integrated and evaluated at $r = \frac{d}{2}$ to obtain the attached growth period

$$t_2 = \frac{\pi\alpha}{3} \ \frac{\rho_v^2 \ h_{fg}^2}{k_1^2 \ T_e^2} \ d^2 \ .$$
(2.35)

The period of bubble migration to the turbulent core has been determined by solving an idealized equation of motion for a vapor bubble leaving the surface. It was assumed that spherical bubbles were present, condensation was neglected, and only forces perpendicular to the plane of the surface were considered. The bubbles were considered to have an apparent mass due to the liquid layer associated with them as reported by Han and Griffith (26). The forces and velocities present for the three experimental surfaces are shown in Figure 9. The general form of the dynamic equation follows:

$$\begin{bmatrix} \text{Normal} \\ \text{Force} \end{bmatrix} + \begin{bmatrix} \text{Drag} \\ \text{Force} \end{bmatrix} = \begin{bmatrix} \text{Apparent} \\ \text{Mass} \end{bmatrix} \times \begin{bmatrix} \text{Rate of} \\ \text{Velocity} \\ \text{Change} \end{bmatrix}.$$
(2.36)

Although the individual forces and physical environment are different in this study, an approach to migrating bubble dynamics has been suggested by Keshock and Siegel (29). Normal forces are perpendicular to the heated surface and are derived for the pressure field of a curved channel in Appendix A. Drag forces are represented according to a drag coefficient based on the Stokes equation for the drag on a sphere (22). The initial velocity, U_o, is computed by evaluating Equation (2.34) at t_2 for each case:

$$U_o = \frac{3}{4\pi\alpha} \ \frac{k_1^2 \ T_e^2}{\rho_v^2 \ h_{fg}^2 \ d} \ .$$
(2.37)

For a straight surface, Equation (2.36) takes the form:
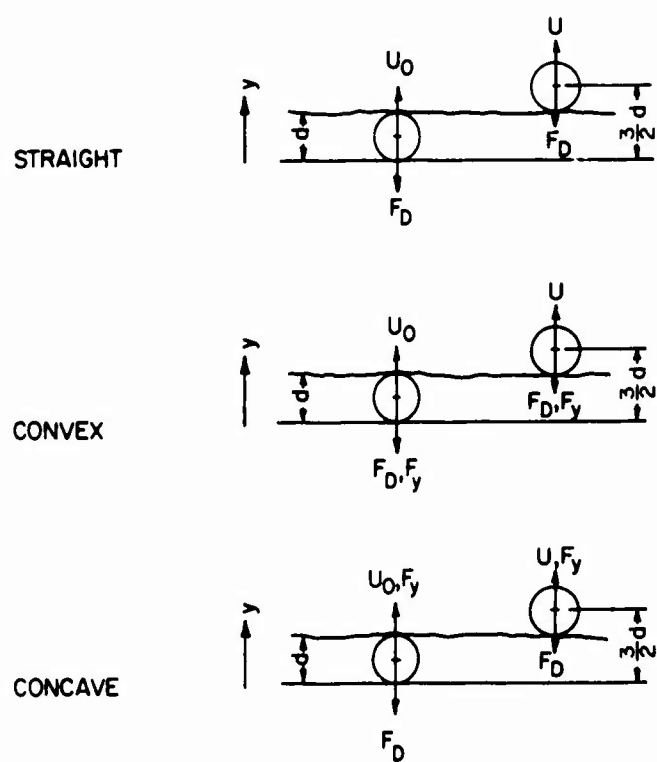
Figure 9   Bubble Forces at Beginning and End of Migration Period

$$- \frac{\pi d}{8} a\mu U = - \frac{11}{16} \rho_1 \frac{\pi d^3}{6} \frac{dU}{dt} \quad, \tag{2.38}$$

which can be simplified to obtain:

$$\frac{dU}{dt} = \frac{12}{11} \frac{a\mu}{\rho_1 d^2} U \quad. \tag{2.39}$$

For simplicity, the following substitution was made:

$$B = \frac{12}{11} \frac{a\mu}{\rho_1 d^2} \quad. \tag{2.40}$$

Equation (2.39) can be solved and evaluated at $y = \frac{3}{2} d$ to obtain the migration period for a straight surface:

$$t_3 = \frac{1}{B} \ln \left(\frac{U_o + Bd}{U_o} \right) \quad. \tag{2.41}$$

For a convex surface, Equation (2.36) is written as:

$$- \frac{\pi d^3}{6} \frac{A \rho_1 V_m^2}{2} - \frac{\pi d}{8} a\mu U = - \frac{11}{16} \rho_1 \frac{\pi d^3}{6} \frac{dU}{dt} \quad, \tag{2.42}$$

and if the following substitution is made,

$$P = \frac{8}{11} A V_m^2 \quad, \tag{2.43}$$

the differential equation of motion is obtained:

$$\frac{d^2 y}{dt^2} - B \frac{dy}{dt} + P \quad. \tag{2.44}$$

Solving Equation (2.44), the integration constants can be evaluated at $t = 0$ where

$$\frac{dy}{dt} = U_o \quad, \tag{2.45}$$

$$y = \frac{d}{2} \quad, \tag{2.46}$$

and a solution for bubble location as a function of time results

$$y = \frac{d}{2} - \frac{1}{B}(U_o + \frac{P}{B}) + \frac{1}{B}(U_o + \frac{P}{B}) e^{Bt} - \frac{P}{B} t \quad . \tag{2.47}$$

An explicit solution of Equation (2.47) for t_3 at $y = \frac{3}{2} d$ is desired, but cannot be directly obtained. If a Taylor series expansion,

$$e^{Bt} = 1 + Bt + \frac{B^2 t^2}{2} \quad , \tag{2.48}$$

is substituted into Equation (2.47), the quadratic equation obtained is

$$t_3^2 + \left(\frac{2U_o}{U_o B + P}\right) t_3 - \left(\frac{2d}{U_o B + P}\right) = 0 \quad . \tag{2.49}$$

The migration can then be determined by a conventional solution of Equation (2.49) which gives

$$t_3 = \frac{U_o}{(U_o B + P)} \left[\sqrt{1 + \frac{2d(U_o B + P)}{U_o^2}} - 1 \right] \quad . \tag{2.50}$$

In serial form, the analogous equations for a concave surface are presented:

$$\frac{d^2 y}{dt^2} - B \frac{dy}{dt} = -P \quad , \tag{2.51}$$

$$y = \frac{d}{2} - \frac{1}{B}(U_o - \frac{P}{B}) + \frac{1}{B}(U_o - \frac{P}{B}) e^{Bt} + \frac{P}{B} t \quad , \tag{2.52}$$

$$t_3^2 + \left(\frac{2U_o}{U_o B - P}\right) t_3 - \left(\frac{2d}{U_o B - P}\right) = 0 \quad , \tag{2.53}$$

$$t_3 = \frac{U_o}{(U_o B - P)} \left[\sqrt{1 + \frac{2d(U_o B - P)}{U_o^2}} - 1 \right] \quad . \tag{2.54}$$

The total period for any surface is the sum of t_1, t_2, and t_3 and it is noted that only the migratory period (t_3) is sensitive

to the surface geometry factor. This is consistent with the assumption that the waiting period and attached growth period occur in a quiescent layer of liquid adjacent to the surface.

The bubble cycle frequency is simply the reciprocal of the sum of the three time periods as follows:

$$f = \frac{1}{(t_1 + t_2 + t_3)} \quad . \tag{2.55}$$

No data exist which could be used for direct comparison with this facet of the model. However, the period of bubble cycles from incipience to collapse have been studied for subcooled pool boiling. For purposes of making crude comparisons, the time for bubble growth to maximum diameter might be cited. The model just developed gives bubble cycle periods ranging from about $.6 \times 10^{-4}$ sec to 8×10^{-3} sec for the limiting cases envisioned in this study. Time periods for growth to maximum diameter have been computed as $.5 \times 10^{-4}$ sec to 5×10^{-4} sec from the work of Robin and Synder (30), 2×10^{-3} sec to 3.2×10^{-3} sec from Kirby and Westwater (31), and 5×10^{-4} to 10^{-3} sec from the work of Forster and Grief (16). Gunther and Krieth (19) have shown growth periods of about 2.5×10^{-4} secs. The data referred to have been generated for a number of fluids in rather dissimilar circumstances, and are intended only to show that the proposed model does not produce totally unreasonable bubble cycle periods.

2.6 Active Nucleation Sites

The criteria for the establishment of active nucleation sites and their role in the nucleate boiling process have been reported by

numerous authors (20, 32-36). To simplify experimental techniques, most investigations have been conducted in pool boiling systems, but Rohsenow (20) has extended this work to the flow boiling regime and supplied an effective nucleation criteria.

In general, all surfaces have a distribution of random sized flaws or pits which serve as potential active boiling sites. In order to be active, a site must contain either a non-condensable gas or some vapor of the fluid to be boiled. A certain liquid superheat, usually only a few degrees, is required to overcome surface tension and initiate bubble growth. Larger characteristic radius active sites require less liquid superheat to support stable bubble growth. Once fully developed boiling begins, the growing vapor bubbles at any active sites present will activate adjacent dormant sites by filling them with vapor. For this reason the hysteresis associated with incipient boiling on increasing heat flux is never present on decreasing heat flux from the fully developed region. The limiting factor at the critical heat flux, therefore, is clearly not one of potential active sites, but rather one of physically accommodating the number of active sites necessary to transmit the imposed heat flux.

It is assumed that as the critical heat flux is approached, a crisis in the packing density of boiling sites occurs. If a certain area of influence is associated with each active site, then the number of such sites multiplied by their area of influence must equal the total heated area at the critical heat flux only

$$N_T \, A_I = A_T$$
(2.56)

The number of active sites per unit area becomes:

$$\frac{N_T}{A_T} = \frac{1}{A_I} \quad , \tag{2.57}$$

and if the area of influence is assumed to be proportional to the area of a departing bubble, the following expression results

$$A_I = K \frac{\pi d^2}{4} \quad . \tag{2.58}$$

Combining Equation (2.57) and Equation (2.58) produces

$$\frac{N_T}{A_T} = \frac{4}{K\pi d^2} \quad . \tag{2.59}$$

This expression represents the number of boiling sites present on a unit area of surface at the critical heat flux. The proportionality factor, K, is assumed to be a function of velocity, subcooling, and the fluid-surface combination; it must be determined experimentally.

2.7   Critical Heat Flux Expressions

Expressions for the critical heat flux on straight, convex and concave surfaces have been developed by combining Equations (2.6), (2.55), and (2.59). The resulting equations, although algebraically cumbersome, have been written in a format that segregates the contributions of the individual terms. This procedure also produced the simplest results of any arrangement attempted. The critical heat flux for a straight surface is represented by,

$$\dot{q}_s{}'' = \frac{2 d_s \rho_v (C_p T_s + 2h_{fg})}{3K\left[\frac{4}{9\pi\alpha}\left(\frac{\rho_v T_c d_s}{\rho_1 T_e}\right)^2 + \frac{\pi\alpha}{3}\left(\frac{\rho_v h_{fg} d_s}{k_1 T_e}\right)^2 + \frac{1}{B} \ln\left(\frac{U_o + B d_s}{U_o}\right)\right]} , \tag{2.60}$$

while the expression for a convex surface is,

$$\dot{q}_i'' = \frac{2d_i \rho_v (C_p T_s + 2h_{fg})}{3K\left[\frac{4}{9\pi\alpha}\left(\frac{\rho_v T_c d_i}{\rho_1 T_e}\right)^2 + \frac{\pi\alpha}{3}\left(\frac{\rho_v h_{fg} d_i}{k_1 T_e}\right)^2 + \frac{U_o}{U_o B + P}\left(\sqrt{1 + \frac{2d_i(U_o B + P)}{U_o^2}} - 1\right)\right]}$$

(2.61)

and the result for the concave surface becomes:

$$\dot{q}_o'' = \frac{2d_o \rho_v (C_p T_s + 2h_{fg})}{3K\left[\frac{4}{9\pi\alpha}\left(\frac{\rho_v T_c d_o}{\rho_1 T_e}\right)^2 + \frac{\pi\alpha}{3}\left(\frac{\rho_v h_{fg} d_o}{k_1 T_e}\right)^2 + \frac{U_o}{U_o B - P}\left(\sqrt{1 + \frac{2d_o(U_o B - P)}{U_o^2}} - 1\right)\right]}$$

(2.62)

The solution of these equations requires the evaluation of the appropriate departure diameter expressions: Equations (2.16), (2.17), and (2.19). Each of these expressions requires a value for W, the dimensionless sublayer thickness, and R_m, the channel radius at which the shear stress is zero. A value of W = 30 has been chosen and corresponds to the boundary of the turbulent core as reported by Martinelli (21). The value of R_m is somewhat more difficult to fix and has been the subject of discussion by various authors. Wattendorf (24) has concluded that R_m is that radius at which:

$$\frac{\partial V}{\partial R} = \frac{V}{R} .$$

(2.63)

If the velocity profile of the channel of interest is known, this radius can be found graphically according to Figure 10. To perform this analysis a velocity profile is needed; since it was not feasible to measure the velocity profile experimentally, an empirical profile,
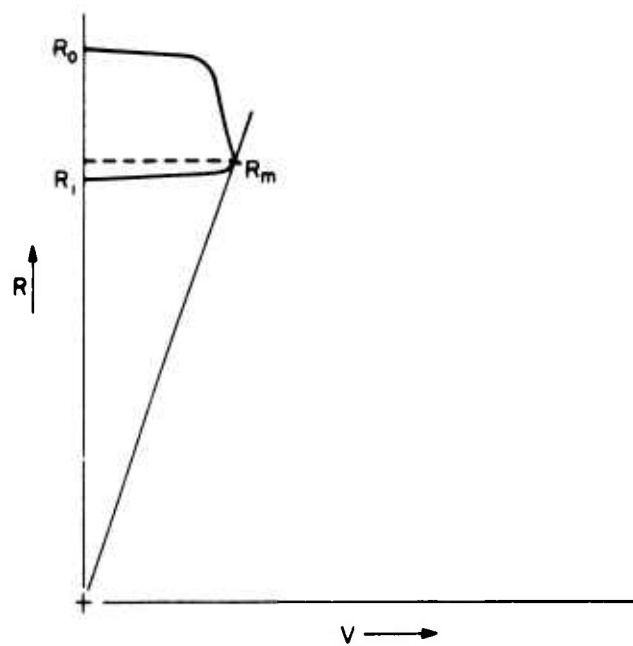
Figure 10 Graphical Location of Zero Shear Radius

suggested by Marris (37) was used. The resulting value was 3.35
inches and was used for analysis purposes. In practice, the
graphical technique could produce values of R_m from 3.33 to 3.38
inches depending on the chosen point of tangency for this apparatus.
In addition, the Marris profile neglects secondary flows which are
certainly present in actual channels. Both of these shortcomings
have been neglected in an attempt to produce a workable model.

The final unknown in Equations (2.60), (2.61) and (2.62) is
the active site proportionality factor, K. Although it cannot be
evaluated without experimental data, if a trial numerical value is
chosen, and if Equations (2.60), (2.61) and (2.62) are evaluated using
saturation properties representative of this work (P = 130 psia),
curves of critical heat flux versus mean velocity can be generated.
The general form of these curves is illustrated in Figure 11. It is
interesting to note that the critical heat flux curves of Figure 11
are quite similar in form to those reported by Stevens, Elliot, and
Wood (8) for the forced flow of Freon in vertical round tubes and by
De Bortoli, et al., (7) for the flow of water in a variety of tube
geometries.

2.8   Critical Heat Flux Ratios

The ratio of the critical heat flux on any two surfaces can
be formed by dividing the appropriate Equations (2.60), (2.61), and
(2.62). If the velocity and subcooling are held constant, the
active site proportionality factor, K, will be eliminated and the
ratio can be calculated directly since no empirical constant remains.
The resulting ratio for the critical heat flux on a concave surface
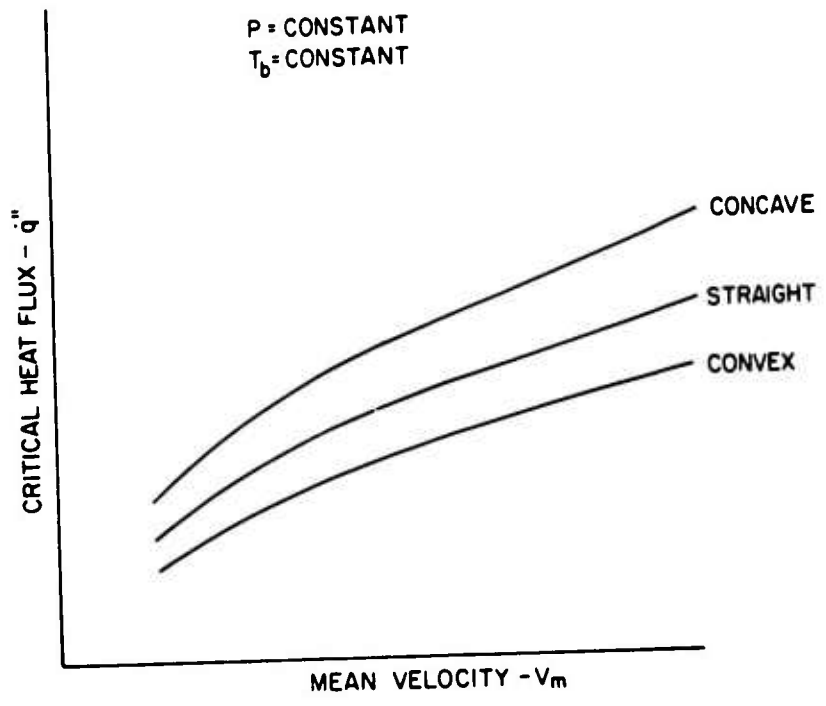
Figure 11   General Form of the Heat Flux Curves

to that on a convex surface is:

$$\frac{\dot{q}_o{''}}{\dot{q}_i{''}} = \frac{d_o\left[\frac{4}{9\pi\alpha}\left(\frac{\rho_v T_c d_i}{\rho_1 T_e}\right)^2 + \frac{\pi\alpha}{3}\left(\frac{\rho_v h_{fg} d_i}{k_1 T_e}\right)^2 + \frac{U_o}{U_o B + P}\left(\sqrt{1 + \frac{2d_i(U_o B + P)}{U_o{}^2}} - 1\right)\right]}{d_i\left[\frac{4}{9\pi\alpha}\left(\frac{\rho_v T_c d_o}{\rho_1 T_e}\right)^2 + \frac{\pi\alpha}{3}\left(\frac{\rho_v h_{fg} d_o}{k_1 T_e}\right)^2 + \frac{U_o}{U_o B - P}\left(\sqrt{1 + \frac{2d_o(U_o B - P)}{U_o{}^2}} - 1\right)\right]}$$

$$(2.64)$$

while the following is obtained for the ratio of straight and convex
surfaces:

$$\frac{\dot{q}_s{''}}{\dot{q}_i{''}} = \frac{d_s\left[\frac{4}{9\pi\alpha}\left(\frac{\rho_v T_c d_i}{\rho_1 T_e}\right)^2 + \frac{\pi\alpha}{3}\left(\frac{\rho_v h_{fg} d_i}{k_1 T_e}\right)^2 + \frac{U_o}{U_o B + P}\left(\sqrt{1 + \frac{2d_i(U_o B + P)}{U_o{}^2}} - 1\right)\right]}{d_i\left[\frac{4}{9\pi\alpha}\left(\frac{\rho_v T_c d_s}{\rho_1 T_e}\right)^2 + \frac{\pi\alpha}{3}\left(\frac{\rho_v h_{fg} d_s}{k_1 T_e}\right)^2 + \frac{1}{B}\ln\left(\frac{U_o + Bd_s}{U_o}\right)\right]}$$

$$(2.65)$$

A graphical representation of these solutions has been
presented in Figure 12 which was plotted for a Freon 113 flow at the
conditions used in this work (p = 130 psia, T_s = 70°F)   The curved
channel was assumed to have a centerline radius 3.5 inches.   It
can be seen that concave surfaces are predicted to sustain heat
fluxes as much   9 times those for convex surfaces, while straight
surfaces are predicted to be as much as 1.2 times as effective as
convex surfaces.
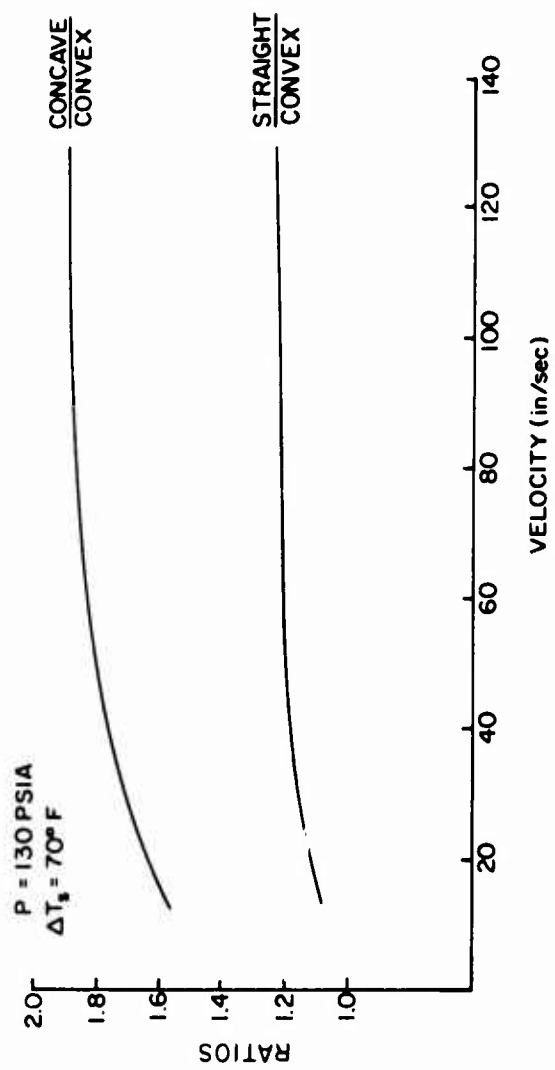
Figure 12 Critical Heat Flux Ratios Predicted by the Analytical Model

CHAPTER III

EXPERIMENTAL INVESTIGATION

3.1   Experimental Concepts

In the development of an apparatus for the experimental
investigation of any boiling process, the pressures, temperatures and
heat fluxes to which the apparatus will be subjected are determined
by the substance chosen as the working fluid. Fluids with low
critical pressures and low heats of vaporization require lower
pressures, temperatures and heat fluxes for the performance of
boiling experiments. As a design objective, it was decided that
the fluid selected for this study should minimize the problems
associated with high pressures and temperatures which challenge
state of the art sealing techniques and overstress common structural
materials. The selection of a working fluid with a low heat of
vaporization alleviates these problems and reduces the magnitude
of the critical heat flux and the surface temperature associated
with it. A low heat of vaporization fluid requires a smaller power
supply, involves smaller temperature gradients, and therefore
reduces attendant problems with heat losses and insulation
techniques. Low heat of vaporization fluids have the added advantage
of permitting investigations of the critical heat flux without
the physical destruction of the heating surface.

These requirements led to the selection of Freon 113 as the
working fluid in this investigation. Freon 113 was selected because
of its low critical point, low heat of vaporization, availability and

well documented thermophysical properties (38-40). In addition,
literature dealing with the forced convection boiling process for
Freon flowing in straight channels is available for comparison
(8, 11, 41). Although similar critical heat flux experiments in
water would probably have more direct applications, the costs and
complexity of such work was judged prohibitive.

Many critical heat flux experiments have been conducted in
test sections heated over their entire length and perimeter. This
procedure produces substantially increasing fluid temperatures and
decreasing fluid pressures in the axial direction, particularly for
fluids having a large heat of vaporization. The net result is
that fluid subcooling changes appreciably as a function of axial
location, and therefore the heated surface is not confronted with
constant fluid properties. The results of such studies are often
difficult to interpret and are normally reported in terms of the
length of heated channel (in $\frac{L}{D}$'s) required to produce a burnout
for specified inlet conditions. In this work these problems were
avoided by designing test sections with minimal bulk fluid
temperature increases ($\sim 2°F$ worst case) and pressure drops (less
than 1 psi). This has been accomplished by using a low heat of
vaporization fluid and heating only a small percentage of the test
section perimeter. For these reasons, fluid conditions adjacent
to the heated surface were considered independent of axial location
in the test section.

Experimental test sections are often difficult and expensive
to replace in critical heat flux studies; therefore, investigators
have devised a number of methods of anticipating the transition to

film boiling in time to prevent the actual burnout of the test
sections. These techniques often involve monitoring the heater
surface temperature and interrupting the power to the test section
when: (1) the magnitude of surface temperature oscillations,
characteristic of an impending transition, reach a certain
predetermined level, or (2) when the rate of surface temperature
increase reaches a high level (7, 8, 11, 41, 42). Other schemes
monitor the resistance of the heated surface and automatically
interrupt the test section power when: (1) the rate of increase of
resistance (related to surface temperature) reaches a present
level, or (2) when the rate of resistance increase of a downstream
portion of the test section becomes substantially greater than that
of either the entire test section or an upstream portion of it (43).

It is apparent that such experimental procedures lend a
"defined" quality to the critical heat flux since the actual
transition to film boiling may never have occurred. These problems
have been avoided in this study by selecting a working fluid and
heater material that allow a brief excursion into the film boiling
regime without the physical destruction of the test section. The
problem of critical heat flux detection was thereby reduced to
observing a rapid rise in surface temperature to a point well above
that associated with nucleate boiling and then terminating the
test.

3.2   Boiling Loop

The nucleate boiling circulation loop has been designed
to supply Freon 113 to the experimental test section at continuously

variable flow rates of 0 to 15 gpm. The design maximums for
circulation loop temperature and pressure are 400°F and 300 psia,
respectively, and each may be varied from ambient conditions to
these values. This was accomplished by assembling a pump, test
section and other auxiliaries into a closed loop as shown in
Figures 13 and 14. Since the loop is closed, the pressure at all
points in it may be raised and lowered by adjusting the helium
pressure in an accumulator attached to the loop. Helium has been
chosen because of its reduced tendency, when compared with other
gases, to dissolve in Freon compounds.

Freon 113 was circulated throughout the loop with a
sealless pump having a combined rotor and impeller assembly driven
by the magnetic field of an induction motor. Such pumps are
compact, light, and leak proof and the need for a rotating shaft
seal is eliminated. The amount of Freon 113 which passed through the
test section was adjusted by two valves, one in the test
section leg and the other in the bypass leg. Each could be opened
or closed relative to the other to provide any flow from zero to
full pump output. Both legs merge downstream of the test section and
pass through a counterflow water cooled heat exchanger and then a
hotwell. The heat exchanger was used to balance the heat addition
in the test section while a resistance type immersion heater in the
hotwell was used to adjust the bulk fluid temperature in the loop.
Variable voltage was supplied to the immersion heater by the
secondary winding of a variac.

Filling and draining were accomplished with a valve and tube
attached to the hotwell. A vent valve for removing extraneous
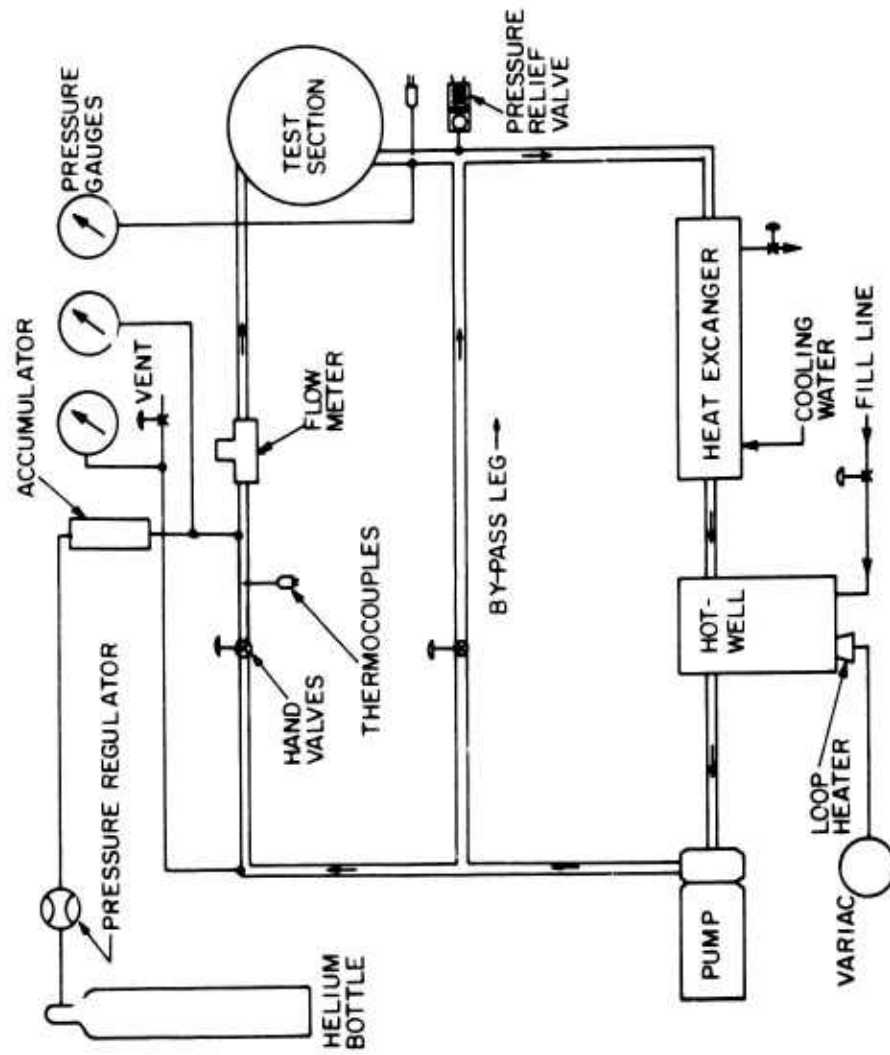
Figure 13 Boiling Loop Schematic
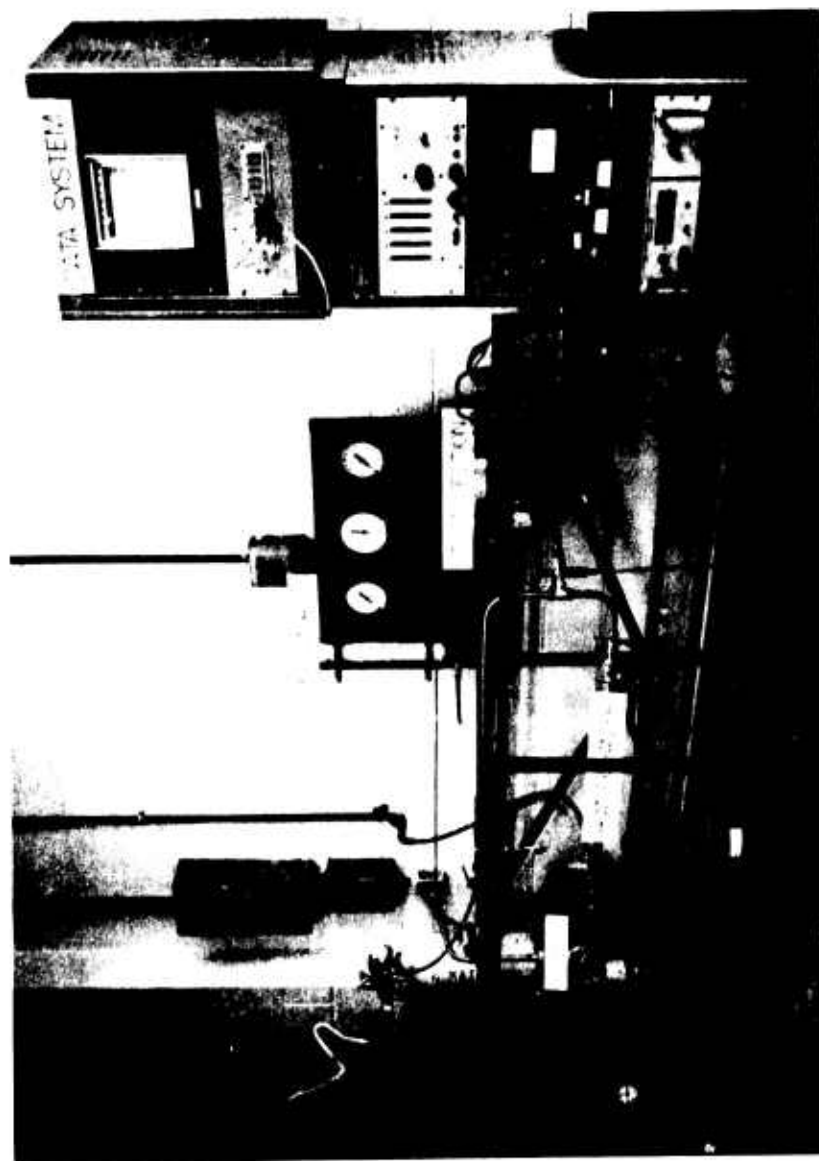
Figure 14 Boiling Loop and Data System

trapped gases was provided in a gas collection tube at the high

point of the loop. Pressures were monitored at the pump discharge,

test section inlet, and test section outlet points in the loop.

Flow was measured at the test section inlet with a turbine type

magnetic impulse flow meter. Inlet and outlet temperatures were

measured for the test section, heat exchanger, and hotwell. A

pressure relief valve was included to insure that the loop was not

operated above its maximum design pressure.

A good general discussion of the difficulties encountered

when experimenting with Freon 113 has been given by Murphy and

Bergles (42). The primary problems center on acid production

through Freon decomposition at high temperatures in the presence of

water and sealing difficulties stemming from the low surface tension

and high vapor pressure of Freon. To avoid acid formation, the

Freon 113 has been passed through a refrigerant dryer (separates

water from Freon) when filling the loop. In addition, the entire

loop has been fabricated from 316 stainless steel and all seals and

packing glands are made of Teflon, which was suggested to be the most

effective sealant material.

3.3 Curved Test Section

The curved test section had a four foot long entrance length

of square stainless tubing which was brazed to a circular stainless

disc into which the circular flow passage had been milled, Figures

15 and 16. An arc of 180° was allowed for the development of

uniform secondary flows. The channel has a square cross section that

is one-half inch wide and one-half inch deep. The inside radius of
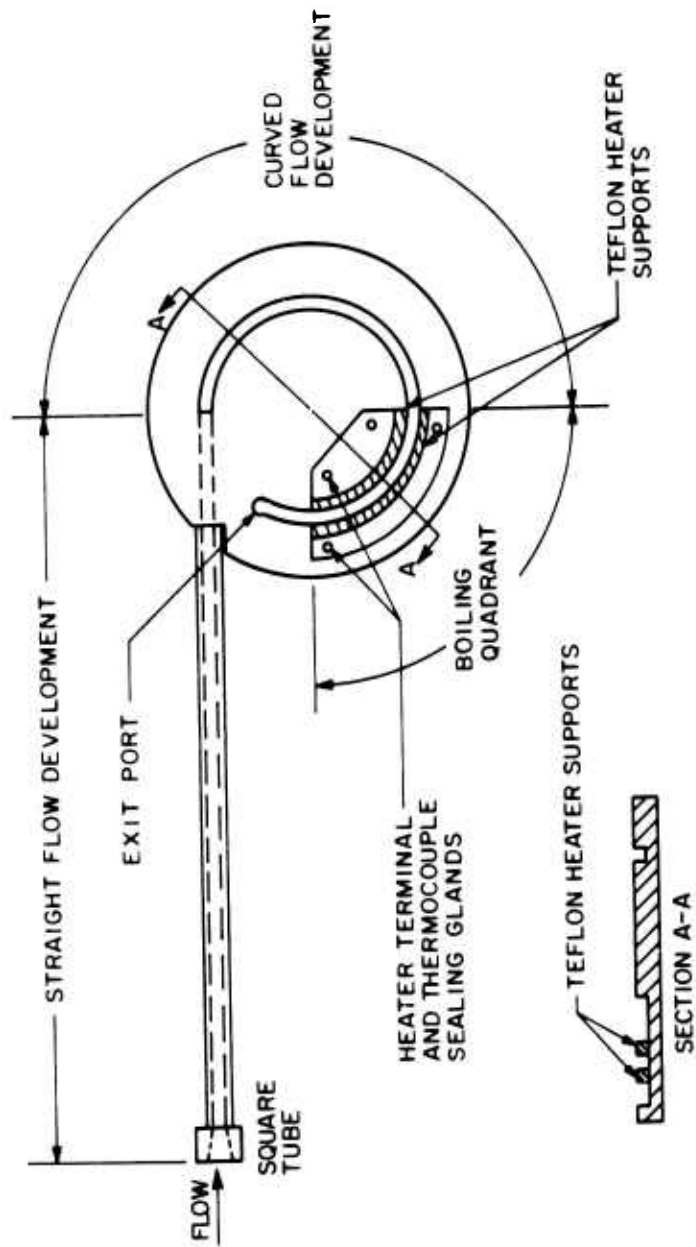
Figure 15   Curved Test Section

Figure 16 Photograph of Assembled Curved Test Section

the channel is three and one quarter inches long. In the region from 180° to 270°, a large truncated pie-shaped area was milled out. The actual boiling experiments were conducted in this region where the flow channel was formed by two circular arcs of Teflon which have been cross-hatched in Figure 15 and are shown in detail in Figures 17 through 19. Strips of Tophet A nichrome heater band were fixed to the Teflon as shown in Figure 17 and Figure 18. The nichrome strips were held in place by spring tensioning brass terminals imbedded in each end of the Teflon arc. The gentle tension of the springs took up any slack in the nichrome strips due to thermal expansion at elevated temperatures. In addition, chromel-alumel thermocouples were butt welded to the back side of the nichrome strip and pulled through holes drilled in the Teflon arcs. Each of these thermocouples was then used in conjunction with a compression spring to hold the nichrome strip tightly against the Teflon arc. This action was particularly important on the concave surface.

Other experiments of this type have encountered substantial difficulties in obtaining heater surface temperature measurements. Most often these difficulties are rooted in the experimenter's inability to place the thermocouple junction on an equipotential line or spot. When this happens, a part of the voltage drop (D.C. heating) or oscillation (A.C. heating) along the heater surface appears as an extraneous signal. To avoid this, the current work made use of a single wire (alumel) butt welded to the nichrome strip with the measurement junction formed 1/32 inch behind it, Figure 20. The nichrome strip temperature was ther   lculated using the

HEATER
TENSIONING
SPRING

HEATER
TERMINAL

THERMOCOUPLE TENSIONING
SPRING & CLAMP

THERMOCOUPLE WIRES

THERMOCOUPLE
JUNCTION

NICHROME STRIP

TEFLON HEATER SUPPORT
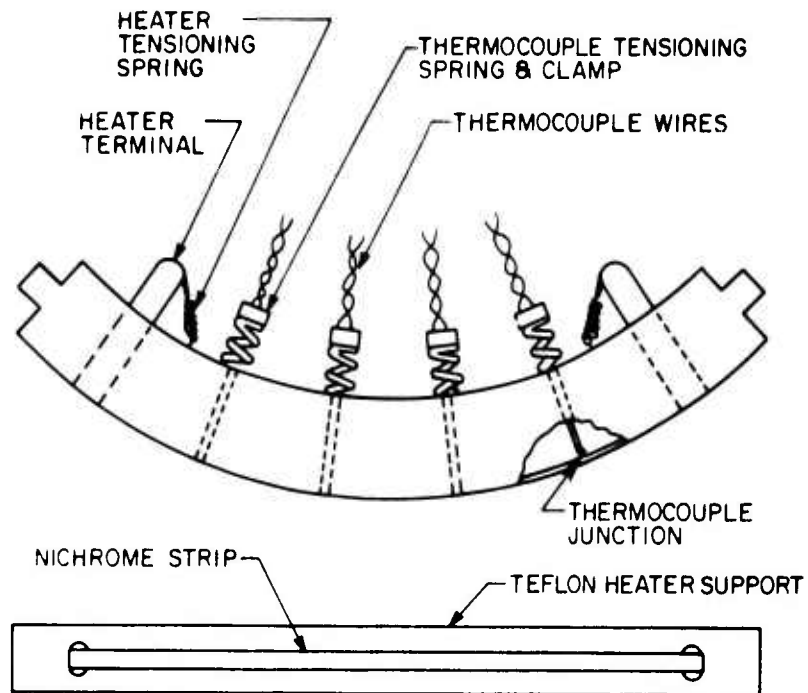
Figure 17   Teflon Supports
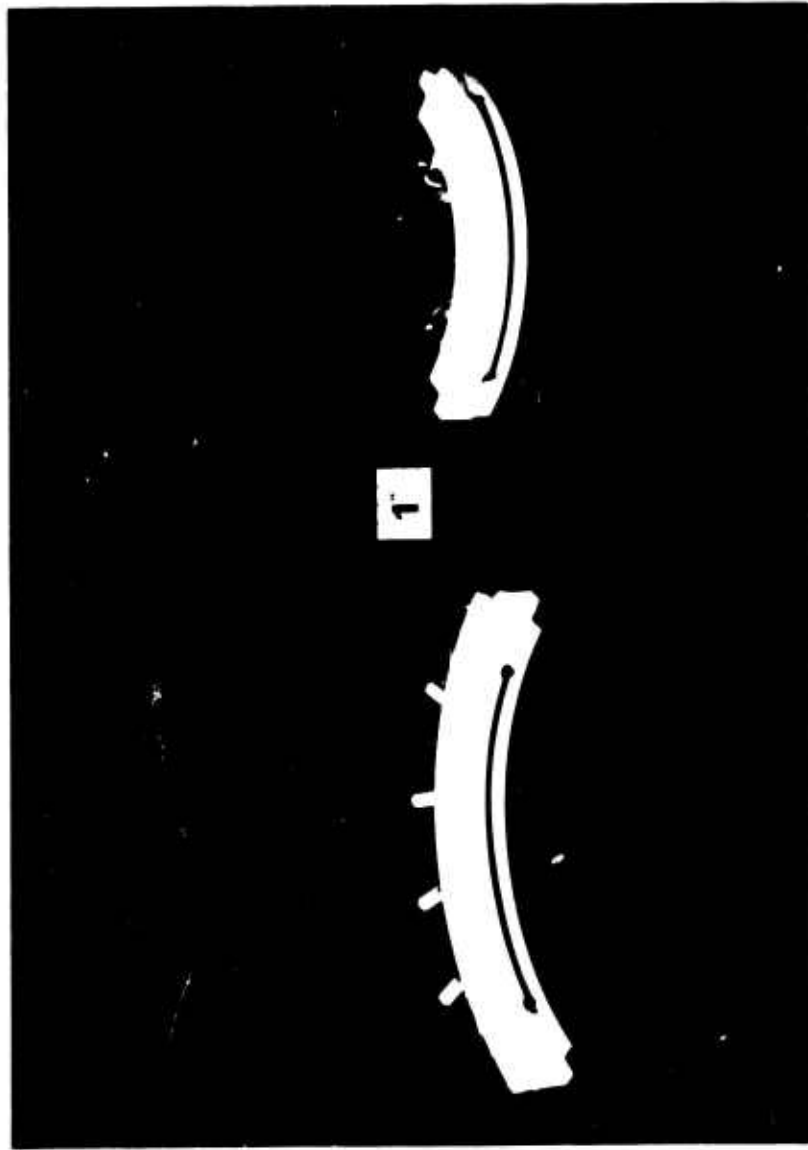
Figure 18 Nichrome Heater Strips Mounted on Flow Side of Teflon Supports
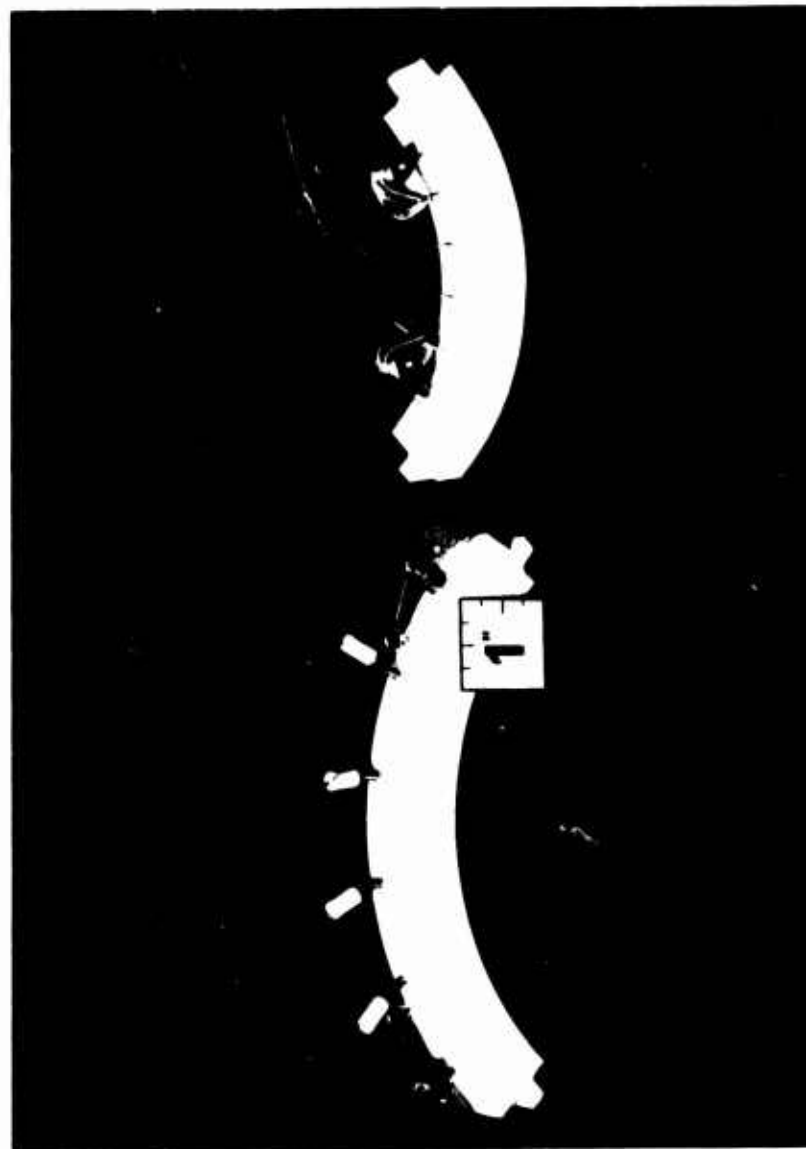
Figure 19   Thermocouples and Power Terminals from Back of Teflon Supports
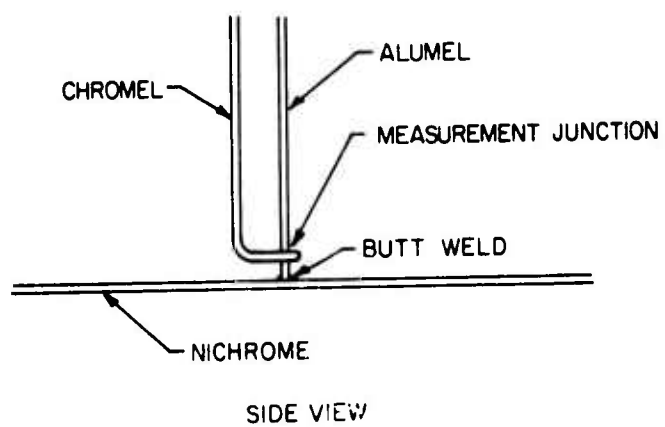
Figure 20   Thermocouple Attachment

observed temperature at the measurement junction. In this work, 24 AWG thermocouple wire has been used with all assemblies.

Although not indicated in Figure 17, a groove was cut in the surface of each Teflon arc so that the heater strip surface was flush with the arc surface. Sealing glands were provided behind each Teflon arc for two 60 amp electric conductors and four pairs of thermocouple wire. An "0" ring groove, Figure 16, was milled around the entire channel in the test section. The test section was then capped with a covering plate of 316 stainless steel which contained a two inch diameter quartz window over the boiling quadrant. The window was sealed with "0" rings and allowed visual observations of the boiling process.

3.4 Straight Test Section

Since no experimental critical heat flux data for concave and convex surfaces are available in the literature, a straight test section was constructed so that some experimental results of this study could be compared to other investigations. In addition, data collected with the straight test section allowed straight and curved surface critical heat flux magnitudes to be compared at equivalent conditions.

The straight test section was directly interchangeable with the curved test section. It conformed to the curved test section with regard to flow development length, cross sectional area, nichrome strip support, and electrical feedthrough seals. Figure 21 shows the top view of the straight test section. Heater strip terminals and tensioning springs can be seen at each end of the Teflon

along with four thermocouple pairs passing through the Teflon support. The thermocouple tensioning springs and electrical sealing glands are seen at the bottom center of Figure 21. Figure 22, the bottom view of the straight test section, shows the power lead glands (Conax EGT-187-A-Cu), the thermocouple seals (Conax MTG-20-A4-T) and the test section pressure tap and discharge port. The pressure tap is the 1/4-inch Swagelok fitting at the bottom center while the discharge port is the 3/4-inch Swagelok fitting at the bottom right.

3.5   Critical Heat Flux Detection

For the test sections used in this study the transition to film boiling occurred rapidly. If the power to the nichrome ribbon was not interrupted within a fraction of a second of the occurrence of the critical heat flux, the Teflon supports would melt locally and deform: in some cases, the nichrome ribbon would overheat and melt. For this reason, it was decided that an automatic critical heat flux detector should be installed to prevent unnecessary damage to the test section and to relieve the experimenter from manually interrupting test section power.

The device designed made use of the surface temperature thermocouples included as an integral part of each heater strip. These thermocouples were used in conjunction with a Leeds and Northrup temperature recorder to measure the nichrome ribbon temperature as the power to the test section was increased. When the critical heat flux was reached, the surface temperature would increase dramatically. A microswitch was added to the potentiometer shaft of the temperature recorder, and was adjusted to trip a power relay when the surface
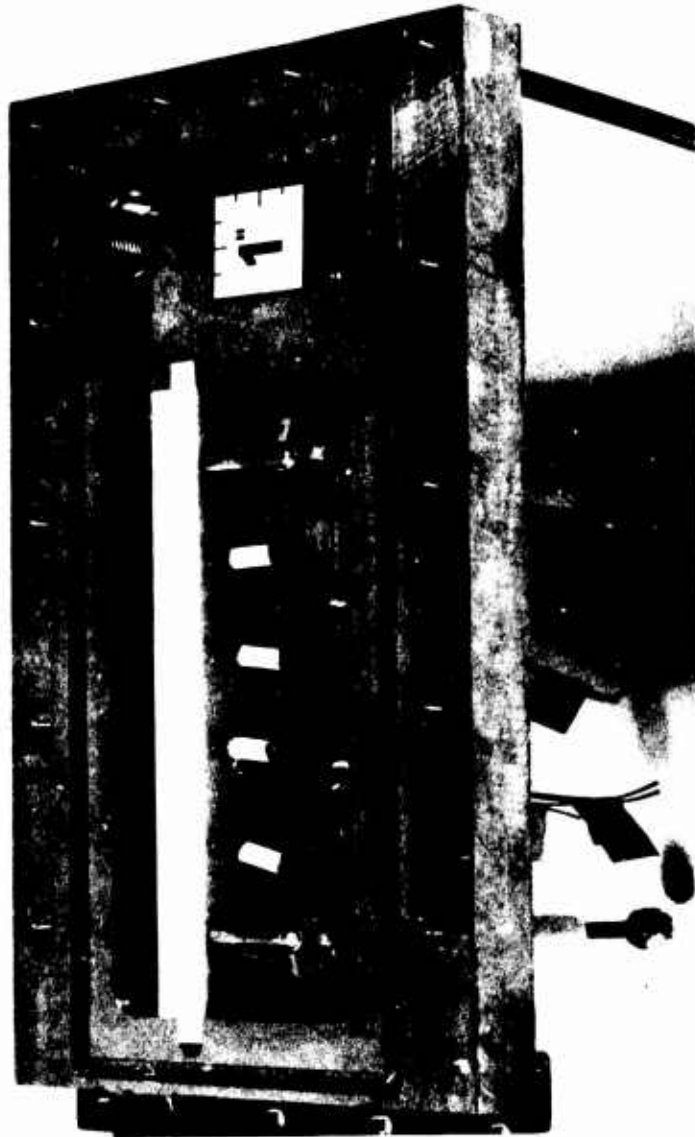
Figure 21 Top View of Straight Test Section
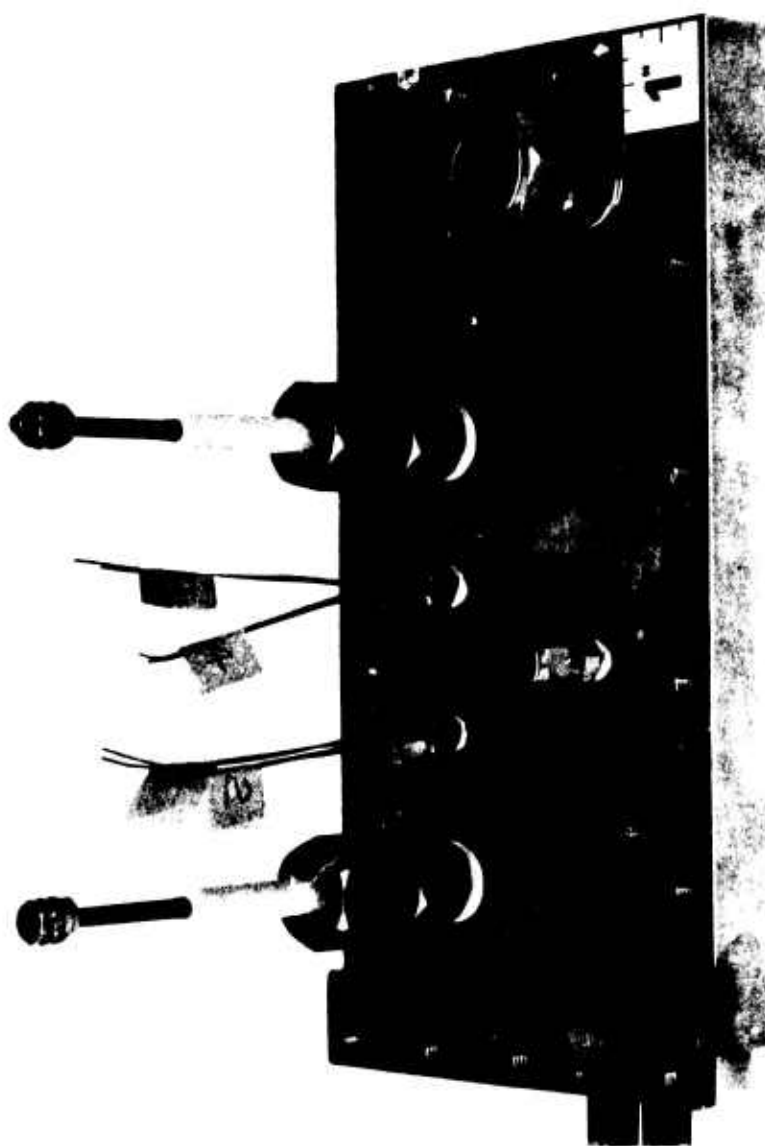
Figure   Bottom View of Straight Test Section

temperature had progressed several hundred degrees into the film boiling regime. Figure 23 is a simplified electrical schematic of the critical heat flux detector. In operation, power to coil A was interrupted with the reset switch prior to each run. When the recorder switch was closed on increasing temperature, coil A was energized and relay A was latched so that the power to coil B was interrupted, thus unlatching the power relay. The power relay remained open until the temperature returned to normal and the reset switch was pushed prior to beginning a new run.

In order to establish the temperature levels at which the transition to film boiling had been irretrievably established, several test sections were allowed to make a full transition to film boiling and "burnout." In fact, the transition to film boiling was so rapid for certain test conditions (high velocity and subcooling) that the thinnest strips used (.0032 inch) would occasionally be destroyed in spite of the presence of the critical heat flux detector.

3 6   Instrumentation

Flows in the boiling loop were measured with a turbine type magnetic pickup flow meter manufactured by Instruments Incorporated (type W2). The number of pulses corresponding to a unit volume flow of Freon 113 were determined by weight calibration. In this procedure, the amount of Freon passing through the flow meter in a certain time was weighed accurately while its pressure and temperature were measured. The output frequency was monitored on a Hewlett Packard Model 521-CR frequency counter and the flow meter pulse
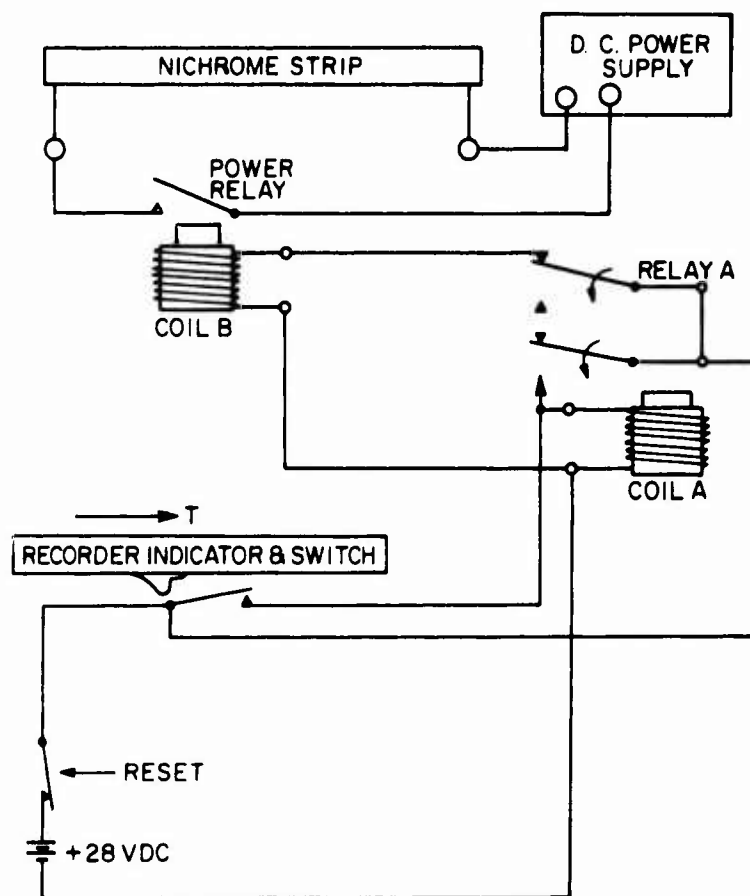
Figure 23 Electrical Schematic of the Critical Heat Flux Detector

factor could then be determined. This procedure was repeated over a range of conditions to establish the frequency versus volumetric flow performance of the system.

The frequency counter was periodically checked with a coherent decade frequency synthesizer, and selected points on the calibration curve were repeated at the conclusion of the experimental program to insure consistent flow meter performance.

Pressures were measured with 316 stainless steel Bourdon tube pressure gauges. A Heise Model CM gauge, with automatic temperature compensation, was used to measure test section pressures. The gauge has an accuracy of 0.1% full scale and was connected to a pressure tap located half-way along the centerline of the boiling channel. Ashcroft Duragauges (Model 1850) were used to measure pump and test section discharge pressures.

A Leeds and Northrup Speedomax H multipoint recorder was used to measure and record temperatures sensed by Chromel/Alumel thermocouples located at the test section inlet and outlet and on the boiling surface itslef. The Leeds and Northrup recorder was calibrated prior to every test series with a General Resistance Model TSC-46 precision thermocouple calibration source. Weksler Type 175-2T bimetal thermometers were used to measure and display the inlet and outlet temperature of the hotwell and heat exchanger coolant water.

The voltage drop across the heated test section was measured with a Hewlett Packard Model 3440A digital volt meter. An internal calibration voltage was used to check the meter operation prior to

every test series. Voltage pickups for the meter were located on the large copper electrodes immediately outside the Conax sealing glands.

A Model 2124 Simpson ammeter and shunt were used to measure current flow to the heated surface. Since an accurate calibration of this device was difficult to obtain, it was used only as a general indicator of the amount of power supplied to the test section.

Power for the test section was supplied by a Hyperion Model HY-TI-36-30 D.C. power supply. The voltage from this power supply could be varied from 0 to 36 volts while the maximum current drawn could be adjusted between 0 to 30 amps.

An overall view of the entire data system is given in Figure 14.

3.7 Test Procedure and Typical Results

Prior to every test series, the boiling loop was filled with a fresh charge of Freon 113. This was done to insure purity and guard against the accumulation of decomposed Freon resulting from the local high temperatures inherent in each brief transition to film boiling at the critical heat flux. To fill the loop, a vacuum pump was first connected to the loop vent and used to evacuate any trapped air present. When the loop held a vacuum with the pump shut off, it was assumed leak tight and the valve in the supply line was opened, allowing Freon to fill the loop. The circulation pump was started and the flow in the test section was observed for the presence of vapor pockets.

If no vapor pockets were observed, a test series was begun by shutting the fill valve and raising the loop to the desired

pressure with the helium bottle and regulator. The loop heater was energized and the variac was adjusted to raise the bulk fluid temperature to the desired value. When the desired bulk temperature was achieved, the variac was adjusted to just balance heat losses so that a steady bulk temperature resulted. The pressure and flow rate were then set at precisely the values desired and attention was shifted to the test section.

To begin a test, the power supply output voltage was set to zero, the critical heat flux detector was reset, and the power jacks were inserted into the desired test section sockets. While observing the heater strip temperature, the voltage on the test section was increased in gradual steps allowing ample time for steady state conditions to be reached at each setting. When the critical heat flux had been reached, the surface temperature would rapidly rise several hundred degrees and trip the power relay through the critical heat flux detector. Since the power relay made an audible "click" when it unlatched, it was possible for the operator to make note of, and record, the voltage necessary to produce the critical heat flux.

This procedure was then repeated several times at each test point. In tests other than the initial test, it was possible to proceed directly to a point 20% below the critical heat flux and thus reduce the time required for each test. During such tests, the heat addition through the test section could be balanced by heat removal at the heat exchanger as required.

Since the bulk fluid temperature was the most sluggish system variable, tests at a number of mean velocities were normally

performed for each surface before the bulk fluid temperature was readjusted.

During a typical test, the surface temperature would rise steadily as the voltage was increased until boiling began. At this point, the surface temperature would be slightly above saturation and vapor bubbles could be observed leaving the heated surface. As the critical heat flux was approached, the surface temperature would begin to oscillate and the surface would be obscured by a steady stream of bubbles. Further increased supply voltage would produce a transition to film boiling accompanied by a rapid surface temperature rise until the power was automatically interrupted. During this transition, the nichrome strip would very briefly glow orange. The orange glow would begin at a random location and spread rapidly over the entire surface. Figure 24 is representative of the records produced by the Leeds and Northrup temperature recorder during a typical test.

In the course of critical heat flux experiments, the nichrome strip and Teflon supports would slowly degrade. The strips would exhibit local irregularities that appeared to be the result of microscopic melting. These locations, thought to be the initial point of transition to film boiling, were randomly located on the heater surface, but were found with increasing frequency in the downstream direction. These brief high temperature excursions caused the Teflon supports to melt locally and therefore distort the surface geometry after a substantial number of runs. Periodic inspections of the surfaces were used to determine when replacements should be
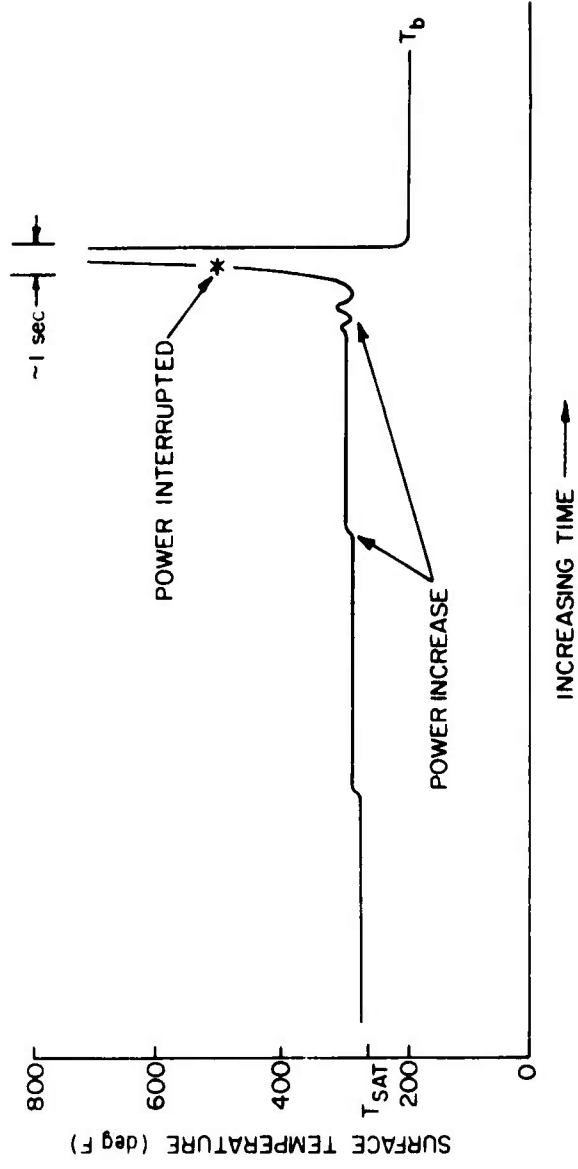
Figure 24   Simulated Temperature Record for a Typical Test

installed. Difficulties of this type were particularly evident on the concave surface.

The speed and intensity of the transition to film boiling was observed to increase with increasing velocity and subcooling. In addition, for constant velocity and subcooling, the speed and intensity of the film boiling transition were observed to diminish between the concave and straight, and the straight and convex surface geometries. In fact, for small velocities and subcoolings, the transition to film boiling on the convex surface exhibited a sort of "lazy" character, with surface temperatures slowly easing upward with an increasing rate of speed.

CHAPTER IV

EXPERIMENTAL AND THEORETICAL RESULTS

4.1   Curved Test Section Data

For all surfaces used in this study, tests were conducted at
five separate mean velocities and four different subcoolings. Each
mean velocity resulted in a unique radial acceleration of the fluid
flowing in the test section. Tophet A nichrome strip was used as the
boiling surface throughout the study. At every combination of radial
acceleration and subcooling, a series of tests were conducted to
determine the voltage necessary to produce the critical heat flux.
An average critical heat flux voltage was then found for each series
of tests and was used to compute the electrical energy supplied to
the surface. The variation of critical heat flux voltage in any
series was never more than 5% and was typically about 1%.

The electrical power supplied to the test section was computed
using the average critical heat flux voltage and the resistance of
the test section in use. Resistances were calculated from published
resistivity data (44) for Tophet A at the average temperature
indicated by the Leeds and Northrup recorder just prior to the
transition to film boiling. The electrical power found in this
manner was then adjusted for conduction losses through electrical
terminals, thermocouples, and the Teflon support blocks as outlined in
Appendix B. It was found that the majority of losses occured by
condution of heat through the electrodes and that the magnitude of
these losses was from 2% to 5% for the concave surface and from 3% to

9% for the convex surface, depending upon the radial acceleration and subcooling of the test.

The distinguishing feature of flow boiling on curved surfaces has been hypothesized to be the presence of the radial acceleration which tends to preferentially wet the concave surface with subcooled liquid and hold vapor near the convex surface. For this reason, the critical heat flux data have been tabulated according to the radial fluid acceleration based on the mean fluid velocity and mean test section radius. This acceleration has been non-dimensionalized by dividing the radial acceleration by the standard acceleration of gravity. Table 1 and Table 2 contain the resulting critical heat flux data for concave and convex surfaces.

Reference to the data indicates that the critical heat flux increases with radial acceleration and subcooling for both concave and convex surfaces. For equal radial accelerations and subcoolings, the concave surface is also observed to produce substantially higher critical heat flux values, as had been hypothesized.

The data of Tables 1 and 2 do not reveal, however, the qualitative differences between the transition to film boiling on a concave surface and a convex surface. Concave surfaces normally gave very little warning of an impending transition to film boiling. Surface temperatures would remain comparatively steady as the power to the surface was increased to the critical heat flux where the transition to film boiling would occur with tremendous rapidity. Convex surfaces, alternately, would undergo temperature oscillations (as much as 20°F) near the critical heat flux, giving warning that

Table 1

Experimentally Determined Critical Heat Flux Values
for the Concave Boiling Surface at 130 psia

Subcooling °F	Non-Dimensional Radial Acceleration $V_m^2/R_{\ell}g$	Heater Strip Dimensions inches	Number of Tests	Critical Heat Flux x 10^{-5} BTU/hr-ft^2
110	1.0	4.58x3/32x0.0052	6	3.40
110	5.0	4.58x3/32x0.0052	6	4.09
110	9.3	4.58x3/32x0.0052	6	4.76
110	14.1	4.58x3/32x0.0052	6	5.70
110	18.5	4.58x3/32x0.0052	5	6.13
90	1.0	4.58x3/32x0.0052	3	3.48
90	5.0	4.58x3/32x0.0052	3	4.06
90	9.3	4.58x3/32x0.0052	3	4.63
90	14.1	4.58x3/32x0.0052	3	5.48
90	18.5	4.58x3/32x0.0052	3	6.18
70	1.0	4.58x3/32x0.0052	3	3.41
70	5.0	4.58x3/32x0.0052	3	3.84
70	9.3	4.58x3/32x0.0052	3	4.50
70	14.1	4.58x3/32x0.0052	3	5.26
70	18.5	4.58x3/32x0.0052	3	5.72
50	1.0	4.58x3/32x0.0052	3	3.03
50	5.0	4.58x3/32x0.0052	2	3.52
50	9.3	4.58x3/32x0.0052	2	4.24
50	14.1	4.58x3/32x0.0052	3	4.93
50	18.5	4.58x3/32x0.0052	2	5.53
90	1.0	4.58x1/8x0.0032	3	3.04
90	5.0	4.58x1/8x0.0032	3	3.67
90	9.3	4.58x1/8x0.0032	3	4.42
90	14.1	4.58x1/8x0.0032	3	4.94
90	18.5	4.58x1/8x0.0032	3	5.15

Table 2

Experimentally Determined Critical Heat Flux Values
for the Convex Boiling Surface at 130 psia

Subcooling °F	Non-Dimensional Radial Acceleration $V_m^2/R_{\ell}g$	Heater Strip Dimensions inches	Number of Tests	Critical Heat Flux x 10^{-5} BTU/hr-ft²
110	1.0	3.97x3/32x0.0052	3	2.21
110	5.0	3.97x3/32x0.0052	2	2.52
110	9.3	3.97x3/32x0.0052	3	2.85
110	14.1	3.97x3/32x0.0052	3	3.20
110	18.5	3.97x3/32x0.0052	3	3.30
90	1.0	3.97x3/32x0.0052	2	2.29
90	5.0	3.97x3/32x0.0052	3	2.48
90	9.3	3.97x3/32x0.0052	2	2.67
90	14.1	3.97x3/32x0.0052	2	3.00
90	18.5	3.97x3/32x0.0052	3	3.33
70	1.0	3.97x3/32x0.0052	3	2.25
70	5.0	3.97x3/32x0.0052	3	2.40
70	9.3	3.97x3/32x0.0052	5	2.52
70	14.1	3.97x3/32x0.0052	4	2.83
70	18.5	3.97x3/32x0.0052	3	3.06
50	1.0	3.97x3/32x0.0052	3	2.00
50	5.0	3.97x3/32x0.0052	3	2.29
50	9.3	3.97x3/32x0.0052	5	2.42
50	14.1	3.97x3/32x0.0052	4	2.72
50	18.5	3.97x3/32x0.0052	4	3.09
110	1.0	3.97x1/8x0.0032	3	2.11
110	5.0	3.97x1/8x0.0032	3	2.32
110	9.3	3.97x1/8x0.0032	3	2.89
110	14.1	3.97x1/8x0.0032	3	3.30
110	18.5	3.97x1/8x0.0032	3	3.70
90	1.0	3.97x1/8x0.0032	3	2.10
90	5.0	3.97x1/8x0.0032	3	2.22
90	9.3	3.97x1/8x0.0032	3	2.65
90	14.1	3.97x1/8x0.0032	3	2.90
90	18.5	3.97x1/8x0.0032	3	3.18
90				

Table 2 (Continued)

Subcooling °F	Non-Dimensional Radial Acceleration $V_m^2/R_i g$	Heater Strip Dimensions inches	Number of Tests	Critical Heat Flux x 10^{-5} BTU/hr-ft^2
70	1.0	3.97x1/8x0.0032	3	1.90
70	5.0	3.97x1/8x0.0032	3	2.16
70	9.3	3.97x1/8x0.0032	3	2.48
70	14.1	3.97x1/8x0.0032	3	2.82
70	18.5	3.97x1/8x0.0032	3	2.94
50	1.0	3.97x1/8x0.0032	3	1.74
50	5.0	3.97x1/8x0.0032	3	1.88
50	9.3	3.97x1/8x0.0032	3	2.16
50	14.1	3.97x1/8x0.0032	3	2.42
50	18.5	3.97x1/8x0.0032	3	2.57

transition was imminent. The rate of surface temperature increase at the critical heat flux was less for the convex surface surface than for the concave surface.

Ratios of the critical heat flux between the concave and convex surfaces have been computed from the combined data of Tables 1 and 2. These ratios appear in Table 3 and increase with increasing radial acceleration and decreasing subcooling. The increasing heat flux ratios are thought to be the result of two related phenomena. First, the radial acceleration results in the motion of more dense subcooled liquid away from the convex surface and toward the concave surface; and second, a radial pressure gradient is created normal to the heated surfaces. This pressure gradient tends to move vapor away from the concave surface and toward the convex surface.

In the curved test section increased radial accelerations are produced by increasing the mean fluid velocity. Although the increasing mean velocity tends to raise the critical heat flux for both surfaces, the accompanying increases in radial acceleration enhance the concave surface performance and detract from the convex surface performance. The probable result of increased radial acceleration can therefore be argued to be increased critical heat flux ratios between concave and convex surfaces, which is what has been observed.

4.2   Straight Test Section Data

Straight test section critical heat flux data has been collected in this study for two reasons: (1) to compare the experimental techniques and results of the present work with other

Table 3

Experimental Results for Critical Heat Flux Ratios
Between Concave and Convex Surfaces

Subcooling °F	Non-Dimensional Radial Acceleration $V_m^2/R_i g$	Concave CHF x 10^{-5} BTU/hr-ft^2	Convex CHF x 10^{-5} BTU/hr-ft^2	Ratio $\dfrac{Concave}{Convex}$
110	1.0	3.40	2.16	1.57
110	5.0	4.09	2.42	1.69
110	9.3	4.76	2.87	1.66
110	14.1	5.70	3.25	1.75
110	18.5	6.13	3.50	1.75
90	1.0	3.48	2.20	1.58
90	5.0	4.06	2.35	1.73
90	9.3	4.63	2.66	1.74
90	14.1	5.48	2.95	1.86
90	18.5	6.18	3.26	1.90
70	1.0	3.41	2.08	1.64
70	5.0	3.84	2.28	1.68
70	9.3	4.50	2.50	1.80
70	14.1	5.26	2.83	1.86
70	18.5	5.72	3.00	1.91
50	1.0	3.03	1.87	1.62
50	5.0	3.52	2.09	1.68
50	9.3	4.24	2.29	1.85
50	14.1	4.93	2.57	1.92
50	18.5	5.53	2.83	1.95

work (no data for concave and convex surfaces are known to exist);
and (2) to obtain straight surface critical heat flux magnitudes for
the conditions investigated in curved flow, so the relative performance
of concave, convex and straight surfaces can be determined. Since
radial accelerations do not exist in straight flows, critical heat
flux data have been obtained for the straight test section at every
mean velocity and subcooling used for the curved test section. The
data have been collected and reduced according to the same procedures
discussed in Section 4.1 and are listed in Table 4. Conduction losses
ranging between 2% and 6% were computed for the straight test section.
The well established pattern of increasing critical heat fluxes for
increasing velocities and subcoolings is corroborated by this data.
If the critical heat flux data for straight surfaces is compared to
that for curved surfaces, Table 5, it is seen that for any given
velocity and subcooling, the magnitude of the critical heat flux for
a straight surface lies between that for the concave and convex
surface.

Critical heat flux ratios between straight and convex surfaces,
at the same velocity and subcooling, have been computed and the results
are listed in Table 6. The straight surface is show.. to accomodate
higher critical heat fluxes than the convex surface at every condition.
Velocity and subcooling have no dramatic effect on the ratio although
it appears to diminish slightly with subcooling.

4.3   Experimental-Theoretical Comparisons

Equation (2.64), which was previously derived, expresses the
ratio between the critical heat flux magnitude on a concave surface and

Table 4

Experimentally Determined Critical Heat Flux Values
For the Straight Boiling Surface at 130 psia

Subcooling °F	Mean Velocity in/sec	$V_m^2/R_{\ell}g$	Heater Strip Dimensions inches	Number of Tests	Critical Heat Flux x 10^{-5} BTU/hr-ft^2
110	37	(1.0)	4.75x3/32x0.0052	3	3.04
110	82	(5.0)	4.75x3/32x0.0052	3	3.50
110	112	(9.3)	4.75x3/32x0.0052	3	4.15
110	138	(14.1)	4.75x3/32x0.0052	3	4.51
110	158	(18.1)	4.75x3/32x0.0052	3	4.52
90	37	(1.0)	4.75x3/32x0.0052	3	2.48
90	82	(5.0)	4.75x3/32x0.0052	3	3.28
90	112	(9.3)	4.75x3/32x0.0052	3	3.57
90	138	(14.0)	4.75x3/32x0.0052	3	4.03
90	158	(18.5)	4.75x3/32x0.0052	3	4.16
70	37	(1.0)	4.75x3/32x0.0052	3	2.24
70	82	(5.0)	4.75x3/32x0.0052	3	3.04
70	112	(9.3)	4.75x3/32x0.0052	3	3.43
70	138	(14.1)	4.75x3/32x0.0052	3	3.84
70	158	(18.5)	4.75x3/32x0.0052	3	3.94
50	37	(1.0)	4.75x3/32x0.0052	3	2.06
50	82	(5.0)	4/75x3/32x0.0052	3	2.69
50	112	(9.3)	4.75x3/32x0.0052	3	2.97
50	138	(14.1)	4.75x3/32x0.0052	3	3.27
50	158	(18.5)	4.75x3/32x0.0052	3	3.44
90	37	(1.0)	4.75x3/32x0.0052	3	2.45
90	82	(5.0)	4.75x3/32x0.0052	3	3.31
90	112	(9.3)	4.75x3/32x0.0052	3	3.76
90	138	(14.1)	4.75x3/32x0.0052	3	3.70
90	158	(18.5)	4.75x3/32x0.0052	3	3.72

Table 5

Summary of Critical Heat Flux Data (BTU/hr-ft^2) for Concave (C),
Straight (S), and Convex (V) Surfaces at 130 psia

Mean Velocity in/sec	Surface	50°F Subcooling	70°F Subcooling	90°F Subcooling	110°F Subcooling
37	C	3.03×10^5	3.41×10^5	3.48×10^5	3.40×10^5
37	S	2.06×10^5	2.24×10^5	2.48×10^5	3.04×10^5
37	V	1.87×10^5	2.08×10^5	2.20×10^5	2.16×10^5
82	C	3.52×10^5	3.84×10^5	4.06×10^5	4.09×10^5
82	S	2.69×10^5	3.04×10^5	3.28×10^5	3.50×10^5
82	V	2.09×10^5	2.28×10^5	2.35×10^5	2.42×10^5
112	C	4.24×10^5	4.50×10^5	4.63×10^5	4.76×10^5
112	S	2.97×10^5	3.43×10^5	3.57×10^5	4.15×10^5
112	V	2.29×10^5	2.50×10^5	2.66×10^5	2.87×10^5
138	C	4.93×10^5	5.26×10^5	5.48×10^5	5.70×10^5
138	S	3.27×10^5	3.84×10^5	4.03×10^5	4.51×10^5
138	V	2.57×10^5	2.83×10^5	2.95×10^5	3.25×10^5
158	C	5.53×10^5	5.72×10^5	6.18×10^5	6.13×10^5
158	S	3.44×10^5	3.94×10^5	4.16×10^5	4.52×10^5
158	V	2.83×10^5	3.00×10^5	3.26×10^5	3.50×10^5

Table 6

Experimentally Determined Critical Heat Flux Ratios
Between Straight and Convex Surfaces

Subcooling °F	Mean Velocity in/sec	Straight CHF x 10^{-5} BTU/hr-ft^2	Convex CHF x 10^{-5} BTU/hr-ft^2	Ratio $\dfrac{\text{Straight}}{\text{Convex}}$
110	37	3.04	2.16	1.41
110	82	3.50	2.42	1.45
110	112	4.15	2.87	1.46
110	138	4.51	3.25	1.39
110	158	4.52	3.50	1.29
90	37	2.48	2.20	1.13
90	82	3.28	2.35	1.40
90	112	3.57	2.66	1.34
90	138	4.03	2.95	1.37
90	158	4.16	3.26	1.28
70	37	2.24	2.08	1.08
70	82	3.04	2.28	1.33
70	112	3.43	2.50	1.37
70	138	3.84	2.83	1.36
70	158	3.94	3.00	1.31
50	37	2.06	1.87	1.10
50	82	2.69	2.09	1.29
50	112	2.97	2.29	1.30
50	138	3.27	2.57	1.27
50	158	3.44	2.83	1.22

on a convex surface. Equation (2.64) results directly from the analysis
of the idealized vapor bubble cycle and involves no empirical constants
or input. In Figures 25 through 28 the analytical and experimental
results for critical heat flux ratios between concave and convex
surfaces are presented. The solid line represents Equation (2.64)
while the circled points represent the average value of all critical
heat flux tests (Table 3) at that particular radial acceleration.
Both the experimental and analytical results for the critical heat
flux ratio appear to approach a constant value as the radial
acceleration is increased.

Equation (2.65) expresses the ratio of the critical heat flux
magnitude between a straight and convex surface. Equation (2.65)
also results from analysis of the idealized vapor bubble cycpe and
involves no empirical inputs. It has been plotted as the solid line
in Figures 29 through 32 which also contain the experimental data of
Table 6. The experimental data is indicated by circled points
representing the ratio of the average critical heat magnitudes for
all tests at that mean velocity. The mean velocity has been used in
plotting the abscissa since the concept of radial acceleration is not
appropriate for a ratio involving straight flow.

The standard deviation of the experimental data from Equations
(2.64) and (2.65) has been computed as outlined in Appendix C. The
results of this analysis are presented in Table 7.

Equations (2.60), (2.61) and (2.62) have been developed from
an analysis of the idealized vapor bubble cycle and relate the critical
heat flux to various fluid and channel properties for straight and
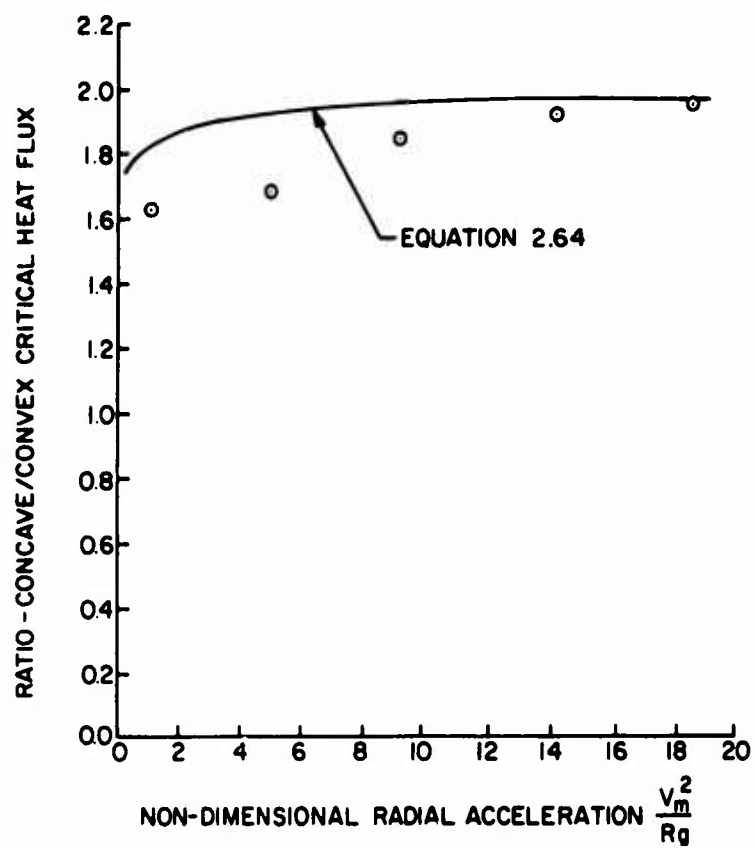curved flows. Each equation contains the area of influence

Figure 25 Analytical and Experimental Critical Heat Flux Ratios
Between Concave and Convex Surfaces Operating at 130
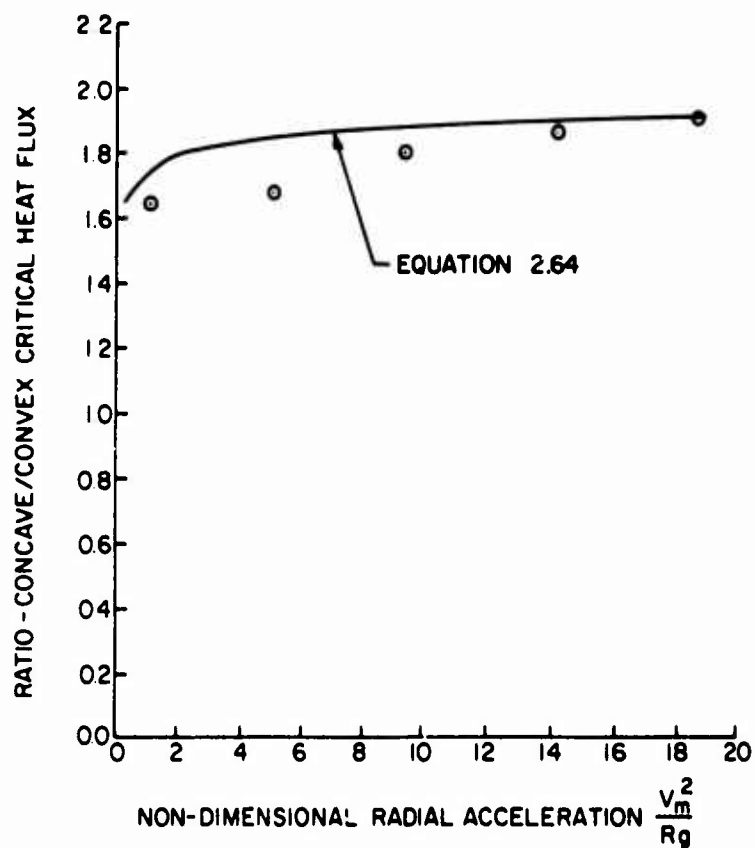psia and 50°F Subcooling

88

Figure 26   Analytical and Experimental Critical Heat Flux Ratios
Between Concave and Convex Surfaces Operating at 130
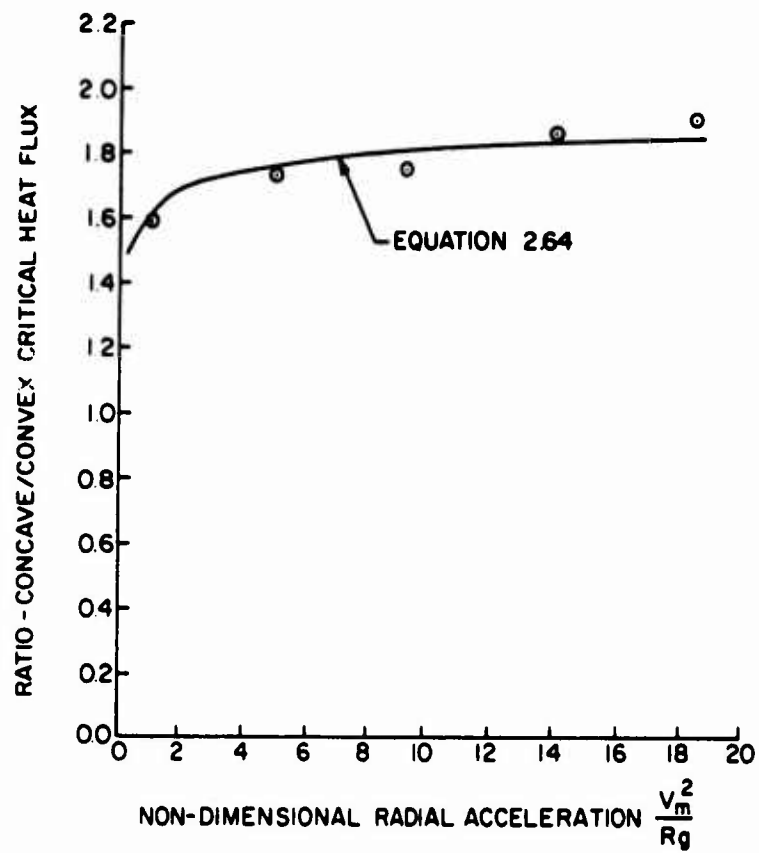psia and 70°F Subcooling

Figure 27   Analytical and Experimental Critical Heat Flux Ratios
Between Concave and Convex Surfaces Operating at 130
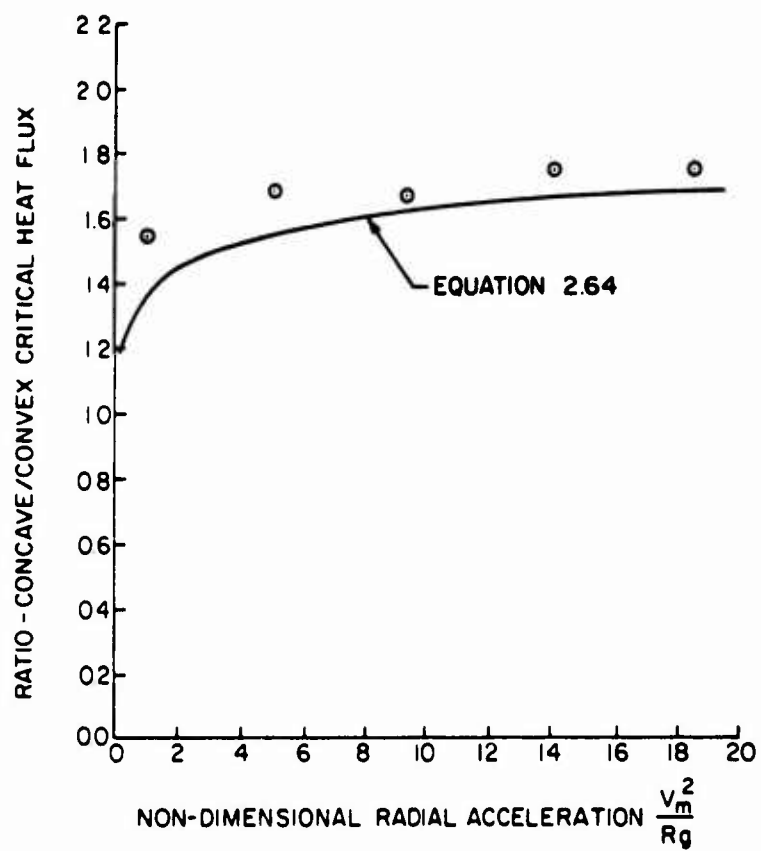psia and 90°F Subcooling

Figure 28   Analytical and Experimental Critical Heat Flux Ratios
Between Concave and Convex Surfaces Operating at 130
psia and 110°F Subcooling
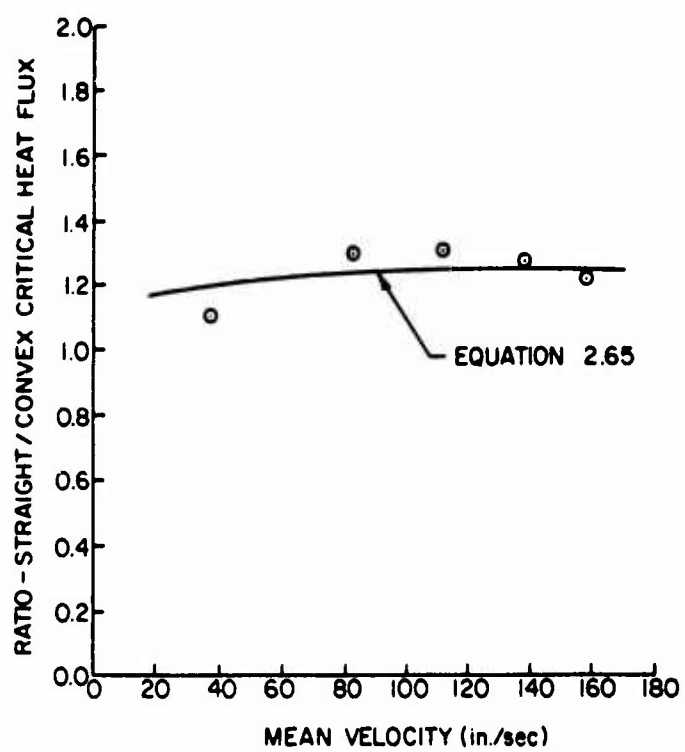
Figure 29   Analytical and Experimental Critical Heat Flux Ratios
            Between Straight and Convex Surfaces Operating at 130
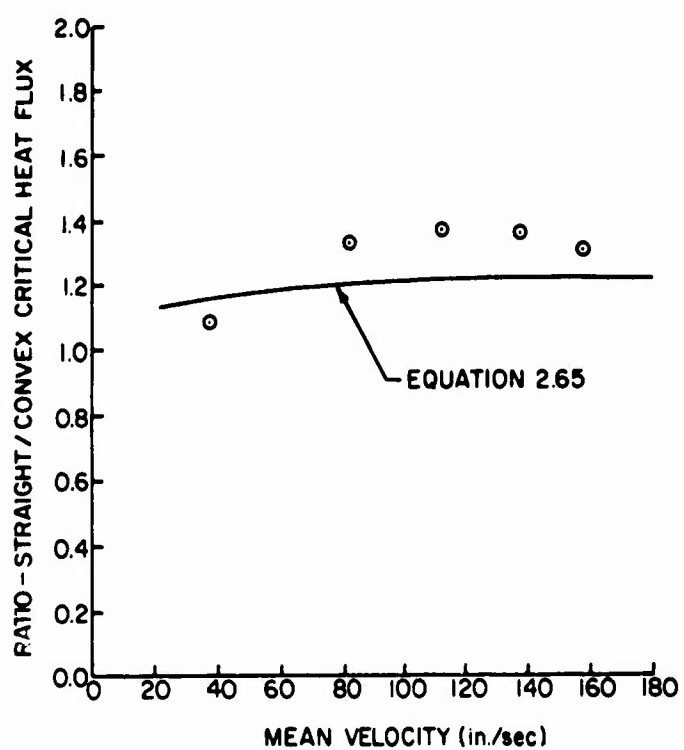   psia and 50°F Subcooling

Figure 30 Analytical and Experimental Critical Heat Flux Ratios
Between Straight and Convex Surfaces Operating at 130
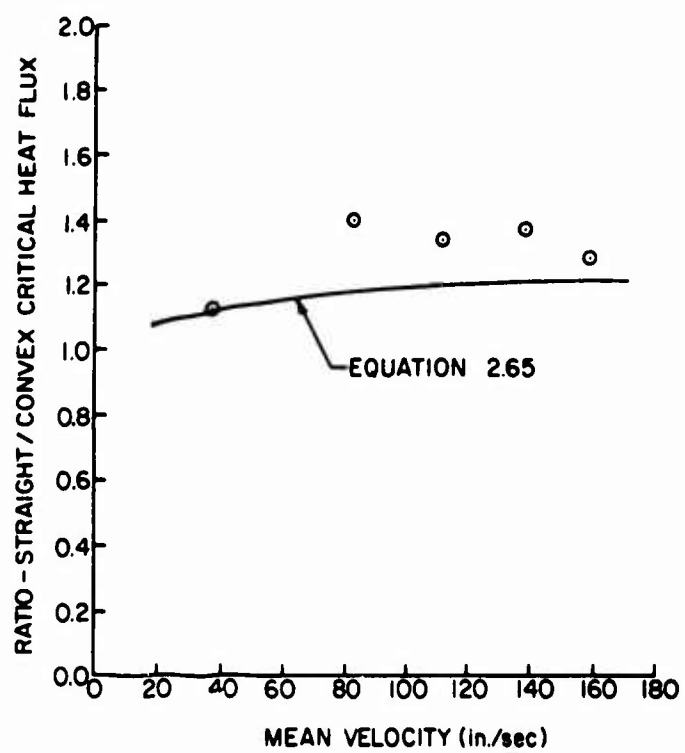psia and 70°F Subcooling

Figure 31 Analytical and Experimental Critical Heat Flux Ratios
Between Straight and Convex Surfaces Operating at 130
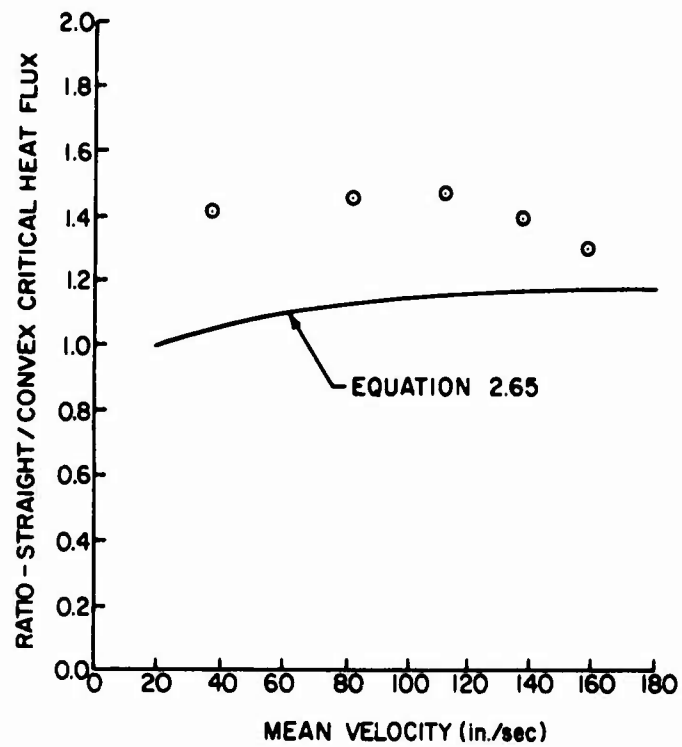psia and 90°F Subcooling

Figure 32 Analytical and Experimental Critical Heat Flux Ratios
Between Straight and Convex Surfaces Operating at 130
psia and 110°F Subcooling

Table 7

Standard Deviation of Experimental Critical Heat Flux Ratios
Compared to Analytical Critical Heat Flux Ratios

Ratio Configuration	Subcooling	σ
Concave/Convex	110	0.14
Concave/Convex	90	0.05
Concave/Convex	70	0.11
Concave/Convex	50	0.16
Straight/Convex	110	0.32
Straight/Convex	90	0.16
Straight/Convex	70	0.14
Straight/Convex	50	0.08

proportionality factor, K, which has been discussed in Section 2.6.
The proportionality factor K, which relates the heater surface area
influenced by a growing bubble to that bubble's departure diameter,
has been assumed to be a function of the mean velocity, subcooling and
the fluid-surface combination.

$$K = f(V_m, T_s) \tag{4.1}$$

This assumption was suggested by the acknowledged influence of mean
velocity, subcooling and fluid-surface combination on critical heat
flux magnitudes.

The proportionality factor, K, was found for each test condition
by solving the appropriate equation ([2.60], [2.61], [2.62]) for the
value of K using the experimentally determined value of the critical
heat flux and fluid properties as input data. The resulting empirical
values of K are reported in Table 8. A simple relationship between
the proportionality factor, K, the mean velocity and the subcooling
was desired. After several trials it was determined that a relationship
of the form,

$$K \propto \frac{\sqrt{V_m}}{T_s} , \tag{4.2}$$

came closest to meeting the objectives of simplicity and explicitness
in the final solution. If the empirical fluid-surface constant
β_{fs} is introduced, Equation (4.2) becomes:

$$K = \beta_{fs} \frac{\sqrt{V_m}}{T_s} . \tag{4.3}$$

Equation (4.3) and the data of Table 8 was then used to compute values
of the fluid-surface constant, β_{fs}, for each test condition, Table 9.

Table 8

Experimentally Determined Values of the Area
of Influence Proportionality Factor, K

Subcooling °F	Mean Velocity in/sec	Concave Surface	Convex Surface	Straight Surface
110	37	0.33	0.38	0.28
110	82	0.58	0.64	0.49
110	112	0.68	0.70	0.55
110	138	0.69	0.73	0.60
110	158	0.72	0.76	0.68
90	37	0.52	0.51	0.51
90	82	0.91	0.90	0.76
90	112	1.07	1.04	0.92
90	138	1.10	1.11	0.98
90	158	1.10	1.13	1.07
70	37	0.67	0.63	0.69
70	82	1.22	1.11	1.01
70	112	1.39	1.33	1.18
70	138	1.44	1.40	1.26
70	158	1.50	1.49	1.39
50	37	0.89	0.79	0.86
50	82	1.57	1.38	1.31
50	112	1.74	1.66	1.57
50	138	1.80	1.77	1.71
50	158	1.82	1.81	1.83

Table 9

Experimentally Determined Values of the Fluid Surface Constant

$$\beta_{fs}\left[°F\sqrt{\frac{sec}{ft}}\right]$$ for Freon 113 and Tophet A Nichrome

Subcooling °F	Mean Velocity in/sec	Concave Surface	Convex Surface	Straight Surface
110	37	5.95	6.88	5.14
110	82	7.12	7.77	5.99
110	112	7.03	7.23	5.70
110	138	6.42	6.81	5.66
110	158	6.33	6.60	5.95
90	37	7.63	7.47	7.45
90	82	9.12	8.98	7.56
90	112	9.12	8.82	7.83
90	138	8.40	8.53	7.50
90	158	7.88	8.10	7.65
70	37	7.72	7.25	7.89
70	82	9.48	8.62	7.80
70	112	9.22	8.79	7.79
70	138	8.58	8.36	7.52
70	158	8.34	8.29	7.72
50	37	7.31	6.49	7.07
50	82	8.68	7.65	7.27
50	112	8.20	7.84	7.42
50	138	7.67	7.54	7.29
50	158	7.23	7.20	7.29

The data of Table 9 were used to compute a mean value of β_{fs} for the combination of Freon 113 and Tophet A. Since experiments at 110°F subcooling were troublesome throughout this investigation, only the data for 50°F, 70°F and 90°F subcoolings were used in the computation of the mean value of β_{fs}. This procedure resulted in an optimized correlation of the 50°F, 70°F and 90°F subcooling data and a less ideal correlation of the 110°F data; and was justified by virtue of the scattered data, undesired heater strip destruction, and Teflon support degradation evident in many experiments conducted with 110°F subcooling. A mean value of β_{fs} = 7.94 was computed and used throughout this study for the correlation of <u>all</u> critical heat flux data reported. The standard deviation of the data of Table 9 from a mean of 7.94 was 0.67, or 8% of the mean.

Although an investigation of the critical heat flux mechanism itself was not the primary objective of this study, it is interesting to note that the substitution of Equation (4.3) and an appropriate diameter expression (Equation [2.16], [2.17] or [2.19] into Equation (2.58) indicates that the packing density of active sites at the critical heat flux is increased by increasing velocity and subcooling through a reduction of the area of influence. Such behavior is at least potentially capable of explaining the influence of velocity and subcooling on the critical heat flux.

The empirically determined value of β_{fs} was used in conjunction with Equations (2.61) and (2.62) to determine the analytical values of the critical heat flux at a series of radial accelerations. The results for concave and convex surfaces are shown in Figures 33 through 36, where the solid lines represent Equations (2.61) and (2.62).
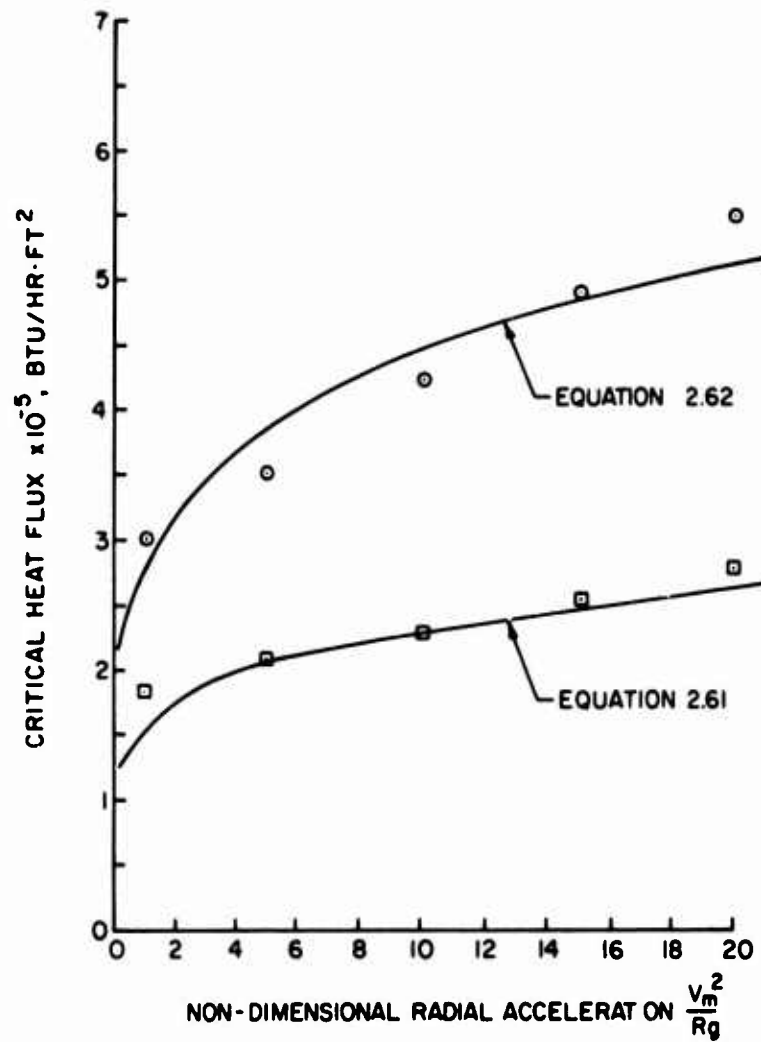
Figure 33 Analytical and Experimental Critical Heat Flux Values for
Concave and Convex Surfaces Operating at 130 psia and
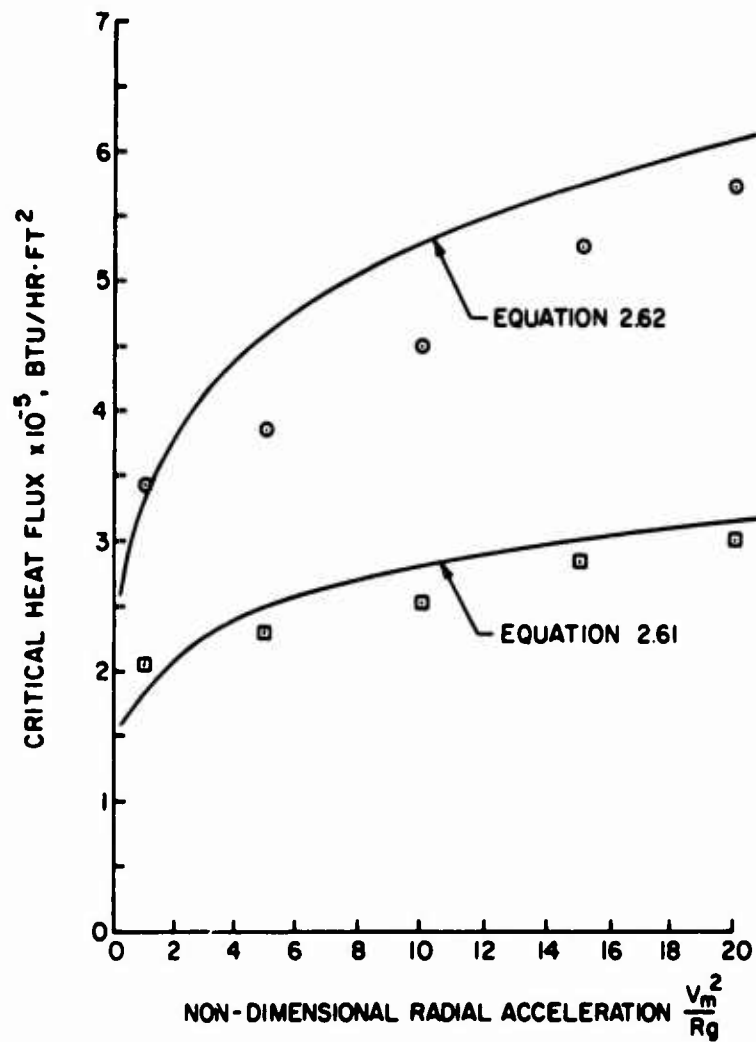50°F Subcooling

Figure 34   Analytical and Experimental Critical Heat Flux Values for
Concave and Convex Surfaces Operating at 130 psia and
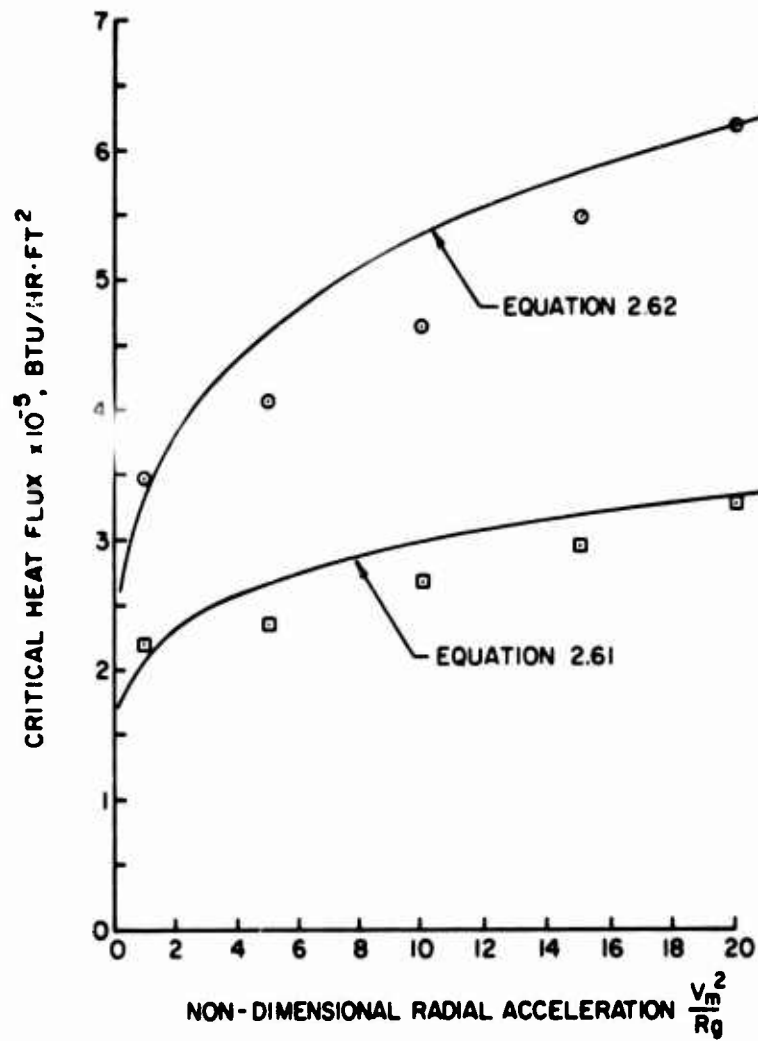70°F Subcooling

Figure 35 Analytical and Experimental Critical Heat Flux Values for
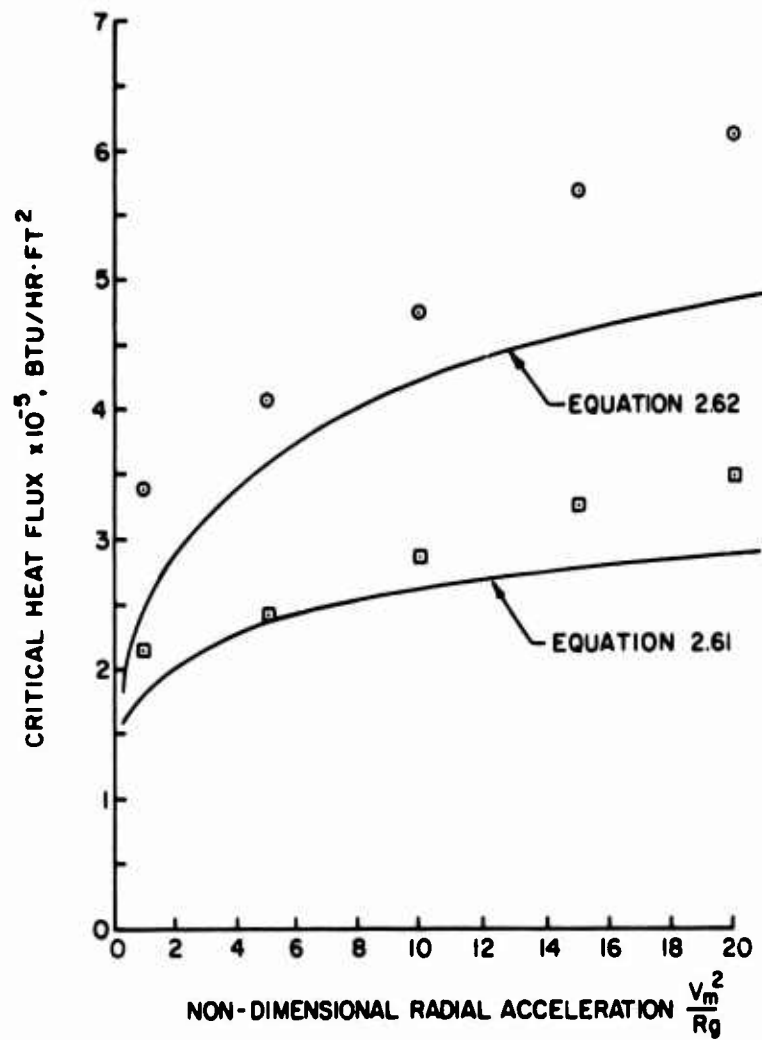Concave and Convex Surfaces Operating at 130 psia and
90°F Subcooling

Figure 36   Analytical and Experimental Critical Heat Flux Values for
Concave and Convex Surfaces Operating at 130 psia and
110°F Subcooling

Experimental data for the concave surface (circles) and convex
surface (squares) have been included. The source of the data was
Tables 1 and 2 of this study. In accordance with the procedures of
Appendix C, the standard deviations of this experimental data about
the analytical curves have been computed and are listed in Table 10.

The results for the straight surface are shown in the same
format in Figures 37 through 40. Mean velocity has been used to
plot the curves since radial acceleration is not meaningful in
straight flow.

A superposition of the straight and curved flow critical heat
fluxes, determined by analysis and experiment, is shown as a function
of mean velocity in Figure 41. Figure 41 serves as an illustration
of the relative magnitudes of the critical heat flux among the surfaces
and is typical of all subcoolings investigated.

The two most unique aspects of the results just discussed are
repeated for emphasis First, the analytical expressions for critical
heat flux ratios contain no empirical constants while the analytical
expressions for critical heat flux magnitudes contain only one
empirical constant; and second, the analytical expressions developed
in this study have as a basis a greatly simplified physical model that
has been solved directly to obtain critical heat flux magnitudes
that compare favorably with experimental observations.

4.4   Comparisons with Other Work

The compatibility of the analytical and experimental results of
this study has been established. It was desired, however, to relate
this work with other work of a similar nature. Since no other

Table 10

Standard Deviation and Percent Variation from the Median Heat
Flux for Experimental Results Compared to Analytical Results

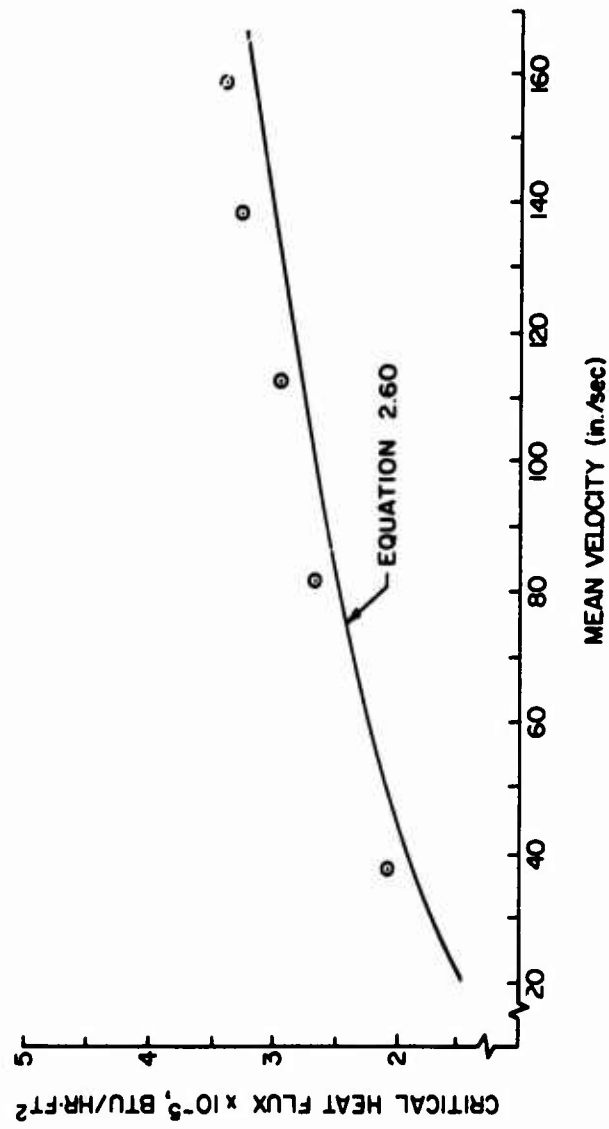| Surface Geometry	Subcooling °F	Number of Tests	$\sigma x\ 10^{-5}$ BTU/hr-ft^2	Percent of Median Heat Flux
Concave	110	28	.91	25
Concave	90	15	.40	8
Concave	70	15	.50	11
Concave	50	12	.27	7
Convex	110	29	.42	18
Convex	90	27	.20	7
Convex	70	33	.18	7
Convex	50	34	.19	9
Straight	110	15	1.16	44
Straight	90	15	.19	6
Straight	70	15	.12	4
Straight	50	15	.23	9

Figure 37 Analytical and Experimental Critical Heat Flux Values for
a Straight Surface Operating at 130 psia and 50°F Subcooling
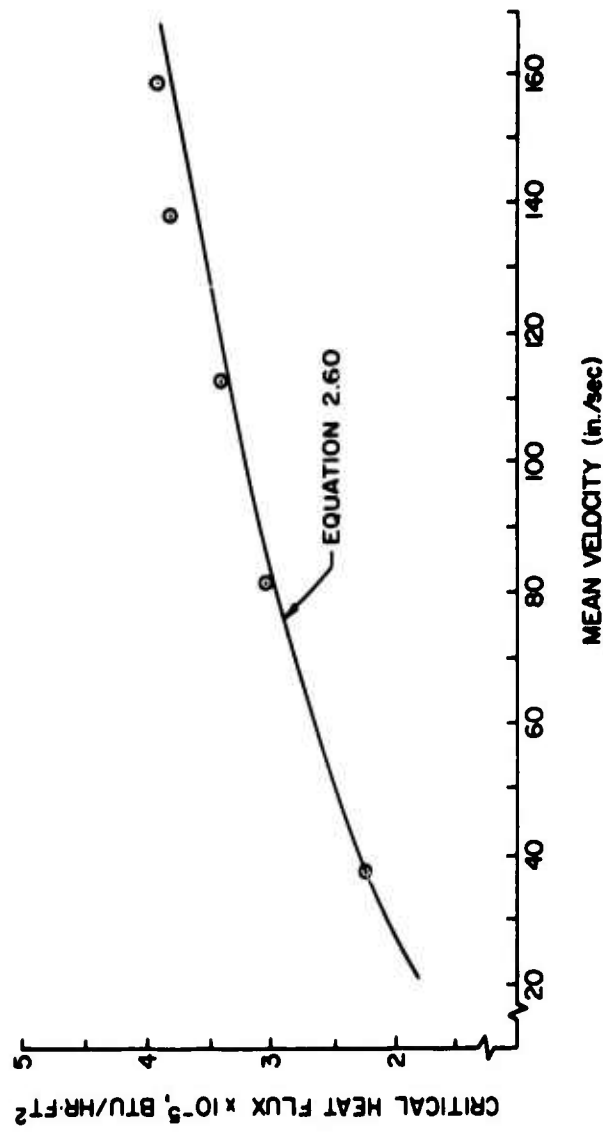
Figure 38   Analytical and Experimental Critical Heat Flux Values for a Straight Surface Operating at 130 psia and 70°F Subcooling
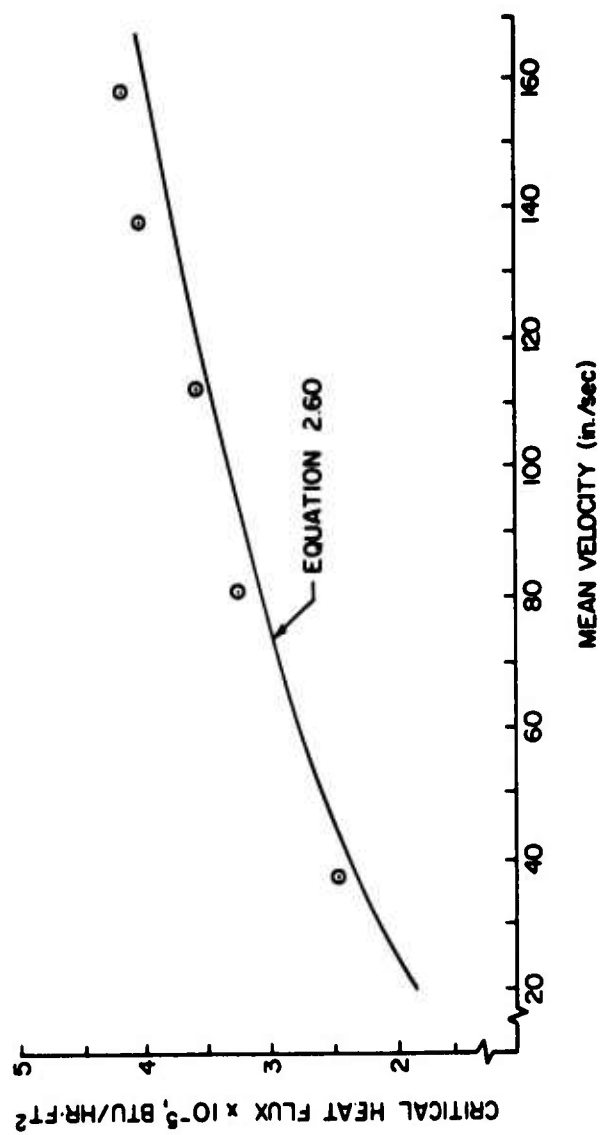
Figure 39 Analytical and Experimental Critical Heat Flux Values for a
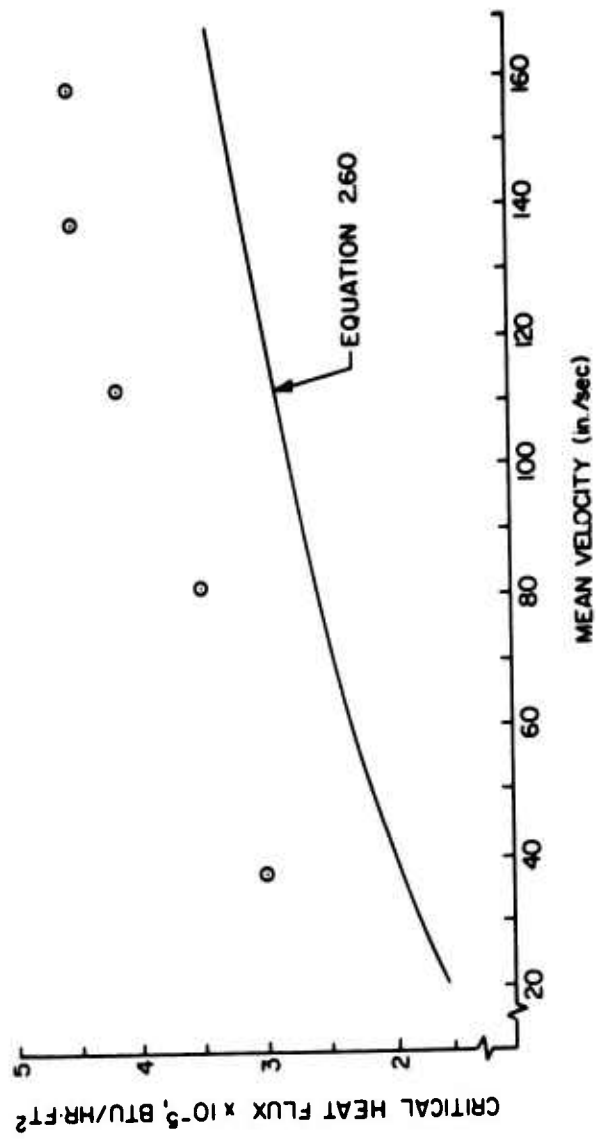Straight Surface Operating at 130 psia and 90°F Subcooling

Figure 40 Analytical and Experimental Critical Heat Flux Values for a Straight Surface Operating at 130 psia and 110°F Subcooling
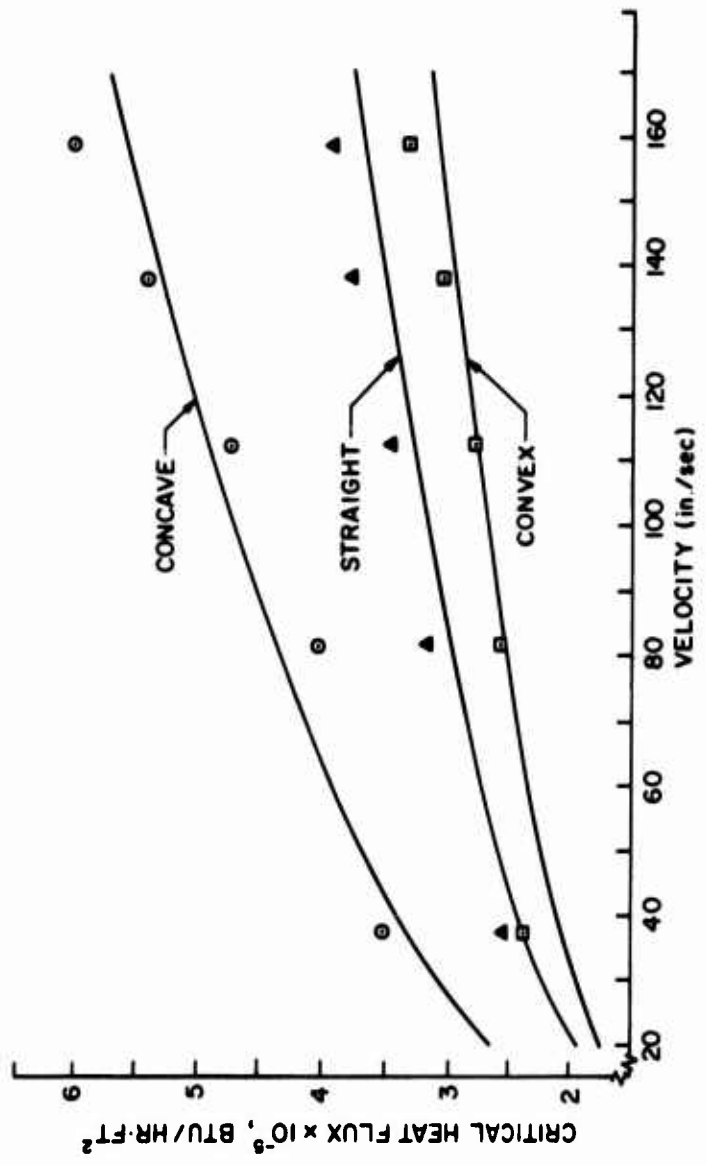
Figure 41   Analytical and Experimental Critical Heat Flux Values at
130 psia and 50°F Subcooling

experimental or analytical results for the critical heat flux on

concave and convex surfaces are known to exist, the experimental

results of several other studies have been compared to the analytical

results of this study for the case of straight flow (Equation [2.60]).

Only experiments using Freon 113 and stainless steel heater surfaces

are considered since the value of β_{fs} found in the present study

cannot reasonably be extended to more diverse fluid surface

combinations.

Mattson (11) has performed critical heat flux experiments

in a straight test section very similar to the one used in this study.

A nichrome heater strip along the bottom of the channel was used as the

boiling surface. Critical heat flux magnitudes at several pressures,

mass velocities and subcoolings are reported in Table C.1 of the

Mattson (11) work. No analytical expression for the critical heat

flux was developed by Mattson (11); instead, the boundary layer

separation model of Dean (45) was used. The model of Dean (45),

based on the vapor injection mechanism, contains three empirical

constants and correlated the data of Mattson (11) to within $\pm 30\%$

Figure 42 shows the data of Mattson (11) compared with Equation (2.60)

evaluated at 150 psia).

Dean (45) performed critical heat flux experiments with and

without vapor injection through the heated surface in an effort to

determine the appropriateness of the boundary layer separation

mechanism as an explanation of the burnout phenomenon. The work was

performed in an annular flow test section with the inner tube

undergoing heating over its entire length and circumference. Such

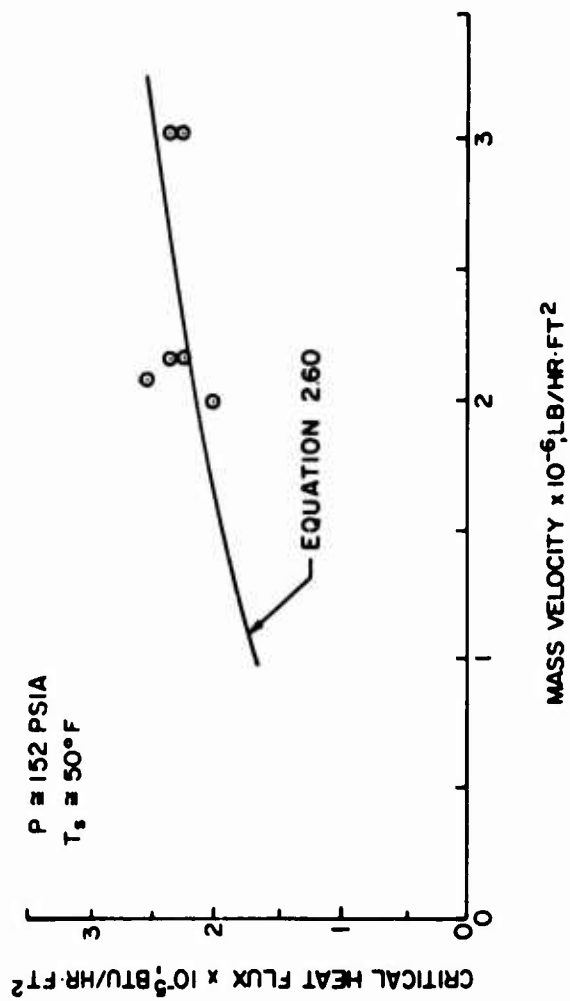practices, as previously discussed, tend to reduce the observed

Figure 42   Comparison of the Critical Heat Flux Predicted by Equation
(2.60) and the Work of Mattson

critical heat flux owing to the increased bulk temperatures and decreased pressures in the flow direction. Equation (2.60) of the present study has been evaluated using the hydraulic diameter of the Dean test section and fluid properties. The results for two bulk temperatures (average of inlet and outlet) are shown in Figures 43 and 44. The circled points represent data reported by Dean (45). It is noted that, in general, the experimental results of Dean (45) fall below the values predicted by Equation (2.60), probably because of axial changes in bulk temperature and pressure in the test section. A correlation function has been developed by Dean (45) and involves the use of three empirical constants.

Dougall and Panian (41) have performed annular flow boiling experiments and correlated the results with a regression analysis allowing three experimentally determined constants. The culmination of each test series was the occurrence of the critical heat flux. Figure 45 compares Equation (2.60) of this study with three experimentally determined critical heat flux values reported by Dougall and Panian (41) at 195 psia.

4.5   Effect of Other Variables

The influence of pressure on the critical heat flux has been considered briefly by a number of investigators (4, 7). Although it is agreed that for pool boiling a maximum critical heat flux is obtained at about one third the critical pressure, no equivalently similar behavior has been ascribed to forced convection boiling. It has been observed, however, that the critical heat flux will vary somewhat with pressure, reaching a peak value at some subcritical pressure.
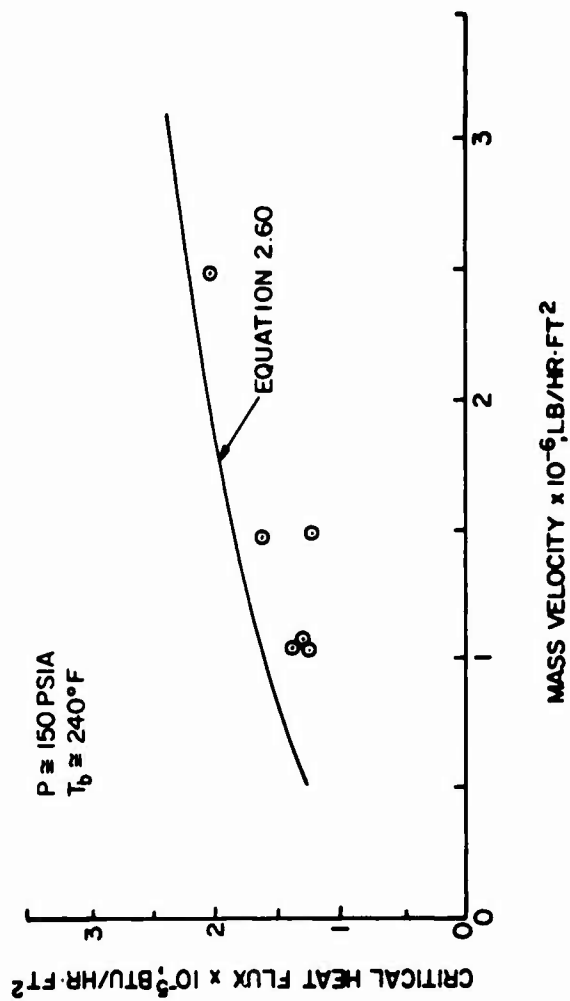
Figure 43 Comparison of the Critical Heat Flux Predicted by Equation
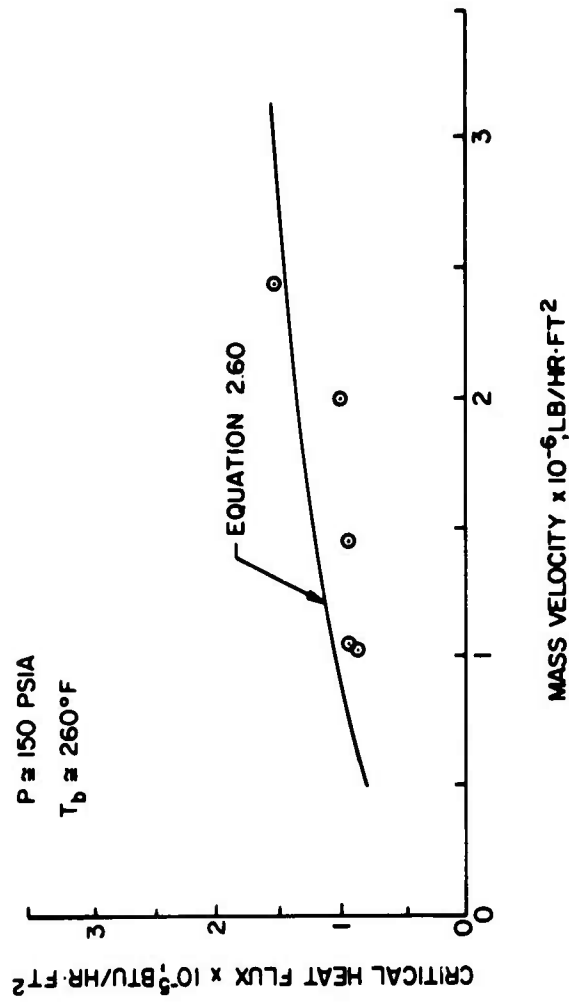(2.60) and the Work of Dean at 47°F Subcooling

Figure 44 Comparison of the Critical Heat Flux Predicted by Equation (2.60) and the Work of Dean at 27°F Subcooling
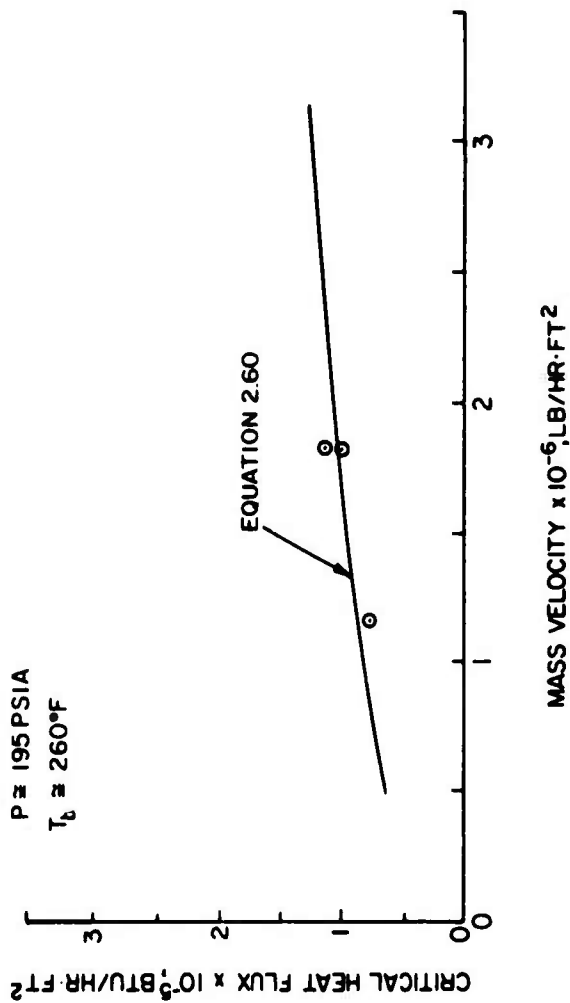
Figure 45 Comparison of the Critical Heat Flux Predicted by Equation
(2.60) and the Work of Dougall and Panian

The data for this study was obtained almost exclusively at 130 psia. This pressure was chosen for convenience in experimentation, to insure experiments in the high pressure boiling regime (11), and to model the boiling process in water at 1000 psia in accordance with the equivalent liquid to vapor density ratio criteria advanced by a number of investigators (11, 46, 47).

Several experiments were conducted at slightly higher and lower pressures at a constant subcooling (70°F) to obtain an assessment of pressure variation effects. The results are contained in Table 11 and show a trend of decreasing critical heat fluxes with increasing pressure. This same trend is produced by the analytical model as shown in Figure 46 where Equation (2.61) has been evaluated for increasing pressures at a subcooling of 50°F. Similar results were obtained at all subcoolings. In addition, Equation (2.60) has been applied successfully to other experimenter's data at a variety of pressures in Section 4.4.

In agreement with all previous work, increases in velocity and subcooling have produced general increases in the critical heat flux in both the analytical and experimental phases of this study. Several exceptions to this trend are contained in the data and are considered to be the result of normal experimental uncertainties. In addition, the analytical results at 110°F subcooling resist the general trend and this is thought to be the result of the imperfect empirical description of β_{fs} at 110°F subcooling.

It is well established that although dissolved gases influence incipient boiling and the transition to fully developed boiling, they have little or no effect on the critical heat flux (7, 20, 42).

Table 11

Experimental Determinations of the Effect
of Pressure on the Critical Heat Flux

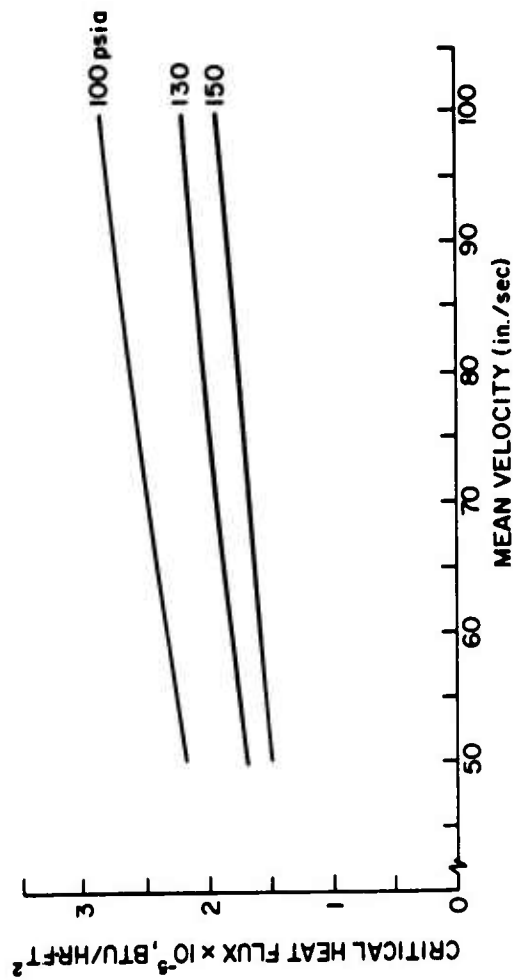| Pressure psia	Subcooling °F	Non-Dimensional Radial Acceleration $V_m^2/\underset{a}{g}$	Number of Tests	Critical Heat Flux x 10^{-5} BTU/hr-ft^2
110	70°F	5.0	3	2.52
130	70°F	5.0	3	2.40
150	70°F	5.0	4	2.32
110	70°F	14.1	3	3.09
130	70°F	14.1	4	2.83
150	70°F	14.1	4	2.71

Figure 46   The Effect of Pressure on the Critical Heat Flux Expression for the Convex Surface at 50°F Subcooling

In spite of this, dissolved gases were held to a minimum in this study
by using helium to pressurize the boiling loop, by degasing before
each test series, and by measuring dissolved gas levels periodically
to insure constant test conditions. Dissolved air concentrations in
Freon samples taken from the boiling loop during selected tests were
measured by gas chromatography. Dissolved air concentrations
between 236 PPM and 256 PPM were found to be present in the samples.

A surface breakin or aging effect was observed in this study.
The initial test with a new boiling surface normally produced slightly
higher values for the critical heat flux than succeeding tests at
equivalent conditions. Once the initial test was performed, the
nichrome would assume a tarnished look and no further changes, other
than geometry degradation, were observed. On several occasions
blocks of data were repeated after numerous intermediate tests at
other conditions. Substantial changes in surface performance were
not observed to occur.

The influence that surface roughness exerts on the critical
heat flux has not been agreed upon by all experimentors. Durant and
Mirshak (48) have reported significantly higher critical heat fluxes
for artifically roughened surfaces while DeBortoli, et al., (7),
in a summary of other work, have concluded that surface roughness
does not affect the critical heat flux for surface roughnesses of
up to 120 microinches. The surface roughness in the Durant study was
obtained by threading, knurling, and sandblasting the boiling surfaces
This gave rise to roughnesses more than an order of magnitude larger
than those in the DeBortoli study, and certainly much greater than
any that would routinely be encountered. For this reason the two

studies are probably not comparable. Brown (49) has concluded that surface finish plays no part in flow boiling at large velocities and subcoolings.

Repeated critical heat flux experiments caused a continual increase in the roughness of the surfaces used in this study. The increasing roughness was visible to the eye and appeared to be the result of local microscopic melting of the nichrome ribbon. In spite of this, no measurable change in the critical heat flux was observed for constant fluid conditions. In an effort to characterize the roughening effects of repeated critical heat flux tests, samples of new nichrome ribbon and used nichrome ribbon were analyzed with a roughness profilometer. It was found that repeated critical heat flux experiments could increase the average surface roughness from less than 100 microinches to more than 165 microinches. The most graphic representation of this finding is the analog output of the diamond tipped stylus used to trave two surface segments 0.222 inches long and 0.040 inches wide. Figure 47 shows the new sample where the dimensions normal to the surface are magnified 12.5 times. For the same magnification Figure 48 shows a used surface segment.

Test sections were constructed with nichrome ribbon taken from different locations on the rolls of 3/32 inch x 0.0052 in Tophet A nichrome and 1/8 inch x 0.0032 in Tophet A nichrome. Variations in material batch and size (very limited range) were found to have no measurable effect on the data. In all, nine individual segments of nichrome ribbon of two widths were used to gather the data for this study.
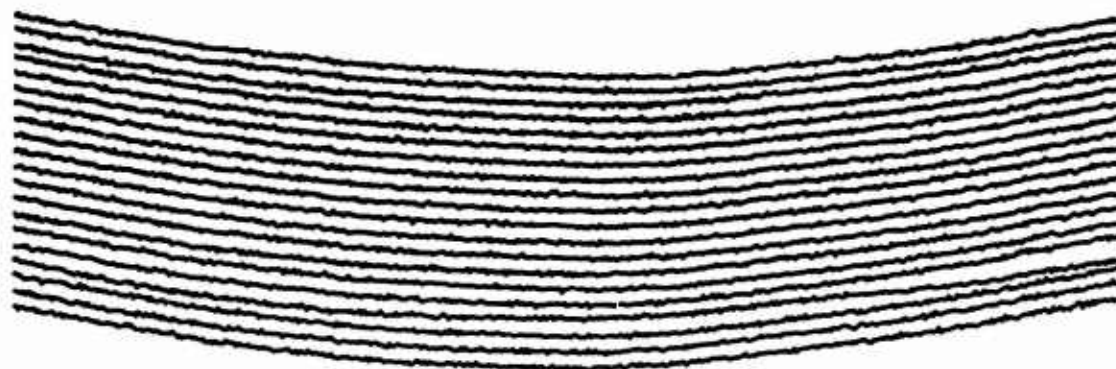
Figure 47   Surface Roughness Profile of Nichrome Strip Before
Critical Heat Flux Tests
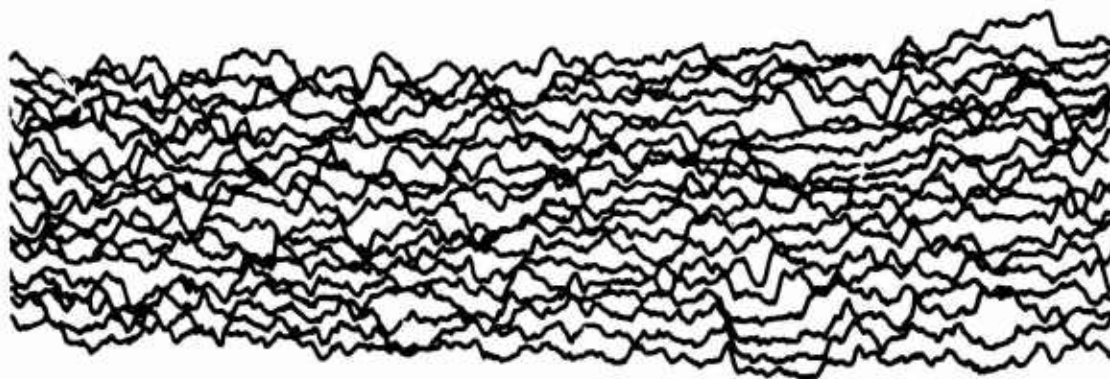
Figure 48   Surface Roughness Profile of Nichrome Strip After Numerous
            Critical Heat Flux Tests

In the course of fabrication, installation and breakin, each boiling surface assembly would assume an individual characteristic "set" in its Teflon support. This would tend to randomly shift the data slightly upward or downward and contributed greatly to experimental data scatter.

Figure 49 Segment of Coiled Tube

An analytical model was developed to predict the critical heat flux for curved and straight flows. A strong physical basis for the model was maintained by defining a greatly simplified ideal vapor bubble cycle, and deriving expressions for the number of active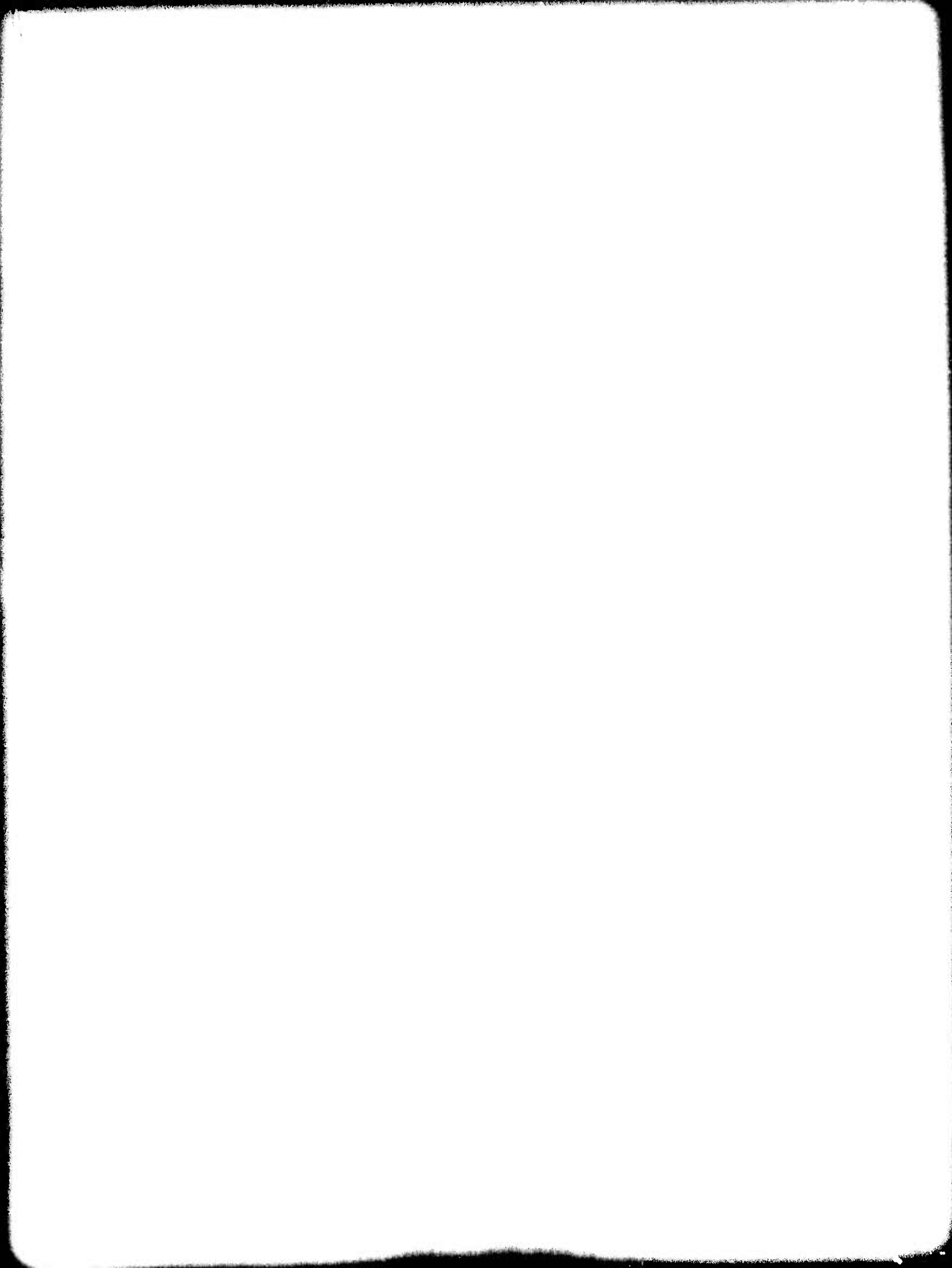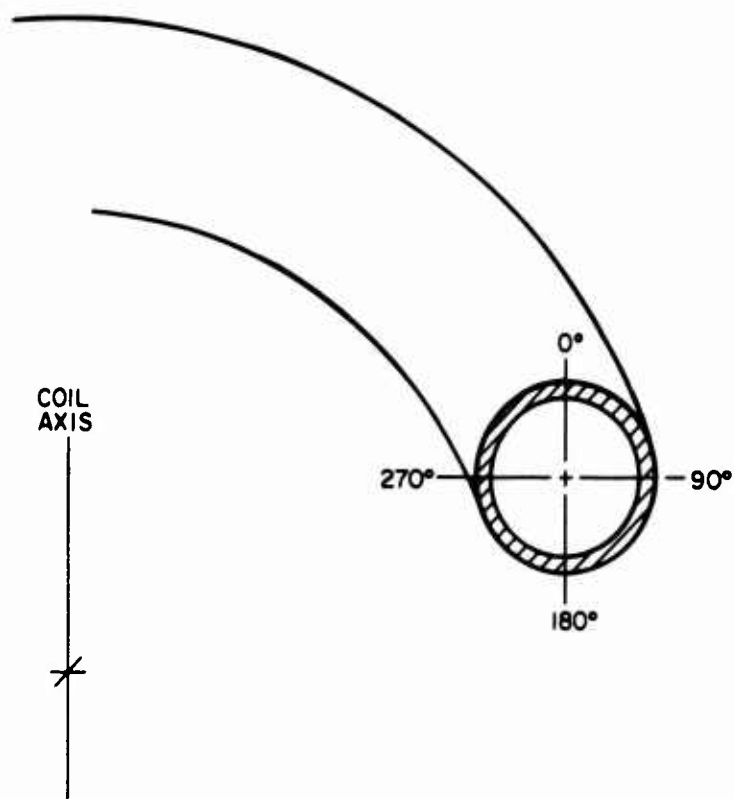 sites, bubble cycle frequency, and energy transfer associated with an average bubble going through the cycle. The product of the energy, frequency and active sites terms yielded the desired critical heat flux expression. In order to develop these expressions, criteria were proposed for the vapor bubble packing density at the critical heat flux and for the average vapor bubble diameter at departure from the heated surface. The resulting critical heat flux expressions contained only one empirical constant, substantially less than the three or more constants commonly associated with linear regression correlation functions.

Ratios of the critical heat flux magnitudes were formed from the critical heat flux equations for concave, convex and straight surfaces. The resulting expressions, comparing concave to convex and straight to convex surfaces, were unique since they contained no empirical constants.

An experimental program was conducted in a closed loop test apparatus using Freon 113 as the working fluid. Freon 113 was chosen to minimize the cost and complexity of the apparatus. Two interchangeable test sections, one curved and the other straight, were used with the boiling loop. The curved test section contained both the concave and convex surfaces. Two separate sizes of Tophet A nichrome strip were used to conduct 274 critical heat flux tests at four subcoolings and five mean velocities. A critical heat flux

detector was developed and used to relieve the experimentor from manually interrupting the test section power at the conclusion of each test.

The results of the analytical and experimental portions of the study have been compared and agree favorably. Both indicate an increasing critical heat flux for all surfaces as the radial acceleration or mean velocity (straight flow) and subcooling are increased. At equivalent subcoolings and radial accelerations (or mean velocities) the concave surface has been shown, by experiment and analysis, to sustain larger critical heat fluxes than the straight surface, which in turn sustains larger critical heat fluxes than the convex surface. The ratios between the critical heat fluxes on concave and convex surfaces have been found to lie between 1.5 and 2.0 while the ratios between straight and convex surfaces were predicted to lie between approximately 1.0 and 1.2 for the conditions investigated in this study.

A fluid-surface empirical constant, β_{fs}, was evaluated with the 50°F, 70°F and 90°F subcooling data for use in the analytical model. Using the resulting value of β_{fs}, the analytical expressions for the critical heat flux correlated the experimental data in this range to within 11%.

Like many investigations into new areas, this study has raised a number of questions that might be answered in future studies. The role of the radial fluid acceleration in curved channels should be considered. It is possible, even likely, that the performance of curved surfaces will be similar for many combinations of mean velocity and channel radius giving the same magnitude of radial acceleration.

Test sections of different centerline radius would be required to investigate this concept.

Additional work on the fluid-surface constant should be performed. The work performed in this study was aimed primarily at demonstrating the feasibility of the concept. Future work should attempt to find a more exact method of relating the area of influence proportionality factor, K, to the fluid surface constant, β_{fs}. There are some indications (Table 9) that a geometry effect should be included in the relationship between K and β_{fs}.

Experiments in a test section of known (measured) velocity profile and wall shear stress would be helpful in determining optimum values of the non-dimensional hydrodynamic boundary layer thickness, W, used to approximate the departure diameter of an average vapor bubble. Such experiments, coupled with a photographic study of concave and convex surfaces operating near the critical heat flux, would provide additional insight into the actual details of the vapor bubble cycle and bubble packing density at burnout, particularly on curved surfaces.

A general expansion of the experimental program to a broader range of pressures, radial accelerations, subcoolings and working fluids would serve to define the practical limits of applicability of the equations derived in this study.

BIBLIOGRAPHY

1. Tong, L. S., "Boundary Layer Analysis of the Flow Boiling Crisis," Int. J. Heat Mass Transfer, II, pg. 1208-1211, 1968.

2. Purcupile, J. C., and Gouse, S. W., Jr., "Reynolds Flux Model of Critical Heat Flux in Subcooled Forced Convection Boiling," ASME, paper No. 72-HT-4, August 1972.

3. Chang, Y. P., "An Analysis of the Critical Conditions and Burnout in Boiling Heat Transfer," United States Atomic Energy Commission Report (Unclassified) TID-14004L, 1961.

4. Jens, W. H., and Lottes, P. A., "Analysis of Heat Transfer, Burnout, Pressure Drop and Density Data for High Pressure Water," Argonne National Laboratory, ANL-4627, 1951.

5. Gambill, W. R., "Generalized Prediction of Burnout Heat Flux for Flowing Subcooled, Wetting Liquids," Chem. Eng. Prog. Symp. Ser., Vol. 59, No. 41, pg. 71, 1963.

6. Bernath, L., "A Theory of Local-Boiling Burnout and Its Application to Existing Data," AIChE Paper No. 110, Third Heat Transfer Conference, August 1959.

7. DeBortoli, R. A., Green, S. J., LeToruneau, B. W., Troy, M., and Weiss, A., "Forced-Convection Heat Transfer Burnout Studies for Water in Rectangular Channels and Round Tubes at Pressures Above 500 psia," Westinghouse Atomic Power Division, No. 188, October 1958

8. Stevens, G F., Elliott, D. R., and Wood, R. W., "An Experimental Investigation Into Forced Convection Burnout in Freon, with Reference to Burnout in Water," United Kingdom Atomic Energy Authority, Atomic Energy Establishment at Winfrith R321 (Unclassified), 1964.

9. Thompson, B., and Macbeth, R. W., "Boiling Water Heat Transfer. Burnout in Uniformly Heated Round Tubes: A compilation of World Data with Accurate Correlations," United Kingdom Atomic Energy Authority, Atomic Energy Establishment at Winfrith R356 (Unclassified), 1964.

10. Milioti, S., "A Survey of Burnout Correlations as Applied to Water-Cooled Nuclear Reactors," The Pennsylvania State University, M S. Thesis, September 1964.

11. Mattson, R. J., "A Photographic Study of Subcooled Flow Boiling and the Boiling Crisis in Freon-113," Michigan University, Ph D. Thesis, January 1972.

12. Carver, J. R., Kakarala, C. R., and Slotnik, J. S., "Heat Transfer in Coiled Tubes with Two-Phase-Flow," Atomic Energy Commission Document TID 20983, 1964.

13. Owhadi, A., "Boiling in Self-Induced Radial Acceleration Fields," Oklahoma State University, Ph.D. Thesis, 1966.

14. Duchatelle, L., DeNucheze, L., and Robin, M. G., "Departure from Nucleate Boiling in Helical Tubes of Liquid Metal Heated Steam Generators," ASME-AIChE Heat Transfer Conference, Paper No. 73-HT-57, 1973.

15. Jiji, L. M., and Clark, J. A., "Bubble Boundary Layer and Temperature Profiles for Forced Convection Boiling in Channel Flow," Transactions ASME, Journal of Heat Transfer, pg. 50, February 1964.

16. Forster, K , and Grief, R., "Heat Transfer to a Boiling Liquid-Mechanisms and Correlations," Transactions ASME, Journal of Heat Transfer, Series C, Vol. 81, No. 1, 1959.

17. Bankoff, S. G., Colahan, W. J., Jr., and Bartz, D. R., "Summary of Conference on Bubble Dynamics and Boiling Heat Transfer," Jet Propulsion Laboratory, California Institute of Technology, 1956.

18. Bankoff, S. G., "On the Mechanism of Subcooled Nucleate Boiling Parts I and II," Chem. Eng. Prog. Symp. Ser., Vol. 57, No. 32, pg. 156, 1961.

19. Gunther, F. C., and Kreith, F., "Photographic Study of Bubble Formation in Heat Transfer to Subcooled Water," Proceedings of the Heat Transfer and Fluid Mechanics Institute, 1949.

20. Rohsenow, Warren M., "Nucleation with Boiling Heat Transfer," ASME, Heat Transfer Conference, Paper No. 70-HT-18, Detroit, 1970.

21. Martinelli, R. C., "Heat Transfer to Molten Metals," Transactions ASME, November 1947.

22. Schlichting, H., Boundary Layer Theory, McGraw-Hill, 1968.

23. Eskinazi, S., and Yeh, H., "An Investigation of Fully Developed Turbulent Flows in a Curved Channel," Journal of Aero. Sci., Vol. 23, pp. 23-34, January 1956.

24. Wattendorf, F. L., "A Study of the Effect of Curvature on Fully Developed Turbulent Flow," Proc. Roy. Soc. London, A, 148, pp. 565-598, 1934.

25. Ito, H., "Friction Factors for Turbulent Flow in Curved Pipes," Transactions ASME, Journal of Basic Engineering, June 1959.

26.   Han, C. Y., and Griffith, P., "The Mechanism of Heat Transfer in Nucleate Boiling," TR 19, Massachusetts Institute of Technology, February 1962.

27.   Carslaw, H. S., and Jaeger, J. C., <u>Conduction of Heat in Solids</u>, Oxford University Press, 1947.

28.   Plesset, M. S., and Zwick, S. A., "The Growth of Vapor Bubbles in Super-heated Liquids," Journal of Applied Physics, Vol. 25, pg. 493, 1954.

29.   Keshock, E. G., and Siegel, R., "Forces Acting on Bubbles in Nucleate Boiling Under Normal and Reduced Gravity Conditions," NASA, Lewis Research Center, Cleveland, 1964.

30.   Robin, T. T. Jr., and Snyder, N. W., "Bubble Dynamics in Subcooled Nucleate Boiling Based on the Mass Transfer Mechanism," International Journal of Heat and Mass Transfer, Vol. 13, pg. 305-318, 1970.

31.   Kirby, D. B., and Westwater, J. W., "Bubble and Vapor Behavior on a Heated Horizontal Plate During Pool Boiling Near Burnout," Chemical Engineering Progress Symposium Series, Vol. 61, No. 57, 1965.

32.   Anderson, D. L. J., Judd, R. L., and Merte, H. Jr., "Site Activation Phenomena in Saturated Nucleate Boiling," ASME, Heat Transfer Conference, Paper No. 70-HT-14, Detroit, 1970.

33.   Thirunavukkarsau, K., "Bubble Growth from a Cavity at a Solid Surface," ASME, Heat Transfer Conference, Paper No. 70-HT-13, Detroit, 1970.

34.   Gaertner, R. F., "Distribution of Active Sites in Nucleate Boiling of Liquids," Chemical Engineering Progress Symposium Series, Vol. 59, No. 41, pg. 52, 1963.

35.   Gaertner, R. F., and Westwater, J. W., "Population of Active Sites in Nucleate Boiling Heat Transfer," Chemical Engineering Progress Symposium Series, Vol. 56, No. 30, pp. 39-48, 1960.

36.   Clark, H. B., Strenge, P. S., and Westwater, J. W., "Active Sites for Nucleate Boiling," Chemical Engineering Progress Symposium Series, Vol. 55, No. 29, pg. 103, 1959.

37.   Marris, A. W., "Radial Distributions of Temporal Mean Peripheral Velocity and Pressure for Fully Developed Flow in Curved Channels, Transactions ASME, Journal of Basic Engineering, Series D, Vol. 82, pp. 528-538, 1960.

38.   Benning, A. F., and McHarness, R. C., "The Thermodynamic Properties of Freon 113," Bulletin T-113A, E. I. duPont de Nemours and Company, Wilmington, Delaware, 1938.

39. Downing, R. C., "Transport Properties of Freon Fluorocarbons,"
     Bulletin C-30, E. I. duPont deNemours and Company, 1967.

40. "Surface Tension of the Freon Compouns," Bulletin D-27,
     E. I. duPont deNemours and Company, 1967.

41. Dougall, R. S., and Panian, D. J., "Subcooled Forced Convection
     Boiling of Trichlorotrifluoroethane," University of Pittsburgh,
     Report No. NASA-CR-2137, 1972.

42. Murphy, R. W., and Bergles, A. E., "Subcooled Flow Boiling of
     Fluorocarbons," Report DSR 71 903-72, Engineering Projects
     Laboratory, Massachusetts Institute of Technology, January 1971.

43. Rohsenow, W. M., Boiling," Annual Review of Fluid Mechanics,
     Vol. 3, pg. 211-236, 1971.

44. "Major Alloys and Their Properties," Wilbur B. Driver Company,
     Newark, New Jersey, 1971.

45. Dean, R. A., "Effect of Vapor Injection on Critical Heat Flux in
     a Subcooled R-113 (Freon) Flow," University of Pittsburgh,
     Ph.D. Thesis, 1970.

46. Cermak, J. O., Tong, L. S., and Motley, F. E., "Scaling Law of
     Flow-Boiling Crisis," Paper B6 12, Fourth International Heat
     Transfer Conference, Paris 1970.

47. Crowley, J. D., and Bergles, A. E., "Fluid-to-Fluid Modelling
     of the Hydrodynamic Stability of Flow in Boiling Channels,"
     ASME, Heat Transfer Conference, Paper No. 70-HT-28, Detroit,
     1970.

48. Durant, W. S., and Mirshak, S., "Roughening of Heat Transfer
     Surfaces as a Method of Increasing Heat Flux at Burnout,"
     E. I. duPont deNemours and Company, Inc., No. 60-284,
     Savanna River Laboratory, 1960.

49. Brown, W. T., "A Study of Flow Surface Boiling," Massachusetts
     Institute of Technology, Ph.D. Thesis, 1967.

50. Rohsenow, W. M., and Choi, H. Y., Heat, Mass and Momentum
     Transfer, Prentice-Hall, 1961.

51. Massier, P. F., "A Forced-Convection and Nucleate-Boiling Heat-
     Transfer Test Apparatus," JPL Technical Report No. 32-47,
     March 1961.

52. Van Stralen, S. J. D., "The Mechanism of Nucleate Boiling
     in Pure Liquids and in Binary Mixtures - Part III," Int. J.
     Heat Mass Transfer, Vol. 10, pp. 1469-1484, 1967.

53. Kenning, D. B. R., and Cooper, M. G., Flow Patterns Near Nuclei and the Initiation of Boiling During Forced Convection Heat Transfer," Proc. Inst. Mech. Engr., Vol. 180, Pt. 3C, Paper 11, 1965-66.

54. Glushchenko, L. F., "Correlation of Experimental Data on Critical Heat Fluxes in Subcooled Boiling," Heat Transfer-Soviet Research, January 1970.

55. Weske, J. R., "Investigation of the Flow in Curved Ducts at Large Reynolds Numbers," Journal of Applied Mechanics, Vol. 15, Transactions ASME, Vol. 70, pg. 344, 1948.

56. Tong, L. W., and Hewitt, G. F., "Overall Viewpoint of Flow Boiling CHF Mechanisms, AIChE-ASME Heat Transfer Conference, Paper No. 72-HT-54, Denver, 1972.

57. Cumming, H. G., "The Secondary Flow in Curved Pipes," Aeronautical Research Council Reports and Memorandum No. 2880, 1955.

58. Rohsenow, W. M., and Clark, J. A., "A Study of the Mechanism of Boiling Heat Transfer," Transactions ASME, Vol. 73, No. 5, 1951.

59. Kreith, F., "The Influence of Curvature on Heat Transfer to Incompressible Fluids," Transactions ASME, Vol. 77, pg. 1247-1256, 1955.

60. Forster, H. K., and Zuber, N., "Growth of Vapor Bubbles in a Superheated Liquid," Journal of Applied Physics, Vol. 25, 1954, pg 475.

61. Bergles, A. E., and Rohsenow, W. M., "The Determination of Forced Convection Surface Boiling Heat Transfer," Transactions ASME, Journal of Heat Transfer, Series C, Vol. 86, No. 3, 1964.

62. Hancox, W. T., and Nicoll, W. B., "On the Dependence of the Flow-Boiling Heat Transfer Crisis on Local Near Wall Conditions," ASME-AIChE Heat Transfer Conference, Paper No. 73-HT-38, Atlanta, 1973.

63. Brown, O. G., and Marris, A. W., "Turbulent Flow of Water in Plane Curved Channels of Finite Depth," Transactions ASME, Journal of Basic Engineering, pp. 377-391, September 1963.

64. Hawthorne, W. R., "Secondary Criculation in Fluid Flow," Proceedings of the Roual Society (London), Ser. A., Vol. 206, 1951, pp. 374-387.

65. Dean, W. R., "The Stream-Line Motion of Fluid in a Curved Pipe," The London, Edinburgh and Dublin Philosophical Magazine and Journal of Science, Vol. 5, 1928, pp. 673-695.

66. Kurihara, H. M., and Myers, J. E., "The Effects of Superheat
     and Surface Roughness on Boiling Coefficients," AIChE
     Journal, Vol. 6, No. 1, pp. 83-91, March 1960.

67. Dix, G. E., "Freon-Water Modelling of CHF in Round Tubes,"
     ASME, Heat Transfer Conference, Paper No. 70-HT-26, Detroit,
     1970.

68. Joy, W., "Experimental Investigation of Shear Flow in
     Rectangular Bends," Massachusetts Institute of Technology,
     Ph.D. Thesis, 1950.

69. Thorgerson, E. J., "Hydrodynamic Aspects of the Critical Heat
     Flux in Subcooled Convective Boiling," E. I. duPont deNemours
     and Company, Savannah River Laboratory, NTIS No. N69-38575, 1969.

70. Hsu, Y. Y., "On the Size Range of Active Nucleation Cavities
     on a Heating Surface," Transactions ASME, Journal of Heat
     Transfer, pp. 207-216, August 1962.

71. Moore, F. D., and Mesler, R. B., "The Measurement of Rapid
     Surface Temperature Fluctuations During Nucleate Boiling of
     Water," AIChE Journal, December 1961.

APPENDIX A

PRESSURE FORCES ON BUBBLES IN CURVED DUCTS

Confining the flow of a fluid to a curved channel creates a radial gradient in the static pressure. For two dimensional steady flow, where viscous and turbulent terms are neglected, the equations of motion give:

$$\frac{dp}{dR} = \frac{\rho_1 V^2}{R} \quad , \tag{A.1}$$

in the absence of secondary flow. This is a substantial simplification of the true situation, but several investigators (24, 37) have found it to render a useful approximation of the static pressure gradient experimentally observed. This conclusion is due mainly to the transmission of pressure forces from the free stream, where the approximation is reasonable, through the viscous sublayer where it is not appropriate.

The radial pressure distribution can be obtained by integrating Equation (A.1) after the substitution of a suitable velocity profile. Such a profile is reported by Marris (37):

$$\frac{V}{V_m} = \frac{R_o - R_1}{\ln\left(\frac{R_o}{R_1}\right)} \left[\frac{1}{R}\right] \quad . \tag{A.2}$$

Substituting Equation (A.2) into Equation (A.1) gives:

$$\frac{dp}{dR} = \frac{\rho_1 (R_o - R_1)^2 \, V_m^2}{\left[\ln\left(\frac{R_o}{R_1}\right)\right]^2} \left[\frac{1}{R^3}\right] \quad . \tag{A.3}$$

which may be integrated to obtain,

$$p = \left\{ \frac{\rho_1 (R_o - R_1)^2 \, V_m^2}{\left[\ln \left(\frac{R_o}{R_1} \right) \right]^2} \right\} \left[-\frac{1}{2R^2} \right] + C \quad .$$ (A.4)

Applying the boundary condition:

$$p = P_{\ell} \quad \text{at} \quad R = R_{\ell} \quad ,$$ (A.5)

the pressure distribution results:

$$p = P_{\ell} + \left\{ \frac{\rho_1 (R_o - R_1)^2}{\left[\ln \left(\frac{R_o}{R_1} \right) \right]^2} \quad \frac{V_m^2}{2g_c} \right\} \left[\frac{1}{R_{\ell}^2} - \frac{1}{R^2} \right] \quad .$$ (A.6)

A coordinate system, used to find the net force on a spherical bubble in a pressure field has been shown in Figure 50. The force on an infinitesimal strip of area for a pressure gradient in the y direction is given by:

$$dF_y = p \, dA_n \quad ,$$ (A.7)

where both P and A_n can be described as functions of ϕ:

$$dA_s = (r d\phi) \times (2\pi r \sin \phi) \quad ,$$ (A.8)

$$dA_n = 2\pi r^2 \sin\phi \, \cos\phi \, d\phi \quad .$$ (A.9)

When Equation (A.6) is substituted into Equation (A.7), the resulting expression cannot be integrated directly. Since the pressure distribution of Equation (A.6) is nearly linear in the curved channel, the pressure distribution in the wall region has been assumed linear with a slope equal to that of Equation (A.6) at the wall:
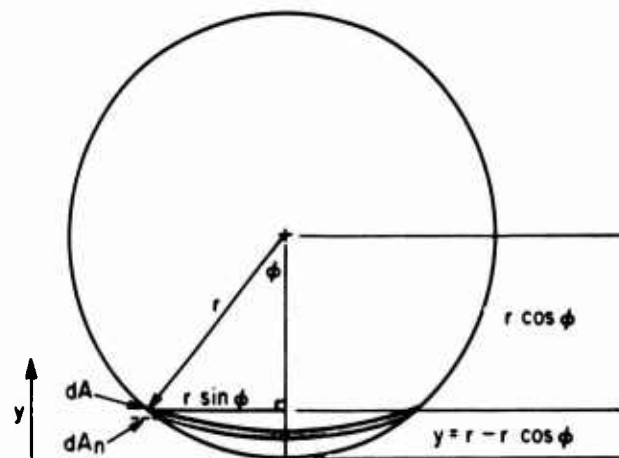
Figure 50   Spherical Bubble in Pressure Field

$$p(\phi) = p_i + \left.\frac{dp}{dR}\right|_{R = R_i, R_o} y \tag{A.10}$$

For a convex surface this expression yields the following pressure distribution,

$$p(\phi) = p_i + \frac{\rho_1 (R_o - R_i)^2}{\left[\ell n\left(\frac{R_o}{R_i}\right)\right]^2 R_i^3} \frac{V_m^2}{g_c} r(1 - \cos\phi) \quad . \tag{A.11}$$

Equation (A.11) and (A.9) were then substituted into Equation (A.7) to obtain a normal force expression:

$$dF_y = \left\{ p_i + \frac{\rho_1 (R_o - R_i)}{\left[\ell n\left(\frac{R_o}{R_i}\right)\right]^2 R_i^3} \frac{V_m^2}{g_c} r(1 - \cos\phi) \right\} 2\pi r^2 \sin\phi \cos\phi \, d\phi . \tag{A.12}$$

Defining the geometry factor,

$$A_{i,o} = \frac{(R_o - R_i)^2}{\left[\ell n\left(\frac{R_o}{R_i}\right)\right]^2 R_{i,o}^3} \quad , \tag{A.13}$$

and integrating Equation (A.12) from $\phi = 0°$ to $\phi = 180°$, the following results were obtained:

$$F_y(\text{Convex}) = - \frac{\pi d^3}{6} A_i \frac{\rho_1 V_m^2}{g_c} \quad , \tag{A.14}$$

$$F_y(\text{Concave}) = \frac{\pi d^3}{6} A_o \frac{\rho_1 V_m^2}{g_c} \quad . \tag{A.15}$$

Results obtained with Equation (A.14) were compared with results obtained by numerically integrating Equation (A.7), using Equation (A.6) for the pressure distribution. Variations of less than 1% were found for bubble diameters representative of this work.

APPENDIX B

CORRECTIONS OF DATA FOR CONDUCTION LOSSES
FROM THE HEATED SURFACE

Although the vast majority of electric power supplied to the
test sections was dissipated by boiling heat transfer, corrections have
been made for heat conduction through thermocouples, Teflon supports,
and electrical terminals. Thermocouples and electrical terminals
have been modeled as fins while the Teflon supports have been
modeled as infinite slabs with a temperature gradient. Figure 51
summarizes the configurations used in conduction loss analyses.

The dimensions of the thermocouples were known and the short
distance between the heated surface and measurement junction was
considered adiabatic. The fluid behind the Teflon support was
considered to be stagnant at the bulk fluid temperature. The solution
to this type problem has been reported by Rohsenow and Choi (50):

$$\dot{q} = \sqrt{hJkS} \ (T - T_b) \ \tanh ML \ , \tag{B.1}$$

where

$$M = \sqrt{\frac{hJ}{kS}} \ . \tag{B.2}$$

The film coefficient has been evaluated for free convection
over a horizontal cylinder and was used in conjunction with the
experimentally determined temperatures to compute the heat lost through
each wire of the thermocouple pair. The total loss was the sum of the
losses for four thermocouple pairs and was found to be less than 1%
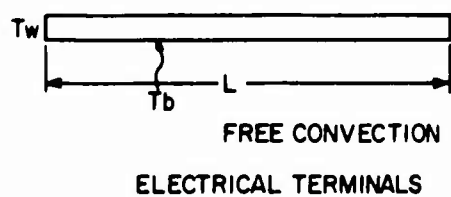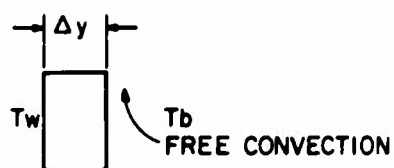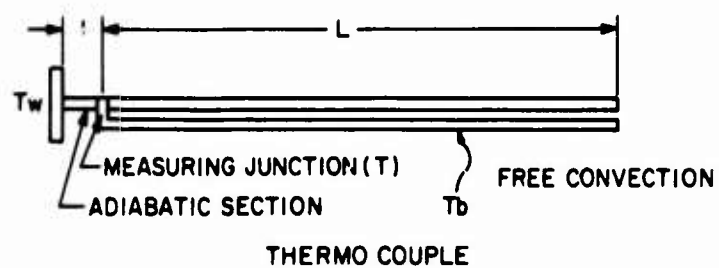of the energy input in the worst case. Actual wall temperatures were

Figure 51 Idealized Models for the Computation of Conduction
Losses Through Thermocouples, Teflon Supports, and
Electric Terminals

then determined using the following expression, derived from a simple conduction analysis of the adiabatic area of the thermocouple:

$$T_W = T + \frac{ql}{kS} \quad . \tag{B.3}$$

The resulting temperatures were used to compute the heat lost by conduction through the Teflon supports. The supports were analyzed as semi-infinite slabs with one surface held at T_W and the other contacting a stagnant pool of liquid at T_b. The film coefficient was evaluated for free convection over a vertical surface and the heat loss per unit area was found to be:

$$\dot{q}'' = \frac{T_W - T_b}{\frac{1}{h} + \frac{\Delta y}{k}} \quad . \tag{B.4}$$

This heat flux was multiplied by the total area of the boiling surface and produced heat losses of much less than 1% in the worst case.

The electric terminals were treated in the same fashion as the thermocouples, using T_W as the driving temperature. Heat losses of 2% to 5% for the concave surface, 3% to 9% for the convex surface, and 2% to 6% for the straight surface were calculated.

APPENDIX C

COMPUTATION OF THE STANDARD DEVIATION OF THE EXPERIMENTAL DATA

In order to assess the variations in the experimental data, the standard deviation has been computed for observed critical heat flux voltages at each test point and for the experimental data compared to the analytical results. Standard deviations were calculated by:

$$\sigma = \left[\frac{\Sigma(X - \bar{X})^2}{N - 1}\right]^{1/2} \quad,$$

where N is the number of points in the sample.

At each test state the mean critical heat flux voltage was substituted for $\bar{X}$ and the individual voltages for each test were used to calculate the standard deviation in volts. For standard deviation calculations comparing experimental and analytical results, the critical heat flux predicted by the model was used for $\bar{X}$ and the experimentally determined critical heat flux values were used for X in order to compute σ. The results are presented in Table 10.

VITA

Thomas G. Hughes was born ████████ ████ ████████ ████████ He was graduated from ████████████████ in [PII Redacted]
May, 1962, and received the degree of Bachelor of Science in Mechanical Engineering from The Pennsylvania State University in March, 1966. In September, 1968, he received the degree of Master of Science with a major in Mechanical Engineering from The Pennsylvania State University.

From March, 1968, to the present the author has been employed as a Research Assistant with the Applied Research Laboratory of The Pennsylvania State University. He is a member of the Pi Tau Sigma and Sigma Tau honorary fraternities.